RAPID THINNING AND COLLAPSE OF LAKE CALVING YAKUTAT GLACIER, SOUTHEAST ALASKA

By

Barbara Lea Trüssel

RECOMMENDED:

Advisory Committee Chair

Chair, Department of Geology and Geophysics

APPROVED:

Dean, College of Natural Science and Mathematics

Dean of the Graduate School

11/25/13

Date

RAPID THINNING AND COLLAPSE OF LAKE CALVING YAKUTAT GLACIER, SOUTHEAST ALASKA

A

DISSERTATION

Presented to the Faculty

of the University of Alaska Fairbanks

in Partial Fulfillment of the Requirements

for the Degree of

DOCTOR OF PHILOSOPHY

By

Barbara Lea Trüssel, Dipl. Natw. ETH

Fairbanks, Alaska

December 2013

Abstract

Glaciers around the globe are experiencing a notable retreat and thinning, triggered by atmospheric warming. Tidewater glaciers in particular have received much attention, because they have been recognized to contribute substantially to global sea level rise. However, lake calving glaciers in Alaska show increasingly high thinning and retreat rates and are therefore contributors to sea level rise. The number of such lake calving systems is increasing worldwide as land-terminating glaciers retreat into overdeepened basins and form proglacial lakes.

Yakutat Glacier in Southeast Alaska is a low elevation lake calving glacier with an accumulation to total area ratio of 0.03. It experienced rapid thinning of 4.43 $\pm$ 0.06 m w.e. yr^{-1} between 2000-2010 and terminus retreat of over 15 km since the beginning of the 20^{th} century. Simultaneously, adjacent Yakutat Icefield land-terminating glaciers thinned at lower but still substantial rates (3.54 $\pm$ 0.06 m w.e. yr^{-1} for the same time period), indicating lake calving dynamics help drive increased mass loss.

Yakutat Glacier sustained a $\sim$3 km long floating tongue for over a decade, which started to disintegrate into large tabular icebergs in 2010. Such floating tongues are rarely seen on temperate tidewater glaciers. The floating ice was weakened by surface ablation, which then allowed rifts to form and intersect. Ice velocity from GPS measurements showed that the ice on the floating tongue was moving substantially faster than grounded ice, which was attributed to rift opening between the floating and grounded ice. Temporal variations of rift opening were determined from time-lapse imagery, and correlated well with variations in ice speeds. Larger rift opening rates occurred during and after precipitation or increased melt episodes. Both of these events increased subglacial discharge and could potentially increase the subaqueous currents towards the open lake and thus increase drag on the ice underside. Simultaneously, increased water input may cause lake level in rifts to rise resulting in faster rift propagation and spreading. Similar formation and disintegration of floating tongues are expected to occur in the glacier's future, as the ice divide lies below the current lake level.

In addition to calving retreat, Yakutat Glacier is rapidly thinning, which lowers its surface and therefore exposes the ice to warmer air temperatures causing increased thinning. Even under a constant climate, this positive feedback mechanism would force Yakutat Glacier to quickly retreat and mostly disappear. Simulations of future mass loss were run for two scenarios, keeping the current climate and forcing it with a projected warming

climate. Results showed that over 95% of the glacier ice will have disappeared by 2120 or 2070 under a constant vs projected climate, respectively. For the first few decades, the glacier will be able to maintain its current thinning rate by retreating and thus losing areas of lowest elevation. However, once higher elevations have thinned substantially, the glacier cannot compensate any more to maintain a constant thinning rate and transfers into an unstable run-away situation. To stop this collapse and transform Yakutat Glacier into equilibrium in its current geometry, air temperatures would have to drop by 1.5 K or precipitation would have to increase by more than 50%. An increase in precipitation alone is unlikely to lead to a stable configuration, due to the very small current accumulation area.

Table of Contents

Page

Page

List of Figures

Page

Page

List of Tables

Page

Acknowledgements

First, I would like to thank the Yakutat Glacier crew for giving me the opportunity to work on this fascinating project.

Martin Truffer was in Switzerland on sabbatical when we first met. At the time, he told me about an upcoming project in Southeast Alaska. A few months later, we both left Switzerland on the same flight: I was moving to Fairbanks, while he was returning. Over the next five years, I learned a lot from him. Beyond sharing his interest-in and knowledge-of glaciology, he was always supportive and patient; giving me the space to make mistakes or work remotely. He always had time for me, providing valuable feedback, suggestions and comments.

Roman Motyka was the principle investigator of the Yakutat Glacier project. It was a pleasure to work with him in the field and in Juneau and I greatly appreciate his trust in letting me lead field campaigns on my own. He was always available for discussions and showed endurance when editing my drafts. Chris Larsen gave valuable advice, both, project specific and thesis/student related, which I appreciated.

Regine Hock was the only committee member who was not part of the Yakutat Glacier crew, yet without her, the modeling part of this work would have not been possible. Her door was always open for questions (especially about mass balance) and I thank her for the valuable comments she provided.

I want to thank a number of people who assisted with field work: Andy Aschwanden, Pat Dryer, Marijke Habermann, Sam Herreid, John Hulth, Austin Johnson, Joe Kennedy, Christian Kienholz, Bob McNabb, David Podrasky, Joanna Young and Lee Zirnheld.

The GI has been a great place to work, so I thank you all for making it to what it is. A special thanks to Jason Amundson, Anthony Arendt, Andy Aschwanden, Tim Bartholomaus, Mark Fahnestock, Ronni Grapenthin, Marijke Habermann, Will Harrison, Sam Herreid, David Podrasky, Anupma Prakash and Joanna Young for their help in various problems. Also thanks to Ed Waddington and the glacier group at the University of Washington to provide a desk for the time I spent in Seattle.

One of the most amazing experiences I had in Fairbanks was being involved in launching *Girls on Ice Alaska* with Marijke Habermann und Joanna Young, with the support of Erin Pettit. Truly, this has been the most rewarding program I have ever been involved in.

My time in Fairbanks would have not been so wonderful without my numerous friends, thank you all. Thanks to Sharon and Lars to let me become a Belfairian. Thanks to Clau-

dine Hauri, Rebecca Hewitt and Lila Tauzer for your support and unforgettable adventures.

Thank you to my family, who have always been supportive and understanding. And finally, a big thank you to Celso Reyes for his endless support and encouragement, especially when things weren't bright and for sharing the "sunny" days.

Again, I feel very fortunate to have had the chance to work on such a fascinating project.

Chapter 1
Introduction

1.1 Background

Glaciers around the globe are undergoing notable retreat and thinning, which is attributed to a changing climate. Particularly, tidewater glaciers have recently received much attention because of their rapid mass loss, which is often attributed to dynamic instabilities. They have been identified as an important contributor to global sea level rise (IPCC, 2007). However, much less is known about calving dynamics in a lake calving (lacustrine) system.

Lacustrine glaciers have only recently been documented to increasingly contribute to sea level rise (Arendt and others, 2002; Larsen and others, 2007), which is mostly due to increased thinning rates, but is also due to undersampling. Larsen and others (2007) showed that highest thinning rates in Southeast Alaska can be found on lake calving glaciers. This could indicate that lacustrine calving processes have an effect on glacier wide surface mass balance and glacier dynamics. At the same time, rapid thinning and retreat could favor the formation of lakes and it remains unclear if lakes are the source or the result of increased thinning rates. However, calving mechanisms in lacustrine systems cannot be neglected, despite calving rates of an order of magnitude smaller than what has been observed on tidewater glaciers (Funk and Röthlisberger, 1989; Warren and Aniya, 1999).

Thinning and terminus retreat are sensitive to climate conditions. As land-terminating glaciers retreat into overdeepened channels formed by glacier erosion (Warren and Aniya, 1999), they can form proglacial lakes and transform into lake calving systems. This transformation modifies glacier dynamics by increasing calving and ice flow, which is then responsible for accelerated thinning and retreat. Hence, once a land-terminating glacier changes into a lacustrine system, it will experience increased mass loss. The number of such shifts in terminus dynamics is growing around the globe as retreat rates increase. This phenomenon is also prominent around the margins of the Greenland Ice Sheet. There, marginal lakes introduce another component to the mass balance of the ice sheet and could significantly increase the contribution to sea level rise. Unfortunately, few data are available to assess the importance of lacustrine glacier dynamics.

In Southeast Alaska, rapid retreat and thinning rates are attributed to climate warming. However, while the link between mass loss due to calving dynamics and a changing climate is complicated, they can be partly decoupled (Larsen and others, 2007). Calving

retreat may cause the glacier surface slope to steepen, which then increases ice flow and extensional thinning. Higher rates of ice flow cause increased crevassing and allow further retreat (e.g. Pfeffer, 2007). This positive feedback loop is not directly coupled to climate and may vary between lake calving and tidewater systems.

Aquatic environments differ greatly between tidewater and lacustrine glaciers. There are three main differences: 1. Lake calving glaciers are not exposed to tidal forcing, but experience seasonal variations in lake level instead. 2. Circulation driven by density difference between warmer saline water and colder subglacial fresh water discharge (Motyka and others, 2003) is only found in tidewater systems. 3. Ocean currents can very effectively transport warm water to the calving front and remove cold glacial discharge, whereas lake calving glaciers are typically part of a closed system without heat exchange with the open ocean.

1.2 General study area

Yakuktat Glacier is located in the northern Gulf of Alaska between Glacier Bay to the south and Icy Bay to the north, surrounded by the coastal Brabazon Range with peaks up to 1500 m a.s.l. Farther inland, peaks of the St. Elias Mountains exceed elevations of 5000 m, a result of a tectonically active area. The Yakutat micro-plate is moving towards the northwest with a block motion of 45 mm yr^{-1} relative to the Southern Alaska block (Elliott and others, 2010). Additionally, the area experiences uplift rates of 32 mm yr^{-1}, which exceeds rapid uplifting of Glacier Bay (30 mm yr^{-1}, Larsen and others, 2005). This region was exposed to large changes in ice volume during late Holocene, which is responsible for isostatic rebound. However, about 40% of the uplift rate in the Yakutat Icefiled area is elastic and can be associated with current ice loss.

The area surrounding Yakutat Glacier hosts a large number of glaciers, including some of the largest temperate land-terminating glaciers in the world, such as Malaspina, a gigantic piedmont glacier. But also active tidewater glaciers are found in the vicinity of Yakutat Glacier, one of them is 115 km long Hubbard Glacier, which is currently advancing. Further, there is a high concentration of surge-type glaciers in the area, including Variegated Glacier and Turner Glacier, the latter is the only surge-type tidewater glacier in Alaska. Most of the glaciers in this region are thinning and retreating and are therefore contributing to global sea level rise (Berthier and others, 2010).

1.3 Objective

The objective of this project was to gain a better understanding of lake calving systems and their contribution to sea level rise. Between May 2009 and September 2011, we collected data on Yakutat Glacier in Southeast Alaska. During that time it became obvious that this glacier maintained a floating ice tongue, which finally started to disintegrate in 2010. Thus, in order to put current dynamic processes into context we studied the glacier's history of rapid retreat and thinning. Next, I described the processes involved in the ongoing large-scale disintegration of the floating tongue, before finally applying a model to predict a range of possible future behaviors.

Chapter 2, which was published in the *Journal of Glaciology*, investigates the past of Yakutat Glacier by looking at rapid retreat and thinning. It addresses the following questions

1. How do lacustrine glaciers behave differently than land-terminating glaciers in terms of retreat and thinning rates?

2. How is mass loss of a lake calving glacier partitioned in terms of surface mass balance versus calving flux?

3. How did the floating tongue form?

4. Yakutat Glacier is a low elevation glacier with a very small accumulation area. How can the presence of the glacier be understood in the context of the glacial history of the area?

As the lead author on this paper, I was involved in data collection, processed, analyzed and visualized data and wrote-up the results. R. Motyka provided guidance with data collection, analysis and edited the manuscript. M. Truffer provided guidance with data processing, analysis and also edited the manuscript. C. Larsen provided guidance with data collection and analysis.

Chapter 3 is planned to be submitted to the *Journal of Glaciology*. It focuses on the present of Yakutat Glacier, looking at the recent and ongoing break-up of the floating tongue by addressing the following questions:

1. What triggered the break-up of the floating tongue?

2. How do rifts evolve and lead to calving?

3. How does the calving style evolve during and after the disintegration of the floating tongue?

As the lead author on this paper, I was involved in data collection, processed, analyzed and visualized data and wrote-up the results. M. Truffer provided guidance with data collection and processing, analysis and edited the manuscript. R. Motyka provided guidance with data collection, analysis and edited the manuscript. C. Larsen provided guidance with data collection and analysis and edited the manuscript.

Chapter 4 will also be submitted to the *Journal of Glaciology*. It predicts the future of Yakutat Glacier by modeling thinning and calving retreat. These future projections address the following questions:

1. How fast does Yakutat Glacier retreat and thin under constant climate conditions versus under projected warming conditions?

2. How much do surface lowering feedbacks contribute to the overall wastage of the glacier?

3. What temperature and precipitation changes would be required to transfer Yakutat Glacier into steady-state and maintain current shape?

As the lead author on this paper, I designed and executed the modeling task, analyzed, visualized and wrote-up the results. M. Truffer provided guidance with modeling, analysis and edited the manuscript. R. Hock provided guidance with her melt model, analysis and edited the manuscripts. R. Motyka edited the manuscript.

Finally, Chapter 5 summarizes the key findings of this thesis and attempts to answer the questions above.

References

Arendt, A., K. A. Echelmeyer, W. D. Harrison, C. S. Lingle and V. Valentine, 2002. Rapid wastage of Alaska glaciers and their contribution to rising sea level, *Science*, **297**(5580), 382–386.

Berthier, E., E. Schiefer, G. K. C. Clarke, B. Menounos and Frédérique Rémy, 2010. Contribution of Alaskan glaciers to sea-level rise derived from satellite imagery, *Nature Geoscience*, **3**(2), 92–95.

Elliott, J. L., C. F. Larsen, J. T. Freymueller and R. J. Motyka, 2010. Tectonic block motion and glacial isostatic adjustment in southeast Alaska and adjacent Canada constrained by GPS measurements, *Journal of Geophysical Research*, **115**(B9), B09407.

Funk, M. and H. Röthlisberger, 1989. Forecasting the Effects of a Planned Reservoir which will Partially Flood the Tongue of Unteraargletscher in Switzerland, *Annals of Glaciology*, **13**, 76–81.

IPCC, 2007. Climate Change 2007: The Physical Science Basis. Contribution of Working Group I to the Fourth Assessment Report of the Intergovernmental Panel on Climate Change.

Larsen, C. F., R. J. Motyka, A. Arendt, K. A. Echelmeyer and Paul E. Geissler, 2007. Glacier changes in southeast Alaska and northwest British Columbia and contribution to sea level rise, *Journal of Geophysical Research*, **112**(F1), 1–11.

Larsen, C. F., R. J. Motyka, Jeffrey T. Freymueller, K. A. Echelmeyer and Erik R. Ivins, 2005. Rapid viscoelastic uplift in southeast Alaska caused by post-Little Ice Age glacial retreat, *Earth and Planetary Science Letters*, **237**(3-4), 548–560.

Motyka, R. J., Lewis Hunter, K. A. Echelmeyer and C.L. Connor, 2003. Submarine melting at the terminus of a temperate tidewater glacier, LeConte Glacier, Alaska, U.S.A., *Annals of Glaciology*, **36**(1), 57–65.

Pfeffer, W. T., 2007. A simple mechanism for irreversible tidewater glacier retreat, *Journal of Geophysical Research*, **112**(F3), 3.

Warren, C. and Masamu Aniya, 1999. The calving glaciers of southern South America, *Global and Planetary Change*, **22**(1-4), 59–77.

Chapter 2
Rapid thinning of lake calving Yakutat Glacier and the collapse of the Yakutat Icefield, Southeast Alaska[1]

Abstract

Both lake calving Yakutat Glacier (337 km^2) and its parent icefield (810 km^2) are experiencing strong thinning, and under current climate conditions will eventually disappear. Comparison of digital elevation models show that Yakutat Glacier thinned at area-averaged rates of 4.76 $\pm$ 0.06 m w.e. yr^{-1} (2000-2007) and 3.66 $\pm$ 0.03 m w.e. yr^{-1} (2007-2010). Simultaneously, adjacent Yakutat Icefield land-terminating glaciers thinned at lower but still substantial rates (3.79 and 2.94 m w.e. yr^{-1} respectively for the same time periods), indicating lake calving dynamics helps drive increased mass loss. Yakutat Glacier terminates into Harlequin Lake and for over a decade sustained a $\sim$3 km long floating tongue, which started to disintegrate into large tabular icebergs in 2010. Such floating tongues are rarely seen on temperate tidewater glaciers. We hypothesize that this difference is likely due to the lack of submarine melting in the case of lake calving glaciers. Floating tongue ice losses were evaluated in terms of overall mass balance and contribution to sea level rise. The post-Little Ice Age collapse of Yakutat Icefield was driven in part by tidewater calving retreats of adjacent glaciers, the lake calving retreat of Yakutat Glacier, a warming climate, and by the positive feedback mechanisms through surface lowering.

2.1 Introduction

The dynamics of tidewater glaciers have received much attention because the large and rapid mass losses often associated with instability of these glaciers is important for sea level rise (Meier and others, 2007; Pfeffer and others, 2008). However, much less is known about the contributions to sea level rise from lake calving (lacustrine) glacier systems despite the growing number of such systems worldwide. Proglacial lakes commonly form at the termini of glaciers as they retreat through overdeepened channels formed by glacier erosion (Warren and Aniya, 1999). These proglacial lakes can then modify glacier behavior through floatation, increased calving and ice flow, and accelerating terminus retreat (e.g. Funk and Röthlisberger, 1989; Warren and Kirkbride, 2003). The shift in terminus dynam-

[1]Published as Trüssel, Barbara L., Roman J. Motyka, Martin Truffer and Christopher F. Larsen, 2013. Rapid thinning of lake calving Yakutat Glacier and the collapse of the Yakutat Icefield, southeast Alaska, USA, J. Glaciol., 59(213), 149-161

ics can play a significant role in lacustrine situations at many spatial scales ranging from small alpine glaciers terminating in cirque basins to valley lakes (Boyce and others, 2007; Dykes and others, 2010), to large lake calving glaciers such as those in Patagonia (Warren and others, 1995; Warren and Aniya, 1999; Naruse and Skvarca, 2000; Warren and others, 2001), to lakes surrounding the Laurentide Ice Sheet at the end of the Last Glacial Maximum (Cutler and others, 2001). The current melting and retreat of the Greenland Ice Sheet is likely to increase the number of ice-marginal lakes there, introducing another component of dynamic and accelerated ice loss. Data on calving flux, ice flow, and surface mass balance on lake calving glaciers are, with few exceptions, virtually non-existent. Thus it is difficult to assess the relative importance of overall ice loss for lake-terminating glaciers and its relevance to global sea level rise.

Most glaciers along the Gulf of Alaska have been retreating and thinning since achieving their Little Ice Age (LIA) maximums sometime between 1750 and 1900 AD, in some cases quite rapidly. This ice loss has contributed significantly to rising sea level and has been linked to climate warming (Arendt and others, 2002). In fact, a majority of temperate mountain glaciers worldwide are thinning and retreating (IPCC, 2007). Although their volume is a small percentage of the world's total land ice mass, they are important contributors to global sea level rise (Meier and others, 2007; Pfeffer and others, 2008; Radić and Hock, 2011). During the period 1961-2003, Alaskan glaciers were responsible for 7.5% of the recent estimate of sea level rise (Berthier and others, 2010). The relationship between glacier thinning/retreat and climate is complicated for glaciers that lose mass through calving (Post and others, 2011). Calving is an important ice-loss mechanism, and can result in much larger volume loss than would be possible through surface ablation alone (van der Veen, 2002). However, studies have shown that calving rates for lake-terminating glaciers tend to be much lower (by up to an order of magnitude) than for their tidewater calving cousins for equivalent water depths (cf. van der Veen, 2002; Benn and others, 2007 for reviews). Furthermore, near-terminus surface slopes of tidewater glaciers are typically steeper than lake calving termini resulting in near terminus ice speeds differing by an order of magnitude with retreating tidewater glaciers often flowing at speeds of 5 - 10 km yr^{-1} compared to 100 - 1000 m yr^{-1} for lake-terminating glaciers.

The reasons for the major differences in terminus dynamics between tidewater and lake calving glaciers remain unexplained. We can distinguish at least three environmental factors that may be partially responsible for these differences: (1) tidal forcing only affects

tidewater glaciers, (2) a strong density contrast exists between fresh water and sea-water for tidal systems, and (3) glacial lakes tend to be colder and less stratified as lakes are closed basins with no heat exchange with the ocean. These differences result in very different circulation patterns, which can drive heat transport and influence calving rates. Despite these differences, calving losses can play a significant role in glacier mass balance for lake-terminating glaciers. For example calving losses at Glaciar Perito Moreno account for 40% of total ice loss there (Stuefer and others, 2007). At the other extreme, calving losses at Mendenhall Glacier, a small valley glacier near Juneau, account for only 4% of the total ice loss (Motyka and others, 2003b; Boyce and others, 2007). As with tidewater glaciers, retreat of lake-terminating glaciers into deeper water can result in positive feedback: as the terminus approaches and exceeds flotation, ice flow may accelerate causing draw down of upglacier ice and extensional thinning. The terminus eventually breaks up into large tabular blocks as ice weakens and fractures. In Southeast Alaska, Larsen and others (2007) found that calving glaciers accounted for over two thirds of the ice loss and found that lake calving glaciers thinned faster per unit area than tidewater glaciers. Yakutat Glacier (Fig. 2.1a) was identified as having one of the highest rates of ice loss during the period 1948-2000 (Larsen and others, 2007).

In this paper, we investigate the continued ice loss of the Yakutat Ice Field (YIF), focusing on the period between 2000 and 2010. We use three digital elevation models (DEMs), one from NASA Shuttle Radar Topography Mission (SRTM) and two from Système Pour l'Observation de la Terre (SPOT) imagery. LiDAR profiles, flown nearly concurrent with the SPOT image acquisitions, provide a check on SPOT DEM reliability. We partition mass loss due to calving versus surface mass balance in order to determine their relative contributions and to assess the role of glacier dynamics in ice loss. YIF consists of both land-terminating and lake calving glaciers, thus allowing comparison of ice losses from systems experiencing different terminus dynamics, but which are affected by the same climate.

2.1.1 Study area

Yakutat Glacier (337 km^2, Raup and others, 2007) lies on the western (maritime) side of the northern Brabazon Range in Southeast Alaska, 50 km east of the village of Yakutat (Fig. 2.1a), where annual precipitation rates exceed 3800 mm yr^{-1}
(http://paya.arh.noaa.gov/clim.php). The glacier is the main outlet of the 810 km^2 YIF (Raup and others, 2007) and consists of two main tributaries, each about 25 km long, that

flow from ice divides at 700 m elevation. Until 2010, the tributaries joined in Harlequin Lake (elev. 28 m) and terminated in a 5-km-wide lake calving front (Fig. 2.1b). The 1973-82 equilibrium line altitude (ELA) at nearby Variegated Glacier averaged around 1000 m with annual variations of up to 300 m (Eisen and others, 2001). Thus, YIF's highest surface elevation is at or below the current ELA for this region, thereby ensuring continuing glacier thinning.

Yakutat Glacier began retreating after reaching its LIA maximum, which likely occured during the mid 18^{th} century (Barclay and others, 2001). By 1903 AD Harlequin Lake had begun to form as the glacier retreated into an over-deepened basin (Fig. 2.2, International Boundary Commission (IBC) maps, IBC, 1952). Harlequin Lake continued to expand as the glacier retreated another 13 km during the 20^{th} century. The lake area was 69 km^2 in 2010. Yakutat Glacier thinned at an average rate of 2.7 ± 0.3 m w.e. yr^{-1} between 1948 and 2000 (Larsen and others, 2007) with similar rates observed at other YIF glaciers. This rapid ice loss has resulted in solid earth uplift rates from glacier rebound, which are currently among the highest in the world ($\sim$32 mm yr^{-1}, Larsen and others, 2005). IBC maps indicate that East and West Nunatak Glaciers were still connected at the terminus and calved into Nunatak Fjord (Fig. 2.2). These glaciers are now land-terminating and have been for at least half a century.

2.2 Methods

2.2.1 Digital elevation models

We compared three DEMs from years 2000, 2007, and 2010 to evaluate glacier thinning. The first DEM was derived from C band data of the SRTM collected in February 2000, with a spatial resolution of 1 arc sec or about 30 m (Rodríguez and others, 2006). Larsen and others (2007) compared the SRTM DEM to LiDAR profiles flown over Southeast Alaska to obtain an estimate of SRTM vertical uncertainties. Their analysis resulted in an elevation dependent correction to address seasonal differences and radar penetration and also provided an estimated grid point uncertainty of 5 m. We have adopted these results for our comparisons of the YIF SRTM DEM to other DEMs.

The other two DEMs have a spatial resolution of 40 m and were generated from SPOT 5 imagery, acquired on 3 September 2007 and 20 September 2010 (Korona and others, 2009). In order to evaluate and correct any elevation errors we compared SPOT DEMs over YIF to light aircraft laser altimetry acquired under Operation Icebridge (Larsen, 2010) and ear-

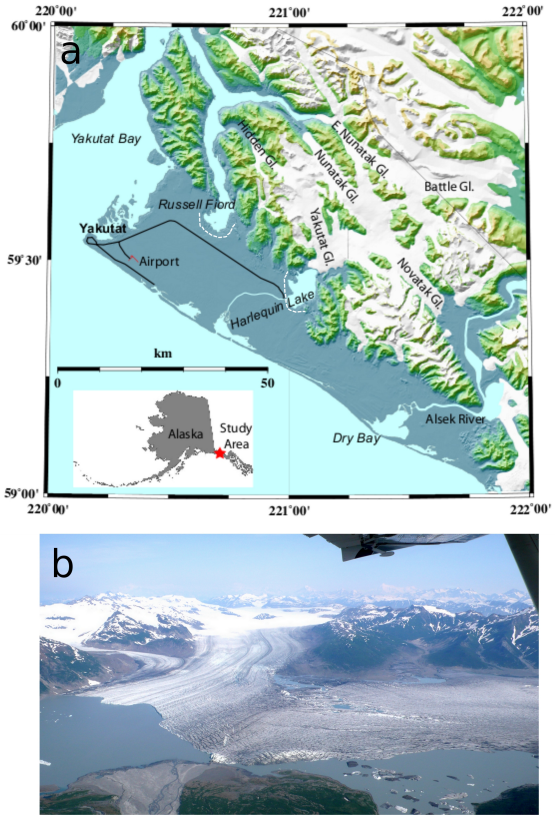

Figure 2.1. a) Yakutat Icefield with Yakutat, Hidden, West Nunatak, East Nunatak, Battle and Novatak Glacier. The Little Ice Age extent at the southern tip of Russell Fjord and for Yakutat Glacier are shown in dashed white. b) Terminus area of Yakutat Glacier 17 July 2009.

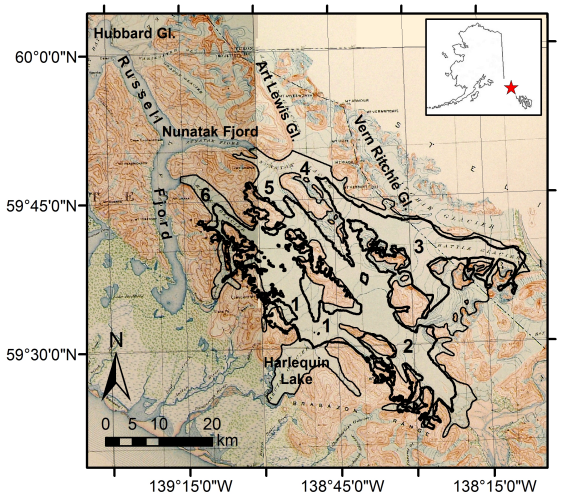

Figure 2.2. International Boundary Commission (IBC) map from 1903 (IBC, 1952) showing YIF with Yakutat Glacier (1), Novatak Glacier (2), Battle Glacier (3), East Nunatak Glacier (4), West Nunatak Glacier (5) and Hidden Glacier (6). Glacier outlines in bold black depict the glacier extent in 2005, based on the GLIMS database. Proglacial Harlequin Lake began forming in 1903, when Nunatak Glacier was still a tidewater glacier (1903 outline in fine black).

lier UAF glacier altimetry. LiDAR data were obtained on 26 August 2007 in profile mode (vertical precision $\pm$ 0.3 m and point-spacing 1.2 m) and on 29 August 2010 in scanning mode (vertical precision $\pm$ 0.3 m and point-spacing 1 m^{-2}), 8 and 22 days before SPOT acquisitions. We corrected for melt between the LiDAR and SPOT acquisition dates. Measurements of summer mass balance for Yakutat Glacier from 2009 and 2010 showed a linear relationship between elevation and melt. A linear function based on these data was then combined with the mean melt recorded by ablation meters (Bøggild and others, 2004) on the floating tongue (0.08 m d^{-1}) to obtain a melting correction for the dates of the 2007 LiDAR and SPOT DEM. We estimate the associated uncertainty at $\pm$ 0.1 m. The same method was used to correct for melting between the 2010 SPOT DEM and LiDAR data, except only August 2010 ablation meter ($\sim$0.08 m d^{-1}) and summer mass balance data were used.

Elevation differences between LiDAR data and the SPOT DEMs were approximately normally distributed with some outliers at either end. Most of these occur in crevassed terminus regions. The others occur over steep bedrock nunataks near the ice divide and probably reflect the difference in grid resolution between the two data sets. We therefore filtered out clear outliers with elevation differences exceeding $\pm$ 10 m, and then corrected

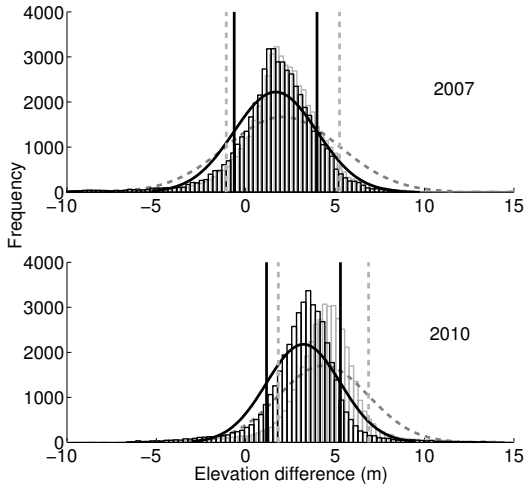

Figure 2.3. Distribution of laser altimetry minus SPOT elevation differences flown over YIF. The raw data (gray) were corrected by excluding elevation differences exceeding ± 10 m and by applying an elevation dependent melt correction function (black). The black curve is a normal fit over the corrected distribution and the dashed gray curve represents a normal fit through raw data. Vertical bars illustrate the area within the standard deviation.

for melt as outlined above. The elevation differences for both uncorrected and corrected data are shown in Figure 2.3. The corrected differences were then used to define a linear elevation dependent vertical bias correction for both years, which were applied to the original SPOT DEMs before differencing.

2.2.2 Digital elevation model differencing

We differenced the DEMs using *Quick Terrain Modeler* (version 7.1.2) to produce an elevation change (ΔZ) DEM with grid spacing of 40 m. The glacier mask for YIF was created using data from GLIMS (Global Land Ice Measurements from Space, (Raup and others, 2007)), Landsat imagery, and USGS Topo maps.

Elevation changes at the glacier margins along steep valley walls can be poorly resolved due to grid spacing and mismatched grid points. Thus, the mask was downscaled by two pixels (pixel size: 40 x 40 m) along the edges to minimize such errors. Outliers in the ΔZ distribution (Fig. 2.3) are from snow covered areas, where the uncertainty of the DEM is large, and from glacier margins. The latter are most likely an artifact of edge proximity that were not caught by downsizing the outline mask. Thus, pixels with ΔZ greater

than +35 m (0.04% of YIF) and less than -105 m (<0.01%) for 2000-2007 and greater than +15 m (0.15%) and less than -45 m (0.01%) for 2007-2010 were eliminated.

We neglected uplift and assumed no changes in elevation of the glacier bed, such as may be caused by erosion and sediment deposition. The uplift rate in YIF area, 32 mm yr^{-1} (Larsen and others, 2005), although large, is negligible compared to the mean $\Delta H/\Delta t$ of the ice field. With the exception of the floating terminus of YIF, ΔZ derived from the differenced DEM can be used directly to calculate ice volume change and thinning rates, $\Delta H/\Delta t$. However, a different strategy must be employed when assessing ice loss for the floating terminus of Yakutat Glacier. We identify four zones: 1) grounded ice, 2) free floating ice, 3) a transition zone between the two, and lastly 4) the area of terminus that retreated between dates of the DEMs (see Appendix). Figure 2.4c and 2.4d show the locations of a series of transects through the differenced DEMs. The change in ΔZ along these transects helps define these different zones (Figs 2.4f and 2.4g). For grounded ice, ΔZ is a direct measure of ice loss. For the floating tongue, buoyancy must be taken into account. Here we assume hydrostatic equilibrium with an ice density of 900 kg m^{-3} and fresh water density of 1000 kg m^{-3} so that ice thinning is given by $\Delta H = 10 \cdot \Delta Z$. Ice in the transition zone was originally grounded, but is now floating. To assess ΔH , we apply a linear trend as a function of distance to evaluate ΔH between the grounding line and the floating tongue.

The fourth zone, the area of the terminus retreat, was identified using SRTM and SPOT images. The area of retreat was assumed to have been in hydrostatic equilibrium, thus surface elevations derived from the DEMs were multiplied by 10 to determine total ice loss. Some regions near lateral margins are likely partially grounded and corrections were thus made for these regions. All four zones changed over time and were determined separately for 2000-2007 and 2007-2010. Details of the treatment of the four zones are provided in section 2.7.

Our geodetic DEM differencing approach assesses the total mass loss of the YIF, including surface mass balance and mass loss due to calving. Retreat of a floating tongue does not lead to mass changes in the local glacier-lake system, and in the transition zone only a portion of the thinning ice leaves the lake-glacier system. To allow comparisons to other results, we evaluate ice loss in two different ways. For example, sensors such as GRACE only measure total mass change, which directly translates to eustatic sea level rise. However, mass balance studies need to account for all ice that is lost, regardless if some of the meltwater remains in the lake. In neither case do the values follow directly from measured

ΔZ.

We now address the question of estimating the uncertainty of determining volume change and geodetic mass balance. The total change in ice volume is determined by differencing the DEMs and summing grid points either over the area of YIF or over individual glaciers. The volume change can in turn be converted to mass (expressed as water equivalent volume, w.e.) if the ice density is known, and further converted to an area-wide specific mass balance by dividing by the area.

When estimating the uncertainty of such calculations, two extreme approaches have commonly been applied (Rolstad and others, 2009). One approach uses the uncertainty of point measurements (i.e., the standard deviation of the elevation error) to represent the integrated uncertainty: the point uncertainty is essentially treated as being totally correlated across the area of integration (Cox and March, 2004; Larsen and others, 2007). At the other extreme, uncertainty of point measurements are treated as random uncorrelated errors (Rignot and others, 2003). In this case, uncorrelated integrated errors will be a factor $n^{1/2}$ smaller than correlated errors, where n is the number of grid points over which the spatial integration is carried out. Following methodology developed by Rolstad and others (2009) and outlined in Motyka and others (2010), we chose an intermediate method of estimating uncertainties, that of using variograms of the differenced DEMs over adjacent land areas to determine an area of correlation, A_c, which is then taken as a measure of error correlation between the two DEMs over the ice.

For comparison of the SPOT DEMs, we found A_c = 0.07 km^2 , which is considerably smaller then the area, A, for both for YIF (810 km^2), and for the individual glaciers. Table 2.1 provides the variance of the mean of the area, $\sigma_{\Delta A}$, and σ_V , the uncertainty in volume change, calculated using relationships discussed in Motyka and others (2010).

Assessing similar uncertainties for the SRTM vs. 2007 SPOT DEMs is more problematic as we are unable to derive suitable variograms due to the seasonal difference. In the most pessimistic case we assume that the elevation difference uncertainty of 5.5 m is correlated across the entire area. The corresponding uncertainty in volume change for YIF is then 4.5 km^3 compared to 0.25 km^3 for an assumed correlation length of 150 m (Table 2.1).

Additional uncertainties accrue from our treatment of the floating tongue. These uncertainties are discussed in the Appendix: they increase the uncertainty in volume change of Yakutat Glacier by 0.01 km^3 but do not influence the remainder of the YIF. Uncertainties due to changes in ice and firn density are considered negligible here, since almost all of the

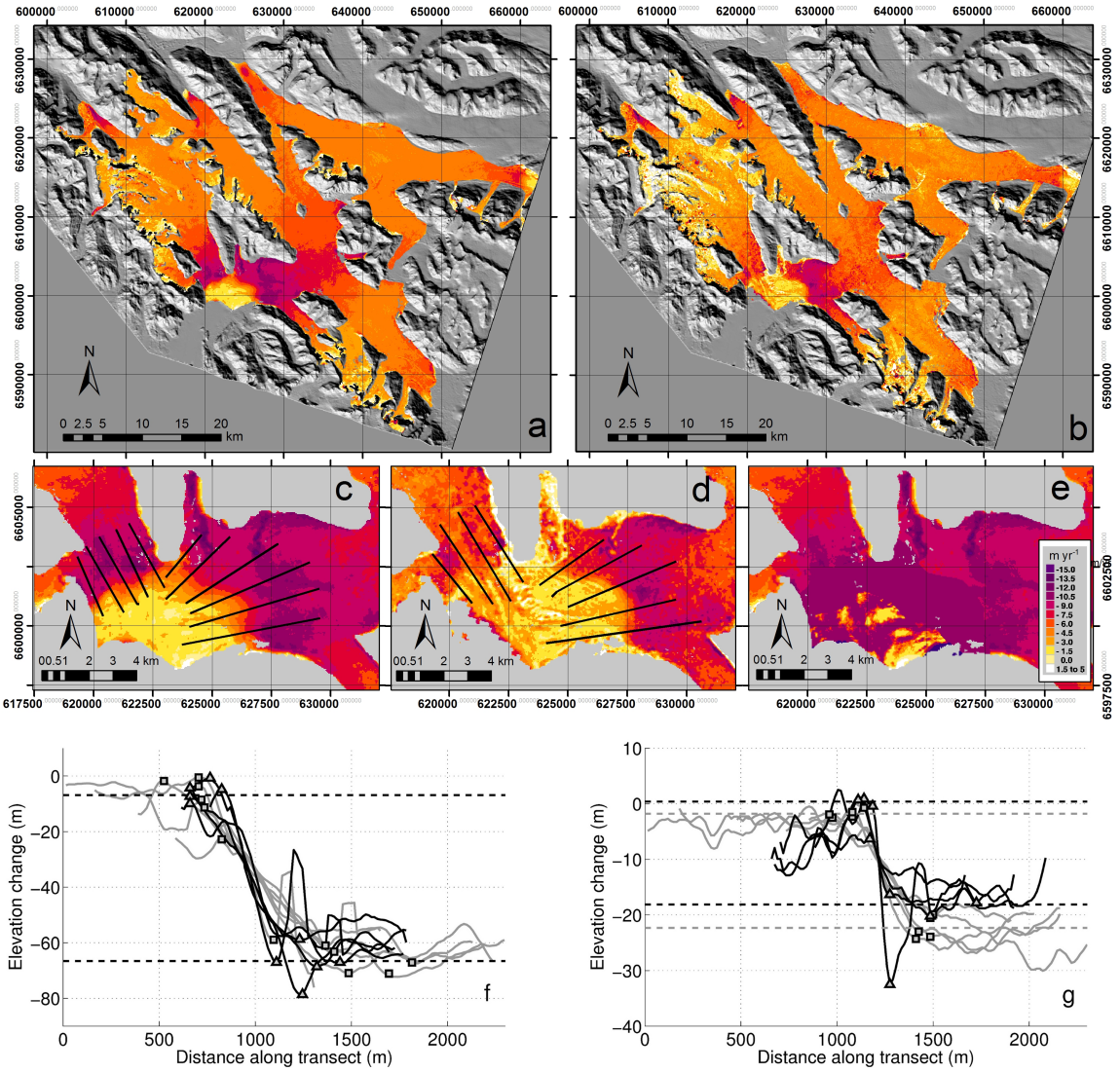

Figure 2.4. Glacier surface elevation change rates ($\Delta Z/\Delta t$ in m yr^{-1}) of Yakutat Icefield before correcting for the floating tongue a) 2000 - 2007 and b) 2007-2010. c) and d) show elevation changes ΔZ and locations of transects for 2000 - 2007 and 2007 - 2010, respectively. e) depicts the corrected ice thickness change ΔH (2000-2007). f) and g) illustrate the transects of the terminus area (c) and d) for location) used to define a transition zone between the grounded ice (right side of each panel defined by large ΔZ) and the floating tongue (left side). Black transects were derived from the western part of the terminus and gray from the eastern part. Points mark the change from one zone to another (squares for the western, triangles for the eastern part). Dashed lines represent the mean ΔZ for the floating (upper) line and grounding (lower) line, based on the hand-picked points.

YIF glacier area is below the snow line.

2.2.3 Calving flux

Calving flux Q_c (m^3 yr^{-1}) is the difference between ice flux arriving at the calving front and the volume change at the terminus (advance/retreat):

$$Q_c = Q_{in} - \frac{dV}{dt} \tag{2.1}$$

where Q_{in} is the ice flux and rate of retreat is $\frac{dV}{dt}$ (O'Neel and others, 2003).

Terminus retreat

We used Landsat 7 satellite imagery (http://glovis.usgs.gov/) panchromatic band (spatial resolution: 15 m) taken on 2 September 2000 and the georeferenced SPOT images for 2007 and 2010 to determine the amount of retreat of Yakutat Glacier. To obtain volume change, we subtracted the lake level elevation from the retreated part of the 2000 DEM for the first time period and 2007 DEM for the second period. The resulting elevation of the ice surface above lake level was multiplied by 10 to obtain the ice thickness assuming hydrostatic equilibrium.

Ice flux

The depth averaged velocity on the floating tongue is essentially equal to the surface velocity, due to the lack of basal drag. However, the velocity is not uniform along the terminus. We obtained a surface velocity field over the terminus area by feature tracking (Scambos and others, 1992) using Landsat 7 imagery (2 September 2000 and 21 September 2001, 16 August 2002 and 10 August 2003, 15 October 2004 and 2 October 2005, 8 October 2007 and 24 September 2008) and orthomosaics based on vertical aerial photography flown on 17 July 2009 and 25 August 2010. These velocities were binned into 150 m sections across the 5 km wide terminus for Landsat images and 80 m sections for the orthomosaics. The velocities varied from year to year due to grounding effects of the floating terminus advancing onto the south shore of Harlequin Lake. We used a mean velocity, v_i, over 2 km length of the floating tongue to represent each bin of width w_i. The ice flux was then determined from

$$Q_{in} = \sum v_i \cdot w_i \cdot h_i \tag{2.2}$$

where h_i is the mean ice thickness of each bin, determined from a cross section (fluxgate) of the SRTM DEM and a DEM generated from 2009 orthophotos (unpublished data by the authors, DEM covers terminus area of Yakutat Glacier). We determined the range of scatter in each bin to assess a mean uncertainty of 5.6 m yr^{-1} for the first period and 12.6 m yr^{-1} for the second.

2.2.4 Longterm retreat

We estimated longterm thinning of YIF by comparing center line contour crossing elevations from 1903 International Boundary Commission (IBC) maps (cf. Fig. 2.2) to the 2010 SPOT DEM. Based on comparisons of land features to USGS Topo maps, the uncertainty for the IBC map elevations is ∼40 m (half contour interval). For reconstruction of the terminus retreat during the 20^{th} century, we used terminus outlines derived from IBC maps (1903), an air photo by B. Washburn (1934), NED DEM (1948), air photos by Austin Post (1960-1978) and Landsat imagery (1973-2010). The outlines were digitized and georeferenced by hand using the software *ENVI* (ver 4.4). We calculated retreat by determining the area defined by a 1400 m wide bar intersecting with terminus positions to ensure a representative retreat rate.

2.3 Results

2.3.1 DEM differencing

DEM differencing revealed that the entire YIF experienced strong thinning for both periods. Thinning rates ranged from 3.0 m yr^{-1} / 2.0 m yr^{-1} at the ice divides and increased down-glacier to ∼10.5 m yr^{-1} near the terminus of Yakutat Glacier (Figs 2.4a and 2.4b). The total ice volume loss and mean mass balance between 2000 and 2007 / 2007 and 2010 for YIF and for the individual glaciers comprising YIF are summarized in Table 2.1, together with error estimates. Table 2.2 presents results specific to Yakutat Glacier. We report results from DEM differencing with and without corrections for the floating terminus. Ice losses in the region of the floating tongue were evaluated as described in sections 2.2 and 2.7: one for mass balance calculations and the other for SLR comparison (Table 2.2). Figure 2.4e shows the differenced DEM (2000-2007) of terminus area of Yakutat Glacier with its floating tongue and after corrections have been applied.

Lake calving Yakutat Glacier experienced the highest area-averaged mass balance of

Table 2.1. Area and volume changes for glaciers comprising YIF with lake calving Yakutat and Battle Glacier and the remaining land-terminating glaciers. The three different lines for Yakutat Glacier reflect values for uncorrected, corrected for the floating tongue in terms of ice loss (MB) and mass loss of the glacier-lake system (SLR). ΔV is the volume change. $\sigma_{\Delta A}$ describes the area elevation uncertainty, σ_V the volume change uncertainty (1 for a correlated uncertainty and 2 for an assumed correlation length of 150 m). $\overline{MB}$ is the mean mass balance. The accumulation-area ratio (AAR) was derived from the 2007 SPOT DEM.

2000-2007	Area (km^2)	ΔV (km^3)	$\sigma_{\Delta A}$ (m)	σ_V 1 (km^3)	σ_V 2 (km^3)	$\overline{MB}$ (m w.e. yr^{-1})	σ_{MB}
Yakutat	337.12	-11.16	0.48	0.16	1.85	-4.25	0.06
Yakutat (MB)	337.12	-12.48	0.48	0.16	1.85	-4.76	0.06
Yakutat (SLR)	337.12	-11.07	0.48	0.16	1.85	-4.22	0.06
East Nunatak	66.43	-1.82	1.08	0.07	0.37	-3.52	0.14
West Nunatak	81.85	-1.86	0.97	0.08	0.45	-2.93	0.13
Novatak	116.08	-2.63	0.82	0.10	0.64	-2.91	0.11
Hidden	58.96	-1.27	1.15	0.07	0.32	-2.77	0.15
Battle	149.06	-3.79	0.72	0.11	0.82	-3.27	0.09
Total (YIF)	809.51	-22.53	0.31	0.25	4.45	-3.58	0.04
YIF corrected (MB)	809.51	-23.85	0.31	0.25	4.45	-3.79	0.04
YIF corrected (SLR)	809.51	-22.44	0.31	0.25	4.45	-3.56	0.04

2007-2010	Area (km^2)	ΔV (km^3)	$\sigma_{\Delta A}$ (m)	σ_V (km^3)	$\overline{MB}$ (m w.e. yr^{-1})	σ_{MB}	AAR (ELA:1000m)
Yakutat	337.12	-3.31	0.36	0.12	-2.95	0.05	0.03
Yakutat (MB)	337.12	-4.11	0.36	0.13	-3.66	0.05	0.03
Yakutat (SLR)	337.12	-3.22	0.36	0.12	-2.87	0.05	0.03
East Nunatak	66.43	-0.71	0.81	0.05	-3.24	0.10	0.02
West Nunatak	81.85	-0.62	0.73	0.06	-2.28	0.09	0.07
Novatak	116.08	-0.85	0.61	0.07	-2.26	0.08	0.06
Hidden	58.96	-0.31	0.86	0.05	-1.62	0.11	0.13
Battle	149.06	-1.32	0.54	0.08	-2.66	0.07	0.02
Total (YIF)	809.51	-7.12	0.23	0.19	-2.64	0.03	0.04
YIF corrected (MB)	809.51	-7.92	0.23	0.19	-2.94	0.03	0.04
YIF corrected (SLR)	809.51	-7.03	0.23	0.19	-2.61	0.03	0.04

Table 2.2. Volume change for the different zones of the Yakutat Glacier as resulting from DEM differencing. MB denotes mass balance calculations and SLR contribution to sea level rise.

	Surface Area (km^2)		Volume change (km^3)	
	2000 - 2007	2007 - 2010	2000 - 2007	2007 - 2010
Differenced DEM	337.12	329.37	-11.16	-3.31
Adjusted differenced DEM (MB)	338.90	328.23	-12.48	-4.11
Adjusted differenced DEM (SLR)	327.47	307.35	-10.07	-3.22
Grounded	311.12	295.24	-10.05	-3.04
Transition	16.35	12.11	-1.14	-0.24
Transition (GRACE)	16.35	12.11	-0.85	-0.17
Floating	9.38	17.21	-0.43	-0.32
Retreated	2.05	3.67	-0.41	-0.51

YIF: -4.76 $\pm$ 0.06 m w.e. yr^{-1} and -3.66 $\pm$ 0.05 m w.e. yr^{-1} for 2000-2007 and 2007-2010, respectively (Figs 2.4a and 2.4b, Table 2.1). In contrast, land-terminating glaciers experienced typically about 1 m w.e. yr^{-1} less mass loss than Yakutat Glacier.

2.3.2 Calving flux

Terminus retreat

The west branch of Yakutat Glacier lost 2.1 km^2 between 2000 and 2007: with a mean calving front width of 4.2 km (4.1 km in 2000 and 4.2 km in 2007), the mean linear retreat rate was 49 m yr^{-1}; and with a total ice volume loss of 0.41 $\pm$ 0.16 km^3 the rate of retreat ($\frac{dV}{dt}$) was 0.06 $\pm$ 0.02 km^3 yr^{-1} for 2000-2007.

Several large tabular icebergs calved from the floating tongue between 2007 and 2010, resulting in a net retreat of 3.67 km^2 and a 5.6 km wide calving front in 2010. The calving was episodic, but the mean linear retreat rate was 273 m yr^{-1}. The total ice volume lost by retreat between 2007 and 2010 was 0.51 $\pm$ 0.04 km^3 resulting in a rate of retreat ($\frac{dV}{dt}$) of 0.17 $\pm$ 0.01 km^3 yr^{-1} for 2007-2010.

Ice flux

The velocity field in the terminus region determined from feature tracking is shown in Figure 2.5a. The binned velocities were averaged for the two time periods (Figs 2.5b and 2.5c). Ice velocities were greatest on the west branch, where the maxima for each time period varied between 139.2 ± 5.6 m yr^{-1} and 150.6 ± 12.6 m yr^{-1} and decreased towards the confluence between the east and west branch. Some velocities varied between years by as much as 88.9 m yr^{-1} between 2007/2008 and 2009/2010. We attribute this change to a local advance onto land at the south end (Fig. 2.5a). A generally stagnant east branch creates a shear zone at the confluence.

The mean ice thickness h_i for each bin, determined from 2000 and 2009 DEMs, was multiplied by the bin's velocity v_i and width w_i. For the first period, Q_{in} was 0.55 km^3 or 0.08 km^3 yr^{-1} over a fluxgate length of 4.95 km. For the second period, mean velocities could only be determined for the first 2.8 km of the fluxgate, for the following 2.2 km, velocities from 2007-2008 were used, resulting in Q_{in} of 0.22 km^3 or 0.06 km^3 yr^{-1}. Combining ice flux and terminus retreat following equation (1) results in a calving flux of 0.14 km^3 yr^{-1} for the first period and 0.23 km^3 yr^{-1} for the second period. Comparing calving flux to total volume loss of Yakutat Glacier shows that for the first period (2000-2007), only about 7.9 % of the total loss is due to calving, whereas for the second period calving accounts for about 16.8 %.

2.3.3 Longterm retreat

To complement and provide perspective to the recent volume losses we also examined longterm trends in thinning and glacier retreat by comparing the center line elevation of the 1903 IBC maps to the 2010 SPOT DEM (Fig. 2.6a), and by plotting terminus positions derived from a variety of resources (Figs 2.6b and 2.6c).

Although glacier contours on the 1903 IBC maps have large uncertainties ($\pm$ 40 m), they do provide some quantification of total ice loss that has occurred over the last century. For example, the ice surface dropped by $\sim$ 400 m during the last century in the region of the 2010 terminus. The maps also suggest that the divides at Yakutat Glacier were about 100 m and 200 m higher on the west and east branches respectively, than they are today.

The outlines of glaciers comprising YIF in 1903 (from IBC maps) vs. 2005 (GLIMS) illustrate the degree of retreat that has transpired during the last century (Fig. 2.2). East

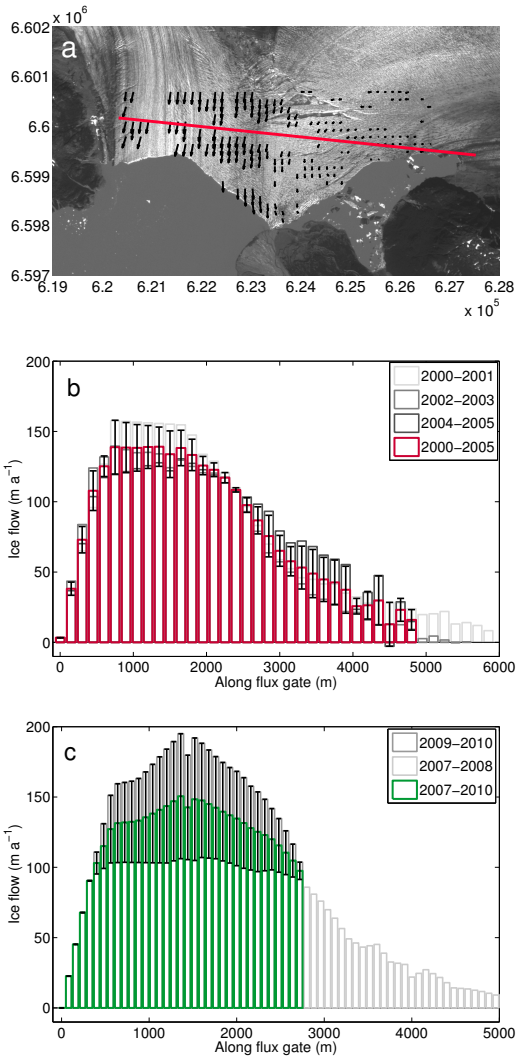

Figure 2.5. Feature tracking from Landsat 7 imagery. a) Spatial distribution and direction of pixel displacements over 349 days (2007-2008). The flux gate is indicated by the red line. b) displacements from four feature tracking datasets through the flux gate in 150 m bins for 2000-2007 and c) in 80 m bins for 2007-2010. Error bars (black) are estimated from the mean displacement scatter over all datasets.

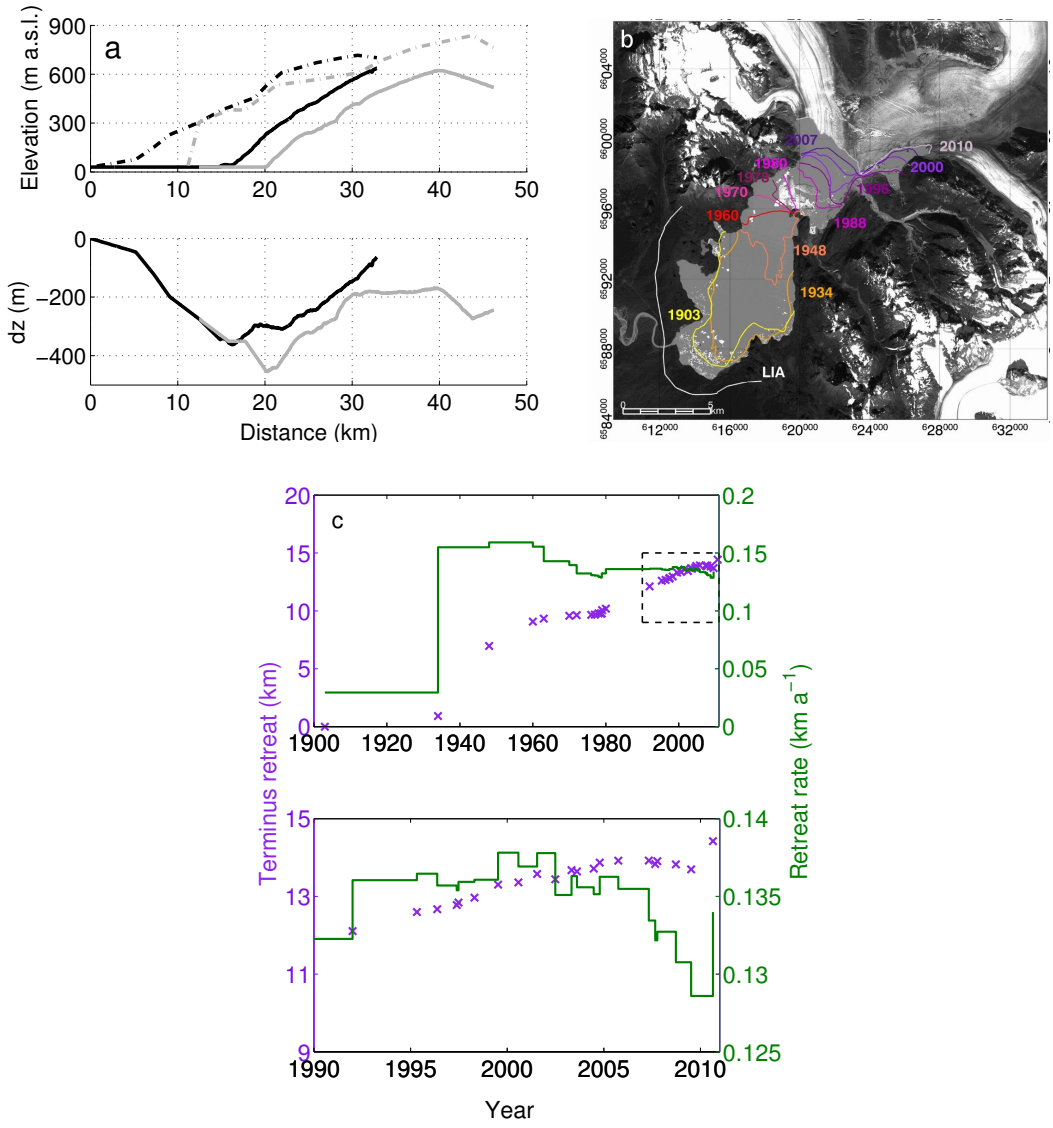

Figure 2.6. Evolution of terminus retreat between 1903 and 2010. a) Elevation of the center line of Yakutat Glacier in 1903 (solid) and 2010 (dashed) for both branches, west branch in black and east branch in gray. Elevation difference (1903 - 2010) of the west branch (black) and east branch (gray) in the lower panel. b) Selected terminus positions overlaying the 2010 SPOT image. c) Terminus retreat in relation to the terminus position in 1903 (purple) and retreat rates (purple). Detailed data in dashed black box are shown in the lower panel.

and West Nunatak were connected as one tidewater glacier in 1903. By 2005, the glacier branches had separated and had retreated 13 km and 10.5 km respectively. Both now terminate on land. Hidden Glacier underwent a retreat of about 7.1 km and Novatak Glacier experienced about 3.1 km terminus retreat between 1903 and 2005, whereas Battle Glacier does not appear to have retreated during this time period. Yakutat Glacier retreated about 14 km, albeit at highly variable rates.

2.4 Discussion

2.4.1 Recent ice losses and comparison to other studies

Yakutat Ice Field experienced a total volume loss of 31.77 $\pm$ 0.31 km^3 between 2000 and 2010, for an average of 3.18 $\pm$ 0.03 km^3 yr^{-1} (Table 2.1). This includes a correction for the elevation change of the floating tongue, which amounts to 5.9% of the total for the first period (2000-07) and 11.2% for the second period (2007-10). Corrections for mass loss calculations of the glacier-lake system are small. For geodetic mass balance calculations (in m w.e. yr^{-1}) we use mass balance, which includes all ice losses (Table 2.2). Previous studies did not include this correction. We report our results for mass balance both with and without the floating tongue contribution. Larsen and others (2007) differenced DEMs from the 1948/62 National Elevation Dataset (NED) and the 2000 SRTM and obtained an average mass balance of -2.7 m w.e. yr^{-1} over this time span. Similar results (-2.5 m w.e. yr^{-1}) were reported by Berthier and others (2010) for DEMs from NED and 2007 SPOT. However, they did not apply the seasonal difference correction as done here from the comparison with 2007 LiDAR data. Doing so would change their mass balance results by about -0.03 m w.e. yr^{-1}. Arendt and others (2008) used laser altimetry data from 2005 and 2007 and reported a mass balance of -2.77 $\pm$ 0.66 m w.e. yr^{-1}, a value similar to the other previous studies.

Our results indicate ice loss significantly accelerated during the first decade of the 21st century for both Yakutat Glacier and for YIF when compared to Larsen and others (2007) and Berthier and others (2010). The reasons for this increase in ice thinning include 1) a positive feedback mechanism, known as the Bodvardsson effect (Bodvardsson, 1955), where thinning lowers the surface elevation and exposes the ice to higher temperatures at lower elevations, causing accelerated ice loss, and 2) climate change. The town of Yakutat has seen a temperature increase of 1.3 °C and annual precipitation increase of 1528 mm during the period 1948-2000 (Larsen and others, 2007). During the last decade (2000-2010),

mean annual temperatures were 0.4 °C higher, following the general trend of the 20^{th} century. Increased temperature elevates the equilibrium line altitude (ELA) and decreases the accumulation area ratio (AAR), resulting in increased ice loss. The study by Arendt and others (2008) covers the time period 2005-2007, part of our study period. They compared NASA's ATM data (2005) with University of Alaska laser altimetry data (2007) and found an area-averaged mass balance for Yakutat Glacier of -2.78 $\pm$ 0.66 m w.e. yr^{-1}, 34% lower than what we found for the period 2000 - 2007, which may reflect inner-annual variations. Additionally, this difference may result from different sources. While laser altimetry data collected along a glacier center flow line may not be representative for an entire glacier (Berthier and others, 2010), this is not likely to be an issue in the case of YIF as the glaciers show uniform surface lowering within elevation bands. However, monthly temperatures from the town of Yakutat reveal a 0.6 °C lower mean annual temperature during the laser altimetry time period (September 2005 to August 2007) compared to 2000-07. Summer temperatures were comparable, but winter temperatures were lower. Precipitation did not show any trends, but the lower temperatures may have led to higher amounts of solid precipitation. Third, the Arendt and others (2008) study did not include losses from the floating tongue. Our results (Table 2.2) indicate that this could account for an additional -0.5 m w.e. yr^{-1}.

Luthcke and others (2008) found 11.6 $\pm$ 0.7 Gt yr^{-1} of the mass loss from GRACE data (mascon region 10) for 2003-2007. Mascon 10 includes YIF as well as large glacier systems such as Malaspina Glacier and large parts of Glacier Bay. Our results indicate that 25% or 2.89 $\pm$ 0.03 Gt yr^{-1} of the mass loss of this GRACE mascon came from YIF.

The results of the five studies are summarized in Figure 2.7. We show corrected as well as uncorrected results for comparison. When we compared equal methods, we did not include adjustments for the floating tongue. Our results show significantly higher volume change rates than all previous studies.

2.4.2 Partitioning of volume loss

Yakutat Glacier loses mass by both surface ablation and calving. Surface ablation is directly influenced by climate. However, dynamic adjustments of the glacier surface can also lead to changing surface mass balance, even under a constant climate. To illustrate this effect, the mean thickness change between 2000 and 2010 was -39 m. A mass balance gradient of 0.0046 yr^{-1} (estimated from unpublished mass balance data by the authors) results in

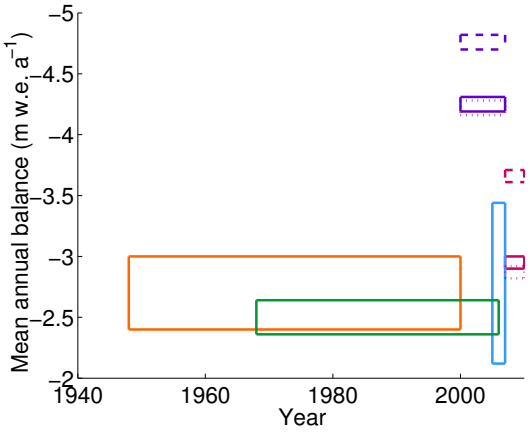

Figure 2.7. Area averaged mass balance for Yakutat Glacier for different years by various authors. The height of the box delineates the uncertainty of the value. Results from our study are depicted by a solid purple box (2000-2007) and by solid red box (2007-2010) for DEM differences uncorrected for the floating tongue. Dashed boxes include corrections for the floating tongue in terms of ice loss (MB) and dotted boxes are corrected with respect of mass loss of the glacier-lake system (SLR). Earlier DEM differencing studies are shown in orange (Larsen and others, 2007, 1948-2000) and in green (Berthier and others, 2010, 1954-2007). The data from a laser altimetry study by (Arendt and others, 2008, 2005-2007) are shown in blue.

a decrease in the surface mass balance of 0.18 m yr^{-1}, due solely to this change in surface elevation. In contrast, ice loss from calving results from dynamic effects and is only indirectly linked to climate. At Yakutat Glacier, large calving events have been episodic in nature, with large tabular sections of the floating tongue periodically breaking away, interspersed with long periods (on the order of months to years) of relative quiescence. The terminus can then steadily advance until the next calving episode. Although tidewater glaciers experience similar patterns of calving retreat followed by slow advance, this periodicity occurs over much shorter time periods, usually days or weeks (O'Neel and others, 2003; Amundson and others, 2008).

The long-term episodic nature of lake calving leads to a ratio of surface mass balance vs. calving flux that fluctuates significantly with time. In our study, for the periods 2000 - 2007 and 2007 - 2010, calving accounted for 7.9% and 16.8% of the total mass loss respectively.

2.4.3 Comparison of Yakutat Icefield glaciers

Currently, two out of six glaciers of the YIF are exposed to calving dynamics, Yakutat Glacier (42% of the icefield) and Battle Glacier (18%). Yakutat Glacier has been a lacustrine glacier for at least one century (see Fig. 2.2, 1903) with the largest retreat of the YIF, whereas Battle Glacier has only recently become a lake calving glacier with almost no terminus retreat since 1903. The highest thinning rates (2000-2010) are found on lake calving Yakutat Glacier. Battle Glacier and land-terminating East Nunatak have the third and second largest thinning rates, respectively (Table 2.1). The remaining land-terminating glaciers generally are thinning at lower but still significant rates. Yakutat, East Nunatak and West Nunatak Glaciers have experienced terminus retreats exceeding 10 km since 1903. We note that they have all been exposed to calving during all or part of the last century.

2.4.4 Evolution and collapse of the icefield

Yakutat Glacier began retreating from its LIA maximum sometime during the 19th century but the rate of retreat has accelerated since 1903 (Fig. 2.6). Total retreat between 1903 and 2010 was 15 km. Retreat rates have not been constant, possibly due to changing climate conditions, the episodic nature of calving at Yakutat Glacier, and lake geometry. Bathymetry (unp. data by authors) shows a relatively shallow sill (150m) across the lake at the narrowest part of the lake, compared to depths of 325 m at the 2010 terminus. The

pinning of the narrows and shallower water may have inhibited calving thereby help stabilize the terminus during the period 1960 - 1980. This sill now entraps the large tabular icebergs that have recently calved from Yakutat Glacier from floating further down lake (Fig. 2.6b).

The ice divide on the east branch of Yakutat Glacier is currently (2010) lower in elevation than on the west branch. In 1903, it was opposite, with the ice divide on the east branch at a higher elevation (Fig. 2.6a). The lowering of the east branch divide may be connected to tidewater glacier dynamics, since the ice divide is shared with West Nunatak Glacier. While it was a tidewater glacier, Nunatak Glacier could draw down ice faster, thus causing the ice divide on the east branch to thin more rapidly than the one on the west branch.

Our results clearly show that the entire YIF is in rapid decline. With little or no accumulation zones (AAR mostly < 0.05), these glaciers are destined to continue their decline into the foreseeable future. Even if the current climate trends are reversed, it would take a substantial change in the regional ELA before these glaciers could begin growing again. We now address the question of how the YIF formed in the first place, and what then led to its collapse, by drawing on published glacial geology (e.g. Barclay and others, 2001), considerations of terrain, and the IBC maps of 1903.

A "typical" alpine glacier with a mass balance of zero will have an accumulation area ratio (AAR) value between 0.5 and 0.7 (Chapt. 3, Paterson, 1994) with coastal Alaska favoring the latter value (Meier and Post, 1962). YIF itself does not have a high elevation accumulation area. Thus, the original LIA YIF must have either been fed from nearby regions and/or been subject to a much colder climate or both. Events leading to the post-LIA collapse of YIF must have preceded the first mapping of the region, because by 1903, the ice divides had already dropped to near the current ELA threshold (Fig. 2.6a), so that the AAR was probably well below that needed to sustain the glaciers. We suggest that YIF is now a remnant icefield. Such remnants exist nearby in Glacier Bay (i.e. Burroughs Glacier) and also in Russell Fjord (Orange Glacier).

During the early 17^{th} century, the east lobe of Hubbard Glacier (a major tidewater glacier to the northwest of Russell Fjord, Figure 2.2) was at its maximum extent and spilled into the south end of Russell Fjord (Barclay and others, 2001). During the same period, Nunatak and Hidden Glaciers advanced into Russell Fjord, where they were then dammed by the east lobe of Hubbard Glacier. By the late 18^{th} century glacier ice had filled the en-

tire southern part of Russell Fjord with a terminus lobe advancing onto land beyond the south end of the fjord. Abetted by the generally cooler LIA climate, these circumstances could have led to the growth of the YIF: ice from the Nunatak and Hidden Glaciers would have backed up because of the Hubbard dam, thereby increasing the height of the YIF ice divides and glacier elevations overall. Ice spilling over to the southeast could have fed the other branches of the YIF. By the end of the 18^{th} century, the main and east lobes of Hubbard Glacier had retreated, and Nunatak Glacier became the primary source of ice into Russell Fjord. The retreat of Hubbard Glacier caused the ice flow direction to reverse in the northwest arm of Russell Fjord. Ice started to retreat from the south end of Russell Fjord in late 18^{th} century (Barclay and others, 2001). Nunutak and probably Hidden Glaciers were tidewater glaciers at this time and a calving retreat likely ensued with the waning of LIA climate conditions. Historically, in the early 1900s, East- and West Nunatak Glaciers were still connected as one tidewater glacier calving into Nunatak Fjord (Tarr and Martin, 1914). However, rapid retreat eventually separated the two arms, with both retreating onto land. The changing climate and the retreat of Nunatak and Hidden Glacier eventually led to the collapse and current condition of the YIF. Such a scenario is not without precedent: Glacier Bay is a prime example where LIA advance and expansion of the main trunk glaciers led to the formation of large peripheral glaciers and ice fields, which then subsequently collapsed once the main trunk glacier retreated (Larsen and others, 2007).

Other potential sources of ice for the growth of the YIF during the LIA are the Art Lewis and Vern Ritchie Glaciers, which lie north of YIF (Fig. 2.2). Both of these glaciers have high elevation accumulation areas and their growth during the LIA may have been sufficient to allow ice to spill over and feed the Nunatak and Battle Glaciers (Fig. 2.2). Given the high precipitation rates in this region, the climate during the LIA may have been sufficiently colder to allow YIF to grow. However, since the current ELA is essentially at or above the current ice divides, the difference would have to have been considerable if this was the only operative process. We also point out that growing ice fields are subject to a positive feedback effect, which would allow it to continue to grow, perhaps rapidly. This instability is similar, but reversed in sign, to what is currently happening.

2.4.5 Tidewater vs. lacustrine glacier

Tidewater glaciers experience calving rates up to order-of-magnitude greater than lake calving glaciers, ice speeds are more than an order of magnitude faster, and near-terminus

surface slopes are steeper. In the following we propose a hypothesis to explain these differences.

We initially assume a temperate glacier in an over-deepened basin near its maximum extent in steady state, with the terminus exposed to calving. If the glacier experiences sufficient thinning, portions of the terminus area can become ungrounded. If the ungrounding allows a cavity to form, a tidewater system will likely react differently than a lacustrine system (Fig. 2.8). In a tidewater situation, a submarine cavity would rapidly be exposed to large basal melt rates, as water circulation driven by subglacial freshwater discharge would transport warm ocean water to the base of the ice. Measurements in Alaska (Motyka and others, 2003a) and in Greenland (Motyka and others, 2011) show that such melt rates can be well in excess of 1 $\mathrm{m\,d^{-1}}$. Thinning due to subglacial melt then decreases the stability of the terminus and ice calves back to the grounding line. Indeed, floating termini are rarely observed in temperate tidewater glaciers, and, when present, appear to be a temporary and unstable feature (Walter and others, 2010). This rapid retreat then steepens the near-terminus surface slope leading to increased extensional ice flow. Faster ice flow causes increased crevassing, which in turn helps drive calving rates (Benn and others, 2007). The glacier thus experiences high calving rates, high flow rates with large extensional gradients, and heavy crevassing. Higher velocities at tidewater glaciers are also facilitated by the denser water at their termini, which leads to lower effective pressures for a given ice thickness (van der Veen, 2002).

In the case of a lacustrine glacier, cavities formed by ungrounding can exist for an extended period of time. The subglacial discharge is not buoyant compared to the lake water, since the temperature and density differences are small. The lake water temperature in Harlequin Lake varies between 0.5 to 1.5 °C, which appears to be typical of other proglacial lakes (Boyce and others, 2007). These lower temperatures are a result of the lake being a closed system with icebergs in it. Thus, water circulation and heat exchange are generally minimal. Therefore, steep surface slopes do not develop and a positive feed-back mechanism between retreat, surface slope, extensional thinning and crevasses is not established. The part of the glacier that is decoupled from its bed appears to be stable for an extended period of time. Indeed floating termini are commonly observed in temperate lake calving glaciers. Lacustrine glaciers can form floating tongues that are stable for months to years or longer, whereas tidewater glaciers in the same climate are unable to maintain a floating terminus, which can lead to steeply sloped terminus areas and attendant high ice fluxes.

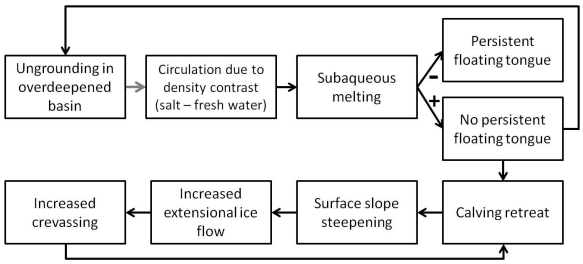

Figure 2.8. Positive feedback mechanisms when a glacier retreats into an over-deepened basin. As the glacier becomes ungrounded due to thinning, the density contrast between warm ocean water and fresh, cold subglacial runoff creates buoyancy driven circulation in a tidewater system that results in submarine melting. This link (gray arrow) is broken in a lacustrine glacier system, because the freshwater density contrast will likely not be strong enough to trigger circulation, and water temperatures are too cold to cause subaqutic melting.

Eventually, continued thinning of a lake calving terminus and lake-level rise can lead to episodic calving of large tabular icebergs. But these events may occur as infrequently as once a year. In tidewater systems, calving occurs much more frequently, often on a daily to weekly basis, abetted by tidal flexure as well as extensional thinning and crevassing.

2.5 Conclusions

The Yakutat Ice Field (YIF) has experienced dramatic thinning: 3.52 ± 0.05 m w.e. yr^{-1} between 2000 and 2010. With an accumulation area ratio of 0.04 (in 2007), the majority of YIF is well-below the equilibrium line altitude (ELA), exposing most of the glacier area to negative surface balance. The entire ice field experiences thinning and the resulting lowering of the ice surface leads to increasingly negative surface balances, even under a constant climate. We thus expect YIF to continue thinning and retreating and predict the eventual disappearance of most of the ice field, even without additional warming.

The evolution of the YIF and transformation into a remnant ice field appears to have been fostered by a combination of factors, including a colder LIA climate, thickening of the Nunatak and Hidden Glaciers and other YIF glaciers as a result of Hubbard Glacier damming Russell Fjord, and spillover of glacier ice from the Art Lewis and Vern Ritchie glaciers. The post-LIA collapse was driven by the tidewater calving retreats of Nunatak and Hidden glaciers, the lake calving retreat of Yakutat Glacier, a warming climate, and by the Bodvardsson feedback mechanism.

Both land-terminating and lake calving glaciers comprise YIF, with the lake calving Yakutat Glacier being the largest glacier, covering 42% of YIF. Yakutat Glacier was able to build and maintain a 17.2 km^2 floating tongue for over a decade. Corrections have to be applied to convert floating tongue elevation changes to thinning rates. Ignoring this effect leads to an underestimate of ice loss and an overestimate of mass loss of the glacier-lake system. Yakutat Glacier has been exposed to calving retreat for more than a century. Calving rates are highly variable with periods of rapid retreat followed by periods of relative stability. The most recent period of rapid retreat began in 2010, when the floating tongue disintegrated into large tabular ice bergs, a process that is common on other lake calving systems (Boyce and others, 2007). The contribution of calving to total mass loss increased from 7.9% (2000-2007) to 16.8% (2007-2010). Yakutat Glacier currently experiences larger mass loss than the land-terminating glaciers of the YIF. This points to the importance of mass loss through calving, not only into the ocean, but also into proglacial lakes. The latter is potentially important for mass balance studies of the Greenland Ice Sheet, where lakes are common, especially along its western perimeter.

Tidewater glaciers in the vicinity of YIF are exposed to a similar climate, but they neither form nor maintain a stable floating tongue nor calve large tabular icebergs, even when retreating into over-deepened basins. We hypothesize that the different calving behavior is caused by a the presence or absence of submarine melt as the glacier retreats into an over-deepening. In the case of a tidewater glacier, submarine melt can be large leading to instability and retreat. In a lacustrine system, subaquatic melt is negligible, allowing floating tongues to form.

2.6 Acknowledgements

A. Post provided terminus outlines based on his air photos. E. Berthier provided mass balance data specifically extracted to our area. M. Fahnestock provided code for the image correlation analyiss. We thank A. Aschwanden, W. Dryer, M. Habermann, S. Herreid, J. Hulth, A. Johnson, J. Kennedy, C. Kienholz, R. McNabb, D. Podrasky, J. Young and L. Zirnheld for assistance with fieldwork. CH2MHill Polar Services provided logistics support, Bill Lucey and Tim Ross supported the work in Yakutat, and Temsco Helicopters and Alsek Air provided aircharter services. The SPOT-5 images used for DEM differencing was provided by the SPIRIT program (CNES). Funding was provided by NSF-OPP (grant ARC 0806463). We thank R. Naruse, an anonymous reviewer and the scientific editor, T.

Scambos, for thorough reviews that helped to focus the manuscript.

2.7 Appendix

For most of the icefield, elevation change (ΔZ) data from the differenced DEM can be used directly to calculate ice volume change and a mean thinning rate ($\Delta H/\Delta t$). However, the terminus of Yakutat Glacier is floating and thus has to be treated separately. We identified four zones: 1) the grounded ice, 2) the free floating ice, 3) the transition zone in between and 4) the retreated zone. To differentiate between these zones, we derived profiles along several transects from the grounded ice to the floating tongue from the differenced DEMs (Figs 2.4c and 2.4d). The largest ΔZ were found in the area of the grounding line followed by a steep increase (more negative to less negative) in a transition zone. The boundary between the transition zone and the free floating part was determined by picking points on each transect by hand (Figs 2.4f and 2.4g). The mean ΔZ of points describing the grounding line was -66.6 m for the first period (2000-2007), and -18.1 m (west branch) and -23.0 m (east branch) for the second period (2007-2010, separated by / from here on). For the border between the transition zone and the free floating part we found a mean ΔZ of -6.9 m / 0.4 m / -1.8 m. Once separated, ΔZ in each zone were weighted differently. In the first zone, the grounded ice, ΔZ directly reflect ΔH, and no further corrections were needed.

The transition zone was handled slightly differently for the two time periods. For period one we applied a linear trend from the grounding line starting with a ΔZ of -66.6 m to the free floating line with a ΔZ of -6.9 m, which was weighted ten times to account for buoyancy of ice in freshwater (measured ΔZ of -6.9 m translate to ΔH values of -69 m). For period two the elevation change at the free floating line was sufficiently different for the two branches to justify defining two separate transition zones, one for the faster flowing west branch and one for east branch. Measured ΔZ at the upstream end of the free floating part were 0.4 m and -1.8 m (Figs 2.4f and 2.4g). These would be interpreted as a thickness changes of +4.0 m and -18.0 m, respectively for east and west branch, and lead to unrealistic thickness change gradients from the grounding line to the free floating part more than 2 km farther downstream. Recognizing the subjectivity in picking these values from transect profiles and the large potential errors due to the hydrostatic compensation, we chose a thickness change value at the free floating part of -21.0 m, which corresponds to the mean of the grounding line values of both branches.

The third zone, the floating tongue, was assumed to be in hydrostatic equilibrium with

an ice density of 900 kg m^{-3} and fresh water density of 1000 kg m^{-3}. Only a tenth of the actual ΔH was accounted for in ΔZ data due to buoyancy. Hence, the value of >-6.9 m for the first period was corrected to -69 m for hydrostatic equilibrium. For the second period we estimated a value of -21 m, as explained above. Smaller values were truncated to -69 m and -21 m respectively to prevent overestimation. Similarly, values greater than zero were set to zero, assuming no thickening in the ablation area.

The fourth zone, the area of the terminus retreat, was identified on Landsat images. The retreated area was then cut out on the earlier DEM and the elevation above lake level was multiplied by 10 to obtain the actual ice thickness of the retreated part. Some values near the lateral margin indicated an ice thickness of over 300 m, which is likely due to a failure of the free-floating assumption. These values were corrected. All four zones changed over time and were determined separately for 2000-2007 and 2007-2010.

Correcting for a floating tongue introduces an additional source of uncertainty. For the second time period (SPOT 2007 to 2010), about 2.2% of the entire surface area of YIF was part of the floating zone. For this area, the uncertainty described in Section 2.2.2 is increased by an order of magnitude, due to the multiplication by 10 to derive ΔH from ΔZ data. The 2000 SRTM DEM was obtained in winter with a frozen, and thus measurable lake level, resulting in negligible uncertainties. For the second period, we assumed a lake level of 28 m a.s.l. based on our lake level measurements using GPS and pressure sensor records for the summer seasons 2009-11. A 1 m error in lake level translates to a volume change of about 0.033 km^3 (or $\pm$ 6.4% of the retreated volume). For the transition zone (1.5%) we estimated a factor 5 increased error, compared to grounded ice. Equivalent corrections apply for the first time period (2000-2007) for the floating zone covering a surface area of 1.2% and a 2.0% transition zone. The adjustments for the retreated part entail further errors. For the first period, eliminating unrealistic values around the edges resulted in a volume decrease of 0.165 km^3 or 0.7% of the total volume change, and a volume increase of 0.003 km^3 for the second period. Volume loss of the retreated part is also affected by uncertainties in lake level. Combining the uncertainties of the retreated part (2007-2010) results in a total volume uncertainty of 0.035 km^3 or 0.4% of the total volume loss of YIF. These additional uncertainties increase the volume uncertainty of Yakutat Glacier from 0.12 km^3 to 0.13 km^3, but do not influence the volume uncertainty of YIF.

References

Amundson, J. M., M. Truffer, M. P. Lüthi, M. Fahnestock, M. West and R. J. Motyka, 2008. Glacier, fjord, and seismic response to recent large calving events, Jakobshavn Isbræ, Greenland, *Geophysical Research Letters*, **35**(22), L22501.

Arendt, A., K. A. Echelmeyer, W. D. Harrison, C. S. Lingle and V. Valentine, 2002. Rapid wastage of Alaska glaciers and their contribution to rising sea level, *Science*, **297**(5580), 382–386.

Arendt, A., S.B. Luthcke, C. F. Larsen, W. Abdalati, W. B. Krabill and M. J. Beedle, 2008. Validation of high-resolution GRACE mascon estimates of glacier mass changes in the St Elias Mountains, Alaska, USA, using aircraft laser altimetry, *Journal of Glaciology*, **54**(188), 778–787.

Barclay, D. J., P. E. Calkin and G. C. Wiles, 2001. Holocene history of Hubbard Glacier in Yakutat Bay and Russell Fiord, southern Alaska, *Geological Society of America Bulletin*, **113**(3), 388–402.

Benn, D. I., R. H. Mottram and S. G. Warren, 2007. Calving processes and the dynamics of calving glaciers, *Earth-Science Reviews*, **82**(3-4), 143–179.

Berthier, E., E. Schiefer, G. K. C. Clarke, B. Menounos and F. Rémy, 2010. Contribution of Alaskan glaciers to sea-level rise derived from satellite imagery, *Nature Geoscience*, **3**(2), 92–95.

Bodvardsson, G., 1955. On the flow of ice-sheets and glaciers, *Jokull*, **5**.

Bøggild, C. E., O. B. Olesen, A. P. Ahlstrøm and P. Jørgensen, 2004. Automatic glacier ablation measurements using pressure transducers, *Journal of Glaciology*, **50**(169), 303–304.

Boyce, E. S., R. J. Motyka and M. Truffer, 2007. Flotation and retreat of a lake-calving terminus, Mendenhall Glacier, southeast Alaska, USA, *Journal of Glaciology*, **53**(181), 211–224.

Cox, L. H. and R. S. March, 2004. Comparison of geodetic and glaciological mass-balance techniques, Gulkana Glacier, Alaska, U.S.A., *Journal of Glaciology*, **50**(170), 363–370.

Cutler, P. M., D. M. Mickelson, P. M. Colgan, D. R. MacAyeal and B. R. Parizek, 2001. Influence of the Great Lakes on the dynamics of the southern Laurentide ice sheet : Numerical experiments, *Geology*, **29**(11), 1039–1042.

Dykes, R. C., M. S. Brook and S. Winkler, 2010. The contemporary retreat of Tasman Glacier, Southern Alps, New Zealand, and the evolution of Tasman proglacial Lake since AD 2000, *Erdkunde*, **2010**(2), 141–154.

Eisen, O., W. D. Harrison and C. F. Raymond, 2001. The surges of Variegated Glacier, Alaska, U.S.A., and their connection to climate and mass balance, *Journal of Glaciology*, **47**(158), 351–358.

Funk, M. and H. Röthlisberger, 1989. Forecasting the effects of a planned reservoir which will partially flood the tongue of Unteraargletscher in Switzerland, *Annals of Glaciology*, **13**, 76–81.

IBC, 1952. International Boundary Commission. International boundary between United States and Canada from Cape Muzon to Mount St. Elias, scale 1:250,000, 13 sheets, Ottawa.

IPCC, 2007. Climate Change 2007: The Physical Science Basis. Contribution of Working Group I to the Fourth Assessment Report of the Intergovernmental Panel on Climate Change.

Korona, J., E. Berthier, M. Bernard, F. Rémy and E. Thouvenot, 2009. SPIRIT. SPOT 5 stereoscopic survey of Polar Ice: Reference Images and Topographies during the fourth International Polar Year (2007–2009), *ISPRS Journal of Photogrammetry and Remote Sensing*, **64**(2), 204–212.

Larsen, C.F., 2010. IceBridge UAF Lidar Profiler L1B Geolocated Surface Elevation Triplets, [29 August 2010], *Boulder, Colorado USA: NASA Distributed Active Archive Center at the National Snow and Ice Data Center*, **Digital media**, http://nsidc.org/data/ilakp1b.html.

Larsen, C. F., R. J. Motyka, A. Arendt, K. A. Echelmeyer and P.E. Geissler, 2007. Glacier changes in southeast Alaska and northwest British Columbia and contribution to sea level rise, *Journal of Geophysical Research*, **112**(F1), 1–11.

Larsen, C. F., R. J. Motyka, J. T. Freymueller, K.A. Echelmeyer and E.R. Ivins, 2005. Rapid viscoelastic uplift in southeast Alaska caused by post-Little Ice Age glacial retreat, *Earth and Planetary Science Letters*, **237**(3-4), 548–560.

Luthcke, S. B., A. Arendt, D. D. Rowlands, J. J. McCarthy and C. F. Larsen, 2008. Recent glacier mass changes in the Gulf of Alaska region from GRACE mascon solutions, *Journal of Glaciology*, **54**(188), 767–777.

Meier, M. F., M. B. Dyurgerov, U. K. Rick, S. O'Neel, R. S. Anderson, W. T. Pfeffer, S. P. Anderson and A. F. Glazovsky, 2007. Glaciers dominate eustatic sea-level rise in the 21st century., *Science*, **317**(5841), 1064–7.

Meier, M. F. and A. Post, 1962. Recent variations in mass net budgets of glaciers in western North America: Variations of the Regime of Existing Glaciers, *International Association of Scientific Hydrology*, **58**, 63–77.

Motyka, R.J., M. Fahnestock and M. Truffer, 2010. Volume change of Jakobshavn Isbræ, West Greenland:: 1985–1997–2007, *Journal of Glaciology*, **56**(198), 635–646.

Motyka, R. J., L. Hunter, K. A. Echelmeyer and C. L. Connor, 2003a. Submarine melting at the terminus of a temperate tidewater glacier, LeConte Glacier, Alaska, U.S.A., *Annals of Glaciology*, **36**(1), 57–65.

Motyka, R. J., S. O'Neel, C. L. Connor and K. A. Echelmeyer, 2003b. Twentieth century thinning of Mendenhall Glacier, Alaska, and its relationship to climate, lake calving, and glacier run-off, *Global and Planetary Change*, **35**(1-2), 93–112.

Motyka, R. J., M. Truffer, M. Fahnestock, J. Mortensen, S. Rysgaard and I. M. Howat, 2011. Submarine melting of the 1985 Jakobshavn Isbræ floating tongue and the triggering of the current retreat, *Journal of Geophysical Research*, **116**(F1), 1–17.

Naruse, R. and P. Skvarca, 2000. Dynamic features of thinning and retreating Glaciar Upsala, a lacustrine calving glacier in Southern Patagonia, *Arctic, Antarctic, and Alpine Research*, **32**(4), 485–491.

O'Neel, S., K. A. Echelmeyer and R. J. Motyka, 2003. Short-term variations in calving of a tidewater glacier: LeConte Glacier, Alaska, U.S.A., *Journal of Glaciology*, **49**(167), 587–598.

Paterson, W. S. B., 1994. The Physics of Glaciers, Pergamon, Oxford, 3 ed., 36.

Pfeffer, W. T., J. T. Harper and S. O'Neel, 2008. Kinematic constraints on glacier contributions to 21st-century sea-level rise, *Science*, **321**(5894), 1340–3.

Post, A., S. O'Neel, R. J. Motyka and G. Streveler, 2011. A complex relationship between calving glaciers and climate, *Eos, Transactions American Geophysical Union*, **92**(37), 305.

Radić, V. and R. Hock, 2011. Regionally differentiated contribution of mountain glaciers and ice caps to future sea-level rise, *Nature Geoscience*, **4**(2), 91–94.

Raup, B., A. Kääb, J. S. Kargel, M. P. Bishop, G. Hamilton, E. Lee, F. Paul, F. Rau, D. Soltesz, S Khalsa and M. Beedle, 2007. Remote sensing and GIS technology in the Global Land Ice Measurements from Space (GLIMS) Project, *Computers & Geosciences*, **33**(1), 104–125.

Rignot, E., A. Rivera and G. Casassa, 2003. Contribution of the Patagonia Icefields of South America to sea level rise, *Science*, **302**, 434–437.

Rodríguez, E., C. S. Morris and J. E. Belz, 2006. A Global Assessment of the SRTM Performance, *Photogrammetric Engineering & Remote Sensing*, **72**(3), 249–260.

Rolstad, C., T. Haug and B. Denby, 2009. Spatially integrated geodetic glacier mass balance and its uncertainty based on geostatistical analysis: application to the western Svartisen ice cap, Norway, *Journal of Glaciology*, **55**(192), 666–680.

Scambos, T. A., M. J. Dutkiewicz, J. C. Wilson and R. A. Bindschadler, 1992. Application of image cross-correlation to the measurement of glacier velocity using satellite image data, *Remote Sensing of Environment*, **42**(3), 177–186.

Stuefer, M., H. Rott and P. Skvarca, 2007. Glaciar Perito Moreno, Patagonia: climate sensitivities and glacier characteristics preceding the 2003/04 and 2005/06 damming events, *Journal of Glaciology*, **53**(180), 3–16.

Tarr, R.S. and L. Martin, 1914. Alaskan glacier studies of the National Geographic Society in the Yakutat Bay, Prince William Sound and lower Copper River regions, The National Geographic Society, Washington.

van der Veen, C. J., 2002. Calving glaciers, *Progress in Physical Geography*, **26**(1), 96–122.

Walter, F., S. O'Neel, D. E. McNamara, W. T. Pfeffer, J. N. Bassis and H. A. Fricker, 2010. Iceberg calving during transition from grounded to floating ice: Columbia Glacier, Alaska, *Geophysical Research Letters*, **37**(15), 1–5.

Warren, C. and M. Aniya, 1999. The calving glaciers of southern South America, *Global and Planetary Change*, **22**(1-4), 59–77.

Warren, C., D. I. Benn, V. Winchester and S. Harrison, 2001. Buoyancy-driven lacustrine calving, Glaciar Nef, Chilean Patagonia, *Journal of Glaciology*, **47**(156), 135–146.

Warren, C. and M. P. Kirkbride, 2003. Calving speed and climatic sensitivity of New Zealand lake-calving glaciers, *Annals of Glaciology*, **36**(1), 173–178.

Warren, C. R., D. R. Greene and N. F. Glasser, 1995. Glaciar Upsala, Patagonia: rapid calving retreat in fresh water, *Annals of Glaciology*, **21**, 311–316.

Chapter 3

The break-up of a lacustrine floating ice tongue, Yakutat Glacier, Alaska[1]

Abstract

Yakutat Glacier in Southeast Alaska maintained a 2 km long floating tongue for over a decade. In early 2010, several rifts opened and intersected, allowing large tabular icebergs to calve. This initiated the break-up of the floating tongue. To investigate the mechanisms that led to this rapid disintegration, we first determine processes, which increase the vulnerability of floating ice and then identify sources of rapid rift opening. In contrast to near-by tidewater glaciers, sub-aqueous melt plays a minor role in thinning and weakening of the floating tongue. However, thinning is the main source of destabilization of the tongue, but could mostly be attributed to surface mass balance. Once the tongue was sufficiently weakened, rift opening rates increased and varied temporally. Larger rates occurred during and after precipitation periods or increased air temperatures. Both of these climatological occurrences increased subglacial discharge and may cause lake level in rifts to rise. Thus we hypothesize that increased rift opening is primarily caused by increased water input into the system.

3.1 Introduction

Glaciers around the world are thinning and experiencing terminus retreat, influenced by a changing climate (Molnia, 2007b). When land-terminating glaciers retreat into an overdeepened basin, a pro-glacial lake can form at the terminus, exposing it to lacustrine calving. With the onset of calving, ice speeds at the terminus can change from essentially zero to potentially the largest anywhere on the glacier. Increased ice flux from higher elevations causes increased dynamic thinning, which then lowers the glacier surface, exposing it to higher temperatures. That, in turn, causes additional melt and retreat. Increases in surface melting can also increase basal sliding through a reduction in effective basal stresses (Pfeffer, 2007), effectively transporting more ice to the calving front. Such positive feedback loops can cause accelerated ice loss and can potentially trigger a run-away process of ice loss. We have observed such feedback loops at lake calving Yakutat Glacier in Southeast Alaska, which has some of the highest thinning rates in Southeast Alaska (Larsen and

[1]Will be submitted to the Journal of Glaciology as: Barbara L. Trüssel, Martin Truffer, Roman J. Motyka and Christopher F. Larsen. The break-up of a lacustrine floating ice tongue, Yakutat Glacier, Alaska.

others, 2007; Trüssel and others, 2013). Worldwide, the number of lake calving glaciers is increasing, causing increased mass loss and increased rates of retreat.

Lake calving and tidewater glaciers both lose ice by calving. However, near-terminus velocities are commonly about an order of magnitude lower in a lacustrine system than at tidewater glaciers (Boyce and others, 2007; Trüssel and others, 2013). Three main differences between the two systems may cause lower terminus velocities at lake calving glaciers. First, lacustrine systems are not exposed to tidal forcing, but instead, are experiencing typically slower and smaller seasonal variations in lake level. Second, a lacustrine system is not exposed to circulation driven by density difference between salt water and subglacial fresh water discharge, as seen in tidewater systems (Motyka and others, 2003). Third, ocean currents can effectively transport warm water to the calving front and exchange cold glacial discharge, whereas lakes are typically a closed system without heat exchange with the open ocean. Trüssel and others (2013) hypothesized that these differences allow floating tongues to form on temperate lake calving glaciers, while the ungrounded tongue of a temperate tidewater glacier is exposed to increased basal melt rates due to density driven circulations. This leads to rapid thinning and calving. Indeed, temperate tidewater glaciers only rarely form floating tongues, which are of relatively small spatial extent and disintegrate rapidly (Walter and others, 2010).

Yakutat Glacier was able to maintain a floating tongue for over a decade (2000-2010). During our study of mass loss at Yakutat Glacier (Trüssel and others, 2013), we also documented the disintegration of this floating tongue by rifting and calving of kilometer-scale tabular icebergs starting in 2010. The style of rifting and calving of large tabular icebergs is more reminiscent of the calving mechanism at cold ice shelves in Antarctica than to neighboring temperate tidewater glaciers. However, there are some differences between lacustrines system and cold ice shelves. First, cold ice has different mechanical ice properties than temperate ice. Second, an ice shelf typically experiences melting close to the grounding line, where temperatures lie above the melting pressure point. The less saline, thus more buoyant water will follow the underside of the shelf as it flows towards the ice front and will sometimes refreeze (Jacobs and others, 1992). A lacustrine ice tongue is generally smaller and less thick and such melting/refreezing mechanisms are less likely to occur.

During the time of the break-up, the glacier was instrumented with ablation wires, time lapse cameras and several GPS units, one of which survived a calving event and

continued to record data as the iceberg floated away. We also acquired repeat surface elevation LiDAR measurements. We also recorded lake level and temperatures in the proglacial lake.

In this paper, we examine the break-up of the floating tongue at Yakutat Glacier, describe periods associated with its disintegration, and explore mechanisms that caused rifting, tabular calving, and loss of the tongue. This well instrumented disintegration of a lacustrine floating ice tongue has never been captured before in such detail.

3.2 Study area

Yakutat Glacier (337 km^2, Raup and others, 2007) is part of the Yakutat Icefield, which is located on the western (maritime) side of the northern Brabazon Range in Southeast Alaska, 50 km east of the village of Yakutat. With ice divides at about 650 m a.s.l., Yakutat Glacier is a low elevation glacier with an accumulation to total area ratio (AAR) of 0.03. The glacier has two main arms, the east and the west branch, both of which calve into Harlequin Lake. The lake covers an area of 69 km^2 with a length of 15 km (2010) and has water depths of over 325 m close to the glacier terminus. It is part of the low elevation Yakutat Icefield (AAR: 0.04) with ice divides at about 650 m a.s.l. Yakutat Glacier experienced annual thinning of 4.43 m w.e. a^{-1} between 2000 and 2010 and retreated of 14.4 km between 1903 - 2010 (Trüssel and others, 2013). This retreat is one of the largest post-Little Ice Age lacustrine retreats in Alaska.

3.3 Methods

3.3.1 Lake and climate measurements

Lake temperature profiles were acquired using a calibrated SeaBird Electronics SeaCAT 19 'plus' conductivity-temperature-depth (CTD) profiler. CTD casts were performed on 24 May 2011 and 12 Sept 2011 and standard procedures were used to measure temperature and other water column parameters that were depth-averaged into 1 m bins.

A HOBO weather station on bedrock measured air temperatures in 15 min intervals near the terminus of Yakutat Glacier on bedrock (59°29'35.66" N / 138 °49'22.94" W). We used precipitation data from the NOAA station PAYA in the town of Yakutat, 47.7 km northwest of our HOBO weather station (http://climate.gi.alaska.edu), due to failure of the precipitation gauge at the HOBO weather station. We suspect that precipitation at the terminus of Yakutat Glacier is likely higher than at PAYA, because of orographic effects.

However, for the purpose of this work, it is the precipitation patterns that matter, not absolute quantity.

Pro-glacial lake bathymetry was determined using a narrow beam (6°) 1 kW depth sounder to measure water depths. The depth sounder was calibrated in situ against known water depths. The estimated accuracy of raw water depth measurements is ± 1.0 m. The bathymetry data were co-registered and logged with GPS data at 5 s intervals. Post processing against a local base station ensured positional accuracy of ± 1.0 m or better. Raw water depth data were adjusted to the Sept 2011 lake level, which we use as our reference zero elevation for our bathymetric map and all depths are referenced to it.

Lake level was measured hourly with a Global Water WL16 Water Level Logger. The logger was located on the east shore of Harlequin Lake in a protected bay, about 1.5 km distance to the glacier terminus.

3.3.2 Laser altimetry - thinning

Light-aircraft laser altimetry data were acquired on 26 August 2009, 29 August 2010, 11 September 2011, and 15 August 2012 in scanning mode (vertical precision ± 0.25 m and point-spacing 1 m^{-2}) by the University of Alaska under National Aeronautics and Space Administration's (NASA) Operation Ice-Bridge program. Earlier LiDAR data were obtained on 26 August 2007 in profile mode (vertical precision ± 0.3 m and point-spacing 1.2 m). Data were processed as described in Johnson and others (2013). We used the software package *Quick Terrain Modeler (version 7.1.2)* to extract surface elevation data along the same 5 m wide flight line for each year, except for 2007, when the east branch was surveyed along a different flight path (Fig. 3.1).

Thinning rates on the floating tongue were calculated by assuming that the ice was in hydrostatic equilibrium with an ice density of 900 kg m^{-3} and a fresh water density of 1000 kg m^{-3}. Lake level was assumed to be constant for assessing thickness changes on the floating tongue in order to avoid errors associated with isostatic adjustment to a changing lake level. In contrast, surface elevations for the grounded ice were kept at their original elevation (WGS84).

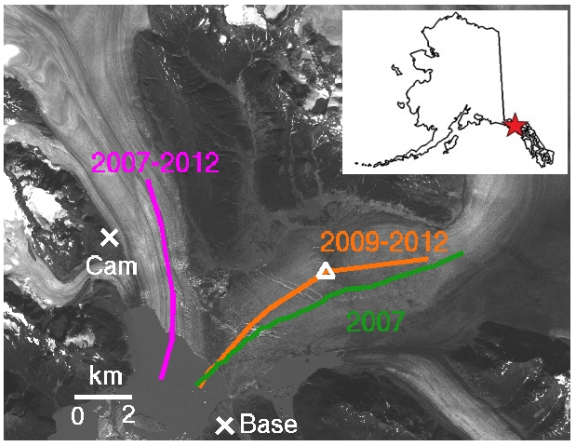

Figure 3.1. Terminus position of Yakutat Glacier (SPOT 2010) and flight lines of the LiDAR missions. The surveyed path on the west branch is shown in magenta, the path for 2009-2012 on the east branch is in orange and the path for 2007 in green. The white triangle on the east branch flight line depicts the grounding line and the white crosses show the location of the camera (Cam) and the GPS base station (Base).

3.3.3 GPS measurements - velocity and strain rate

Continuous GPS observations were conducted at five sites on the west branch of Yakutat Glacier, two sites were on the floating tongue, two sites were on grounded ice and the base station was on bedrock located near the terminus on the southeast end of Harlequin Lake. We used dual-frequency GPS receivers (Trimble 5700 and Trimble NetRS). The antennas of three sites on the glacier were mounted on metal tetrahedra allowing the antenna to "float" at a constant height above the ice surface as surface ablation lowered the unit. For one unit on the floating tongue (SD2M, see Fig. 3.7), the antenna was mounted on stakes drilled several meters into the ice: this allows measurements of the emergence velocity. On-ice GPS data (15 sec interval) were processed against the base station (distance between 4.7 - 8.1 km) using the differential kinematic processing tool Track (http://www-gpsg.mit.edu/ simon/gtgk/). GPS positions were then processed using a robust weighted local regression smoothing method implemented in MATLAB (version 7.7), over 6 h windows.

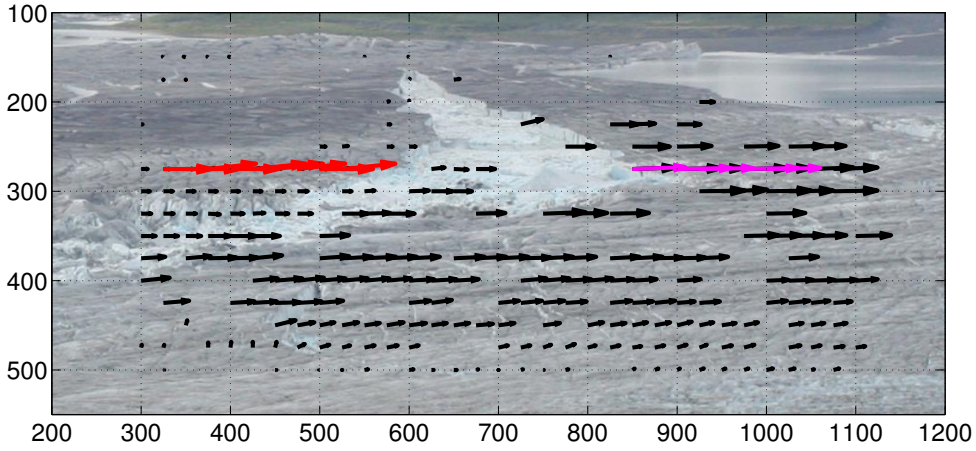

Figure 3.2. Pixel displacement/ice flow between two time-lapse images is shown with arrows. Displacements along one trajectory are used to calculate rift opening speeds by subtracting the mean uprift displacement (mean of red displacements) from the mean downrift displacement (mean of magenta displacements).

3.3.4 Feature tracking - rift opening

A Canon 40D camera was used to collect time-lapse imagery of the terminus area from 25 May - 21 July 2011 with a time interval of 20 min. The location of the camera is shown in Fig. 3.1 (59.55378°N, 138.89080°W) and was oriented towards the southeast (153°from N). The images were down-sampled to one frame per day, then referenced to each other to eliminate small shifts and rotations in the image frame. Next, feature tracking (Scambos and others, 1992) was used to obtain pixel displacements on either side of a specific rift between an image pair. Mean displacements along a flow line for each side of the rift were then subtracted from each other to obtain a rift opening speed in pixels per day (Fig. 3.2).

3.3.5 Terminus positions and orthomosaics

To assess terminus retreat and thinning, we obtained high resolution vertical aerial photos of the terminus region on 17 July 2009, 25 August 2010, and 26 September 2011. The photos were digitized and orthorectified using ground control points. We then produced digital elevation models (DEMs) at 10 m grid spacing using the photogrammetry software BAE

Socet Set. Estimated vertical accuracy of the DEMs based on comparison to LiDAR data over the terminus region is $\pm$ 1.5 m. Orthomosaics were then generated from the DEMs. We also used SPOT imagery and DEMs from 3 Sept 2007 (Trüssel and others, 2013) and from 20 September 2010 to create a chronology of changes in the terminus area.

3.4 Results

3.4.1 Lake bathymetry and temperature

We sounded lake depths during each field season and the composite bathymetric map is shown in Fig. 3.3. Lake level itself is $\sim$28 m a.s.l (EGM96). A 325 m deep, nearly featureless basin, $\sim$1.5 x 2.5 km, lies in front of the terminus. The flatness is likely a result of glacier sedimentation; the basin itself lies about 300 m below sea level. Assuming hydrostatic equilibrium, ice surface elevations determined from photogrammetry and GPS show that much of the terminus region was probably afloat during the past decade. With glacier retreat, our 2011 soundings revealed a ridge extending under the West Branch terminus (Fig. 3.3). This ridge had a depth of 180 m below water level, and might have led to local grounding.

Harlequin Lake underwent seasonal water level changes of about 2.5 m with the minimum occurring between December and April when the lake is frozen; in spring, lake level increased followed by a rapid increase of about 2 m over 2 months. Fluctuations of 0.5 to 1.0 m occur on shorter time scales (days) throughout the summer and early fall. These fluctuations correlated well with precipitation measured in Yakutat. Additionally, diurnal variations of about 2 cm are observed all year long, even in winter.

Lake water temperatures remained below 1.5°C for the entire year (Fig. 3.4). The lake froze every winter for several months and generally thawed sometime in May. On 25 May 2011, just a few days after the seasonal lake ice completely disappeared, water temperatures were relatively homogeneous throughout the entire water column and varied between 0.35 and 0.5°C. Measurements at the same location (site CTD, Fig. 3.3) on 10 September 2011 (Fig. 3.4) showed water temperature increased to 1.35°C between 50 and 200 m and to about 0.8°C below 200 m. However, except for the surface layers, density profiles (Fig. 3.4) show a stable water column in both cases. Overall, water temperatures in Harlequin Lake were well below the density maximum of 4°C year-around. Little stratification and no semi-annual turn-over were observed. Low temperatures indicate that cooling from melting ice and glacial runoff greatly offset solar heating.

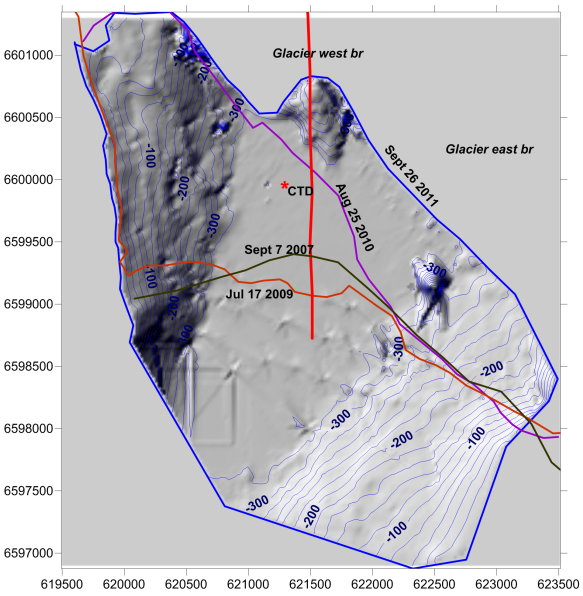

Figure 3.3. Proglacial bathymetry of Harelquin Lake. The broad main channel is 325 m deep. Approximate terminus positions are shown with solid lines, the position of the mooring is depicted by a red star (CTD). Lidar flight track is shown by a red line. Note that the rectangular feature in the southwest corner and equally spaced point features across the lower part are interpolation artifacts.

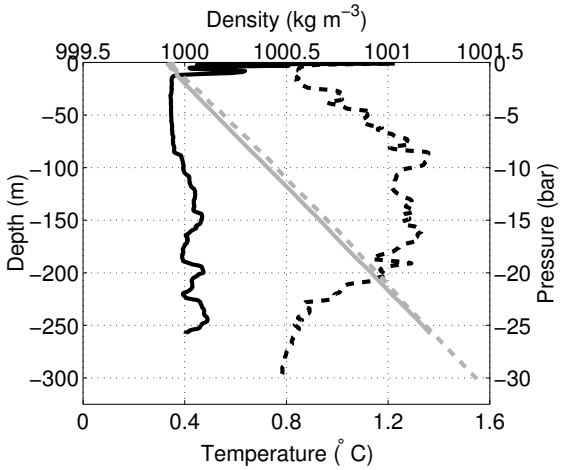

Figure 3.4. Temperature (black) and density (grey) profile of the water column close to the terminus on 25 May 2011 (solid) and 10 September 2011 (dashed). Measurement location is shown in Fig. 3.3.

3.4.2 Surface elevation change and terminus retreat

The centerline surfaces elevation from laser altimetry data for 2007-2012 are shown in Fig. 3.5a and b for the west and east branch, respectively. For inter-annual comparison, we extracted 2009-2012 data along the same line from the laser swath. The west branch (Fig. 3.5a) experienced retreat of over 2.5 km between these dates, which led to the separation of the two branches in late 2011 (Fig. 3.6). Observations in 2012 showed that the terminus of the west branch was very crevassed. These observations show that the terminus has lost most or all of its floating tongue and has likely calved back to its grounding line. However, the east branch (Fig. 3.5b) still retained a floating tongue. The average elevation change on the east branch floating tongue between 3.1 and 4.5 km of the LiDAR track were 55.5 $\pm$ 30 cm yr^{-1} (2009-2010), 87.9 $\pm$ 30 cm yr^{-1} (2010-2011) and 63.7 $\pm$ 30 cm yr^{-1} (2011-2012). For the same time periods, elevation changes on the grounded ice (at 6.5 km) were 8.44 $\pm$ 0.30 m yr^{-1}, 9.14 $\pm$ 0.30 m yr^{-1} and 5.84 $\pm$ 0.30 m yr^{-1}. The last time period 2011-2012 was shorter with 338 days compared to previous 2009-2010 with 368 days and 2010-2011 with 378 days.

Two apparently free-floating icebergs were surveyed by LiDAR, one in 2009 and another in 2012. Assuming hydrostatic equilibrium, an ice density of 900 kg m^{-3}, and using the observed free board, their mean thicknesses were estimated to be 190 $\pm$ 3 m and 207 $\pm$ 3 m m for the 2009 and 2012 iceberg, respectively. Another iceberg captured by our 2011 DEM had a mean thickness of 197 $\pm$ 15 m.

3.4.3 Velocities and strain rates

Summer evolution

GPS measurements (Fig. 3.7 and 3.8) show that the floating tongue was moving twice as fast as adjacent up-glacier grounded ice. Ice velocity increased towards the terminus, both on the floating tongue and grounded ice (Fig. 3.8). All time series showed diurnal variations with a peak around 16:00 local time (AKDT) and a minimum around 4:00.

Ice velocities varied spatially and temporally and in particular, the GPS measurements captured major rifting episodes and a calving event on day of the year (DOY) 249 (Fig. 3.8). A rifting episode appears to have begun around DOY 180. Both GPS stations on the floating ice experienced a series of accelerations and decelerations starting around 9:00 AKDT on 1 July 2011 (DOY 182) that lasted for about three days. Velocities increased grad-

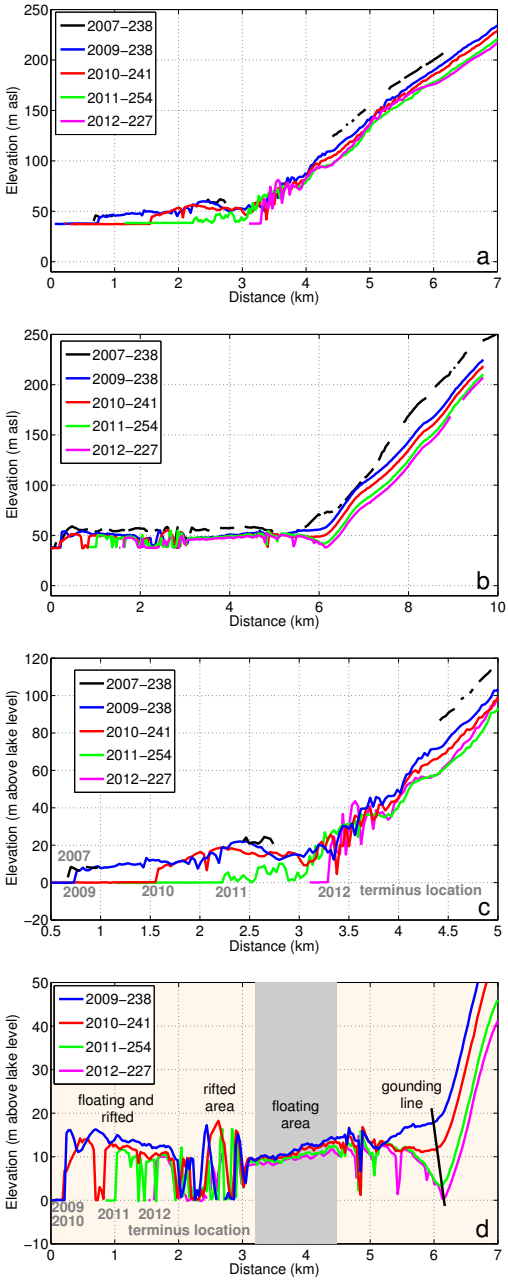

Figure 3.5. LiDAR profiles 2007-2012 a) of the west branch of Yakutat Glacier with a terminus retreat of 2.5 km between 2009 and 2012 and b) of the east branch. The first 3.5 km along flight line show a number of rifts and crevasses that had moved over the 6 year period. c) LiDAR profiles of the terminus area of the west branch show the terminus positions between 2007 and 2012. d) Profiles of the terminus area of the east branch, the shaded area represents the area used to determine surface elevation change for the floating area. The inferred grounding line is shown in black.

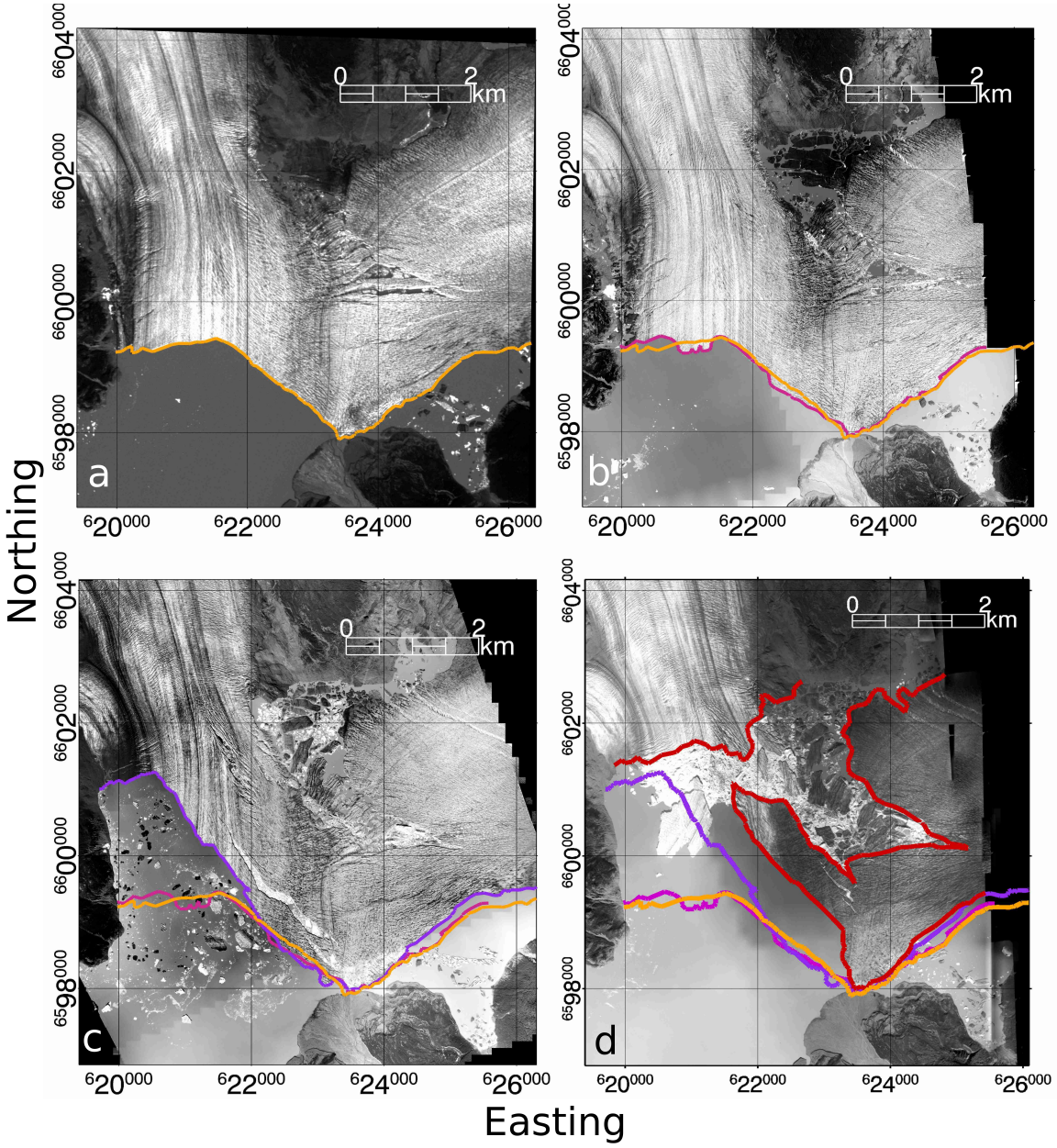

Figure 3.6. Time series of the break-up and rifting of the terminus area from a) 3 September 2007 (orange outline), b) 17 July 2009 (magenta outline), c) 25 August 2010 (purple outline) and d) 26 September 2011 (red outline). In 2011, the west branch retreated to is grounding line and the two branches were separated.

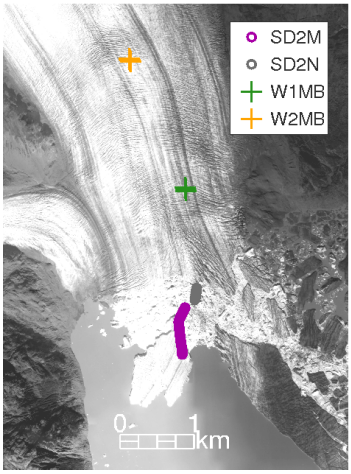

Figure 3.7. GPS unit positions and movement during summer 2011. Units in green and orange were on the grounded ice, magenta and grey were on the floating tongue.

ually at first then strongly accelerated beginning on DOY 182. Velocities then dropped and fluctuated on DOY 184 before rapidly increasing to a peak of 6 $\mathrm{m\,d^{-1}}$. Velocities then abruptly dropped to pre-event speeds then slowed even further in the following days. Similar events occurred later in the summer (DOY 230 - 250) culminating in a calving event on DOY 249 (Fig. 3.8). However, all except the forward most GPS unit on the tongue stopped recording before the calving event, thus strain rates are not available for this period.

Strain rates on the floating tongue were much higher than on the grounded ice (Fig. 3.9). While the strain rate on the grounded ice was relatively constant, strain rates on the floating tongue experienced a sign change, with extension until ∼DOY 180, switching to compression until ∼DOY 200. DOY 182 began with a relatively high extensional strain rate, then slowly relaxed over a period of 33.5 h and was followed by almost 5 h of decrease in strain rate and a switch to compression. The low strain rate was maintained for about 12 h, which overlapped mostly with the time period of decelerating ice speeds. Compression lasted for about 15 days, after which the floating tongue returned to its original regime of extension.

Strain rates between grounded and floating ice (Fig. 3.9) showed a steep increase in extensional strain during this period, with a double peak separated by 16.5h. The peak corresponded to the switching of regimes on the floating ice. Peak strain rates were a magnitude higher than before the ∼DOY 180 event. Strain rates across the grounding line remained relatively stable during the early part of the record and were 3-4 times greater

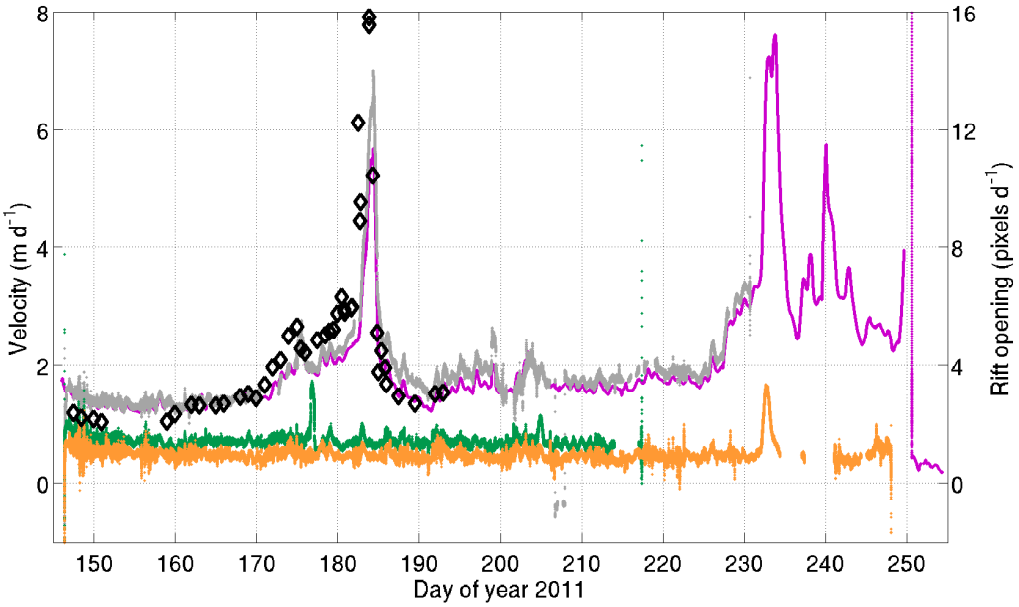

Figure 3.8. Ice velocities of grounded (orange and green) and floating (magenta and grey) ice and rift opening velocities (black diamonds) in pixels per day. See Fig. 3.7 for GPS locations.

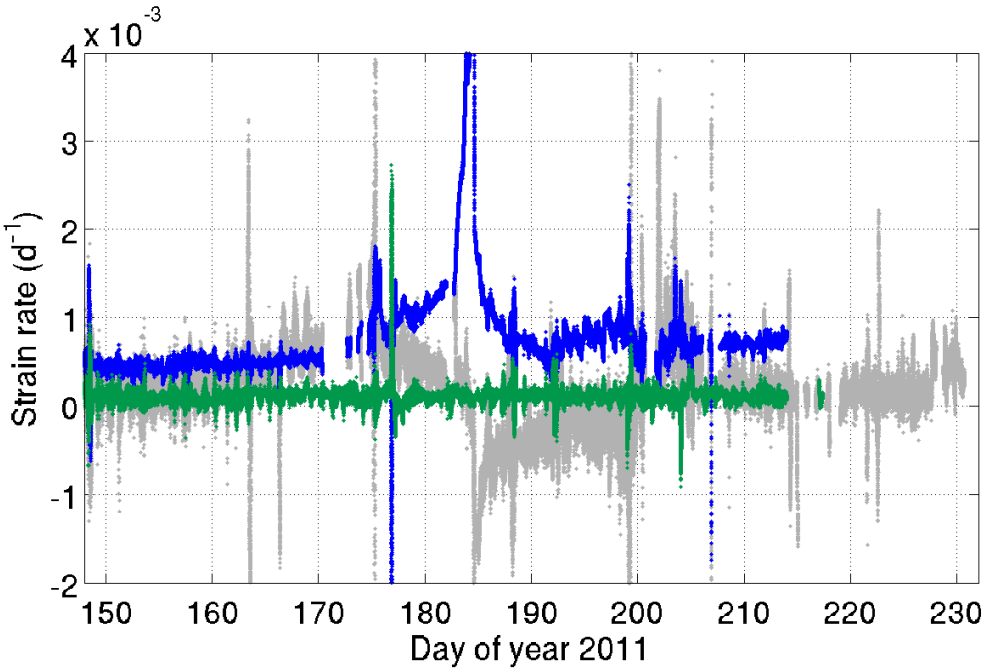

Figure 3.9. Strain rates between the two GPS units on grounded ice (green), floating ice (grey) and across the grounding line (blue).

than grounded ice strain rates (4-5 $\cdot 10^{-4}$ d^{-1} vs. 1-1.5 $\cdot 10^{-4}$ d^{-1}). From DOY 190-199, strain rates increased continuously from 6-10 $\cdot 10^{-4}$ d^{-1}, then experienced another peak at 20 $\cdot 10^{-4}$ d^{-1} at DOY 199 and finally dropped down to a constant 7 $\cdot 10^{-4}$ d^{-1} until the end of our record. Compared to the strain rate on grounded ice, which stayed constant during the entire period, the strain rate across the grounding line was also constant, with the exception of some peak events, but the rate itself increased from about 4-5 to 7 $\cdot 10^{-4}$ d^{-1}.

The results of feature tracking using time lapse imagery are shown in Fig. 3.8. The time series also nicely captures the DOY 182 rift opening episode. The temporal variability in this rift opening is highly correlated with velocity variability. The location of this rift is east of both GPS units on the floating tongue.

On 26 July 2011, we observed a rift up-glacier from both GPS units on the floating ice, while servicing the GPS units. This indicates that the GPS locations on the floating ice were de-coupled from the grounded ice and experienced velocity fluctuations due to rift opening.

Calving event: 6-7 September 2011

A large tabular iceberg calved off the terminus during 6-7 September 2011 (DOY 249-250, Fig. 3.6d). Fortuitously, a GPS unit on the iceberg continued operating during and after the event and captured the motion of the iceberg. Fig. 3.10 shows details of the GPS record as well as precipitation recorded in Yakutat, temperature and lake level at the terminus and the vertical position of the floating ice during the 3.5 weeks prior to the calving event. Lake level increased after several large precipitation episodes (DOY 227-228, 232-239), but then slowly decreased as the number and intensity of rain episodes dropped. A second series of precipitation periods then led to a further rise in lake water level (DOY 246-249). High air temperatures caused increased glacier melt, which also contributed to lake level rise. The calving occurred on DOY 249 once the lake level reached the height of its previous summer maximum. The GPS antenna was anchored in the ice. Its vertical position mimics lake level changes. The seasonal trend is explained by the hydrostatic adjustment to thinning ice.

Fig. 3.11a shows the vertical and horizontal GPS motion during the calving event. Changes during the calving event were characterized by a cascade of three rapid horizontal displacements: 1) 330 m over 15 min accompanied by a steady vertical uplift of 42 cm (15:26-15:41 ADT); 2) 35 m over 10 min (17:20-17:30 ADT); and 3) 45 m over 8 min (23:32-23:40 ADT). No vertical displacements occurred during the second two phases. The three phases exhibited different characteristics as shown in Figure 3.11b. Displacement one and three underwent symmetric acceleration and deceleration whereas displacement two experienced a fast acceleration followed by a slower deceleration. Displacement three started and ended with some motion in reversed direction.

3.5 Discussion

3.5.1 Thinning of the floating tongue

Laser altimetry data (Fig. 3.5d) show that elevation change on the floating tongue is about an order-of-magnitude less than that on the adjacent grounded ice. This result would be expected if we assumed that the floating part was in hydrostatic equilibrium (ice density: 900 $\mathrm{kg\,m^{-3}}$) and if dynamic thinning and subaqueous melt were negligible. This assumption is backed up by radar data showing that the measured ice thickness on the floating part of the west branch corresponds to ice thicknesses calculated by assuming hydrostatic equilibrium (not shown). To evaluate the contribution of surface ablation to the total thin-

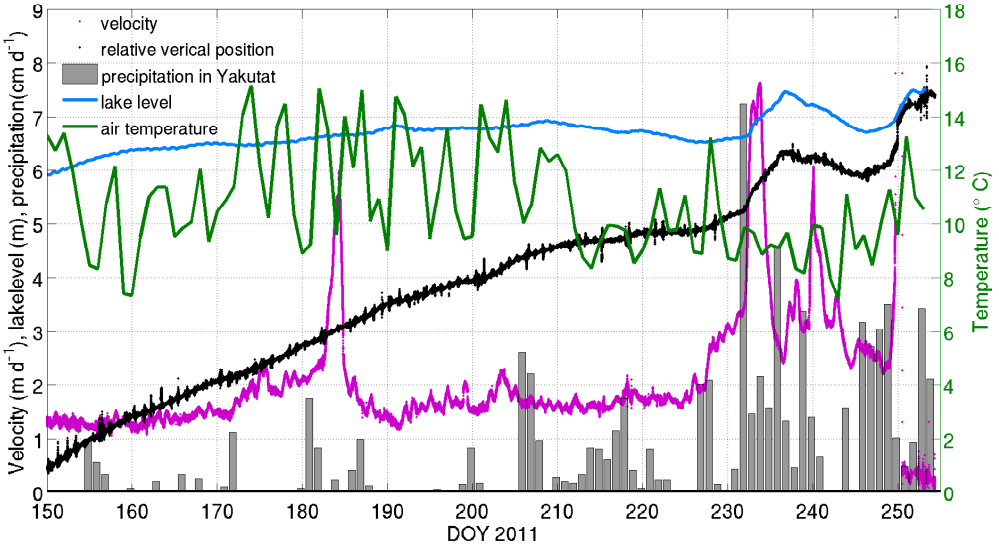

Figure 3.10. Vertical position (black) and velocity (magenta) of floating tongue. Lake level (blue) and air temperature (green, daily maxima) were measured close to the glacier terminus. Precipitation data were measured by NOAA in Yakutat, 47 km northwest of the terminus.

ning, we compared stake measurements from 20 May 2009 - 24 May 2011 (-6.91 m yr^{-1} at east branch) to LiDAR elevation change from 26 August 2009 - 11 September 2011 on the floating part of the east branch. The mean surface elevation change was -1.47 $\pm$ 0.25 m, which corresponds to -7.2 $\pm$ 2.5 m yr^{-1} thinning when assuming hydrostatic equilibrium. Part of the difference between stake and LiDAR measurements can be attributed to different time intervals, stake data were measured in spring and LiDAR data were collected in fall. To validate the seasonal influence we compared nearby point balance stake measurements from 2009 and 2011. They showed a daily melt rate of 4.75 cm d^{-1} for the summer 2009 and 4.93 cm d^{-1} for the summer 2011. We adjusted the stake interval to the LiDAR interval, giving an adjusted surface ablation of 7.25 m yr^{-1} for the interval. These results show that the elevation change on the floating tongue was mostly due to surface ablation and support the hypothesis that subaqueous melt was insignificant. Low lake water temperatures and the lack of an 'engine' for density driven circulation further support this hypothesis.

Thinning of the floating tongue is about ten times the surface elevation changes determined from LiDAR and from DEM differencing. Our DEMs (Trüssel and others, 2013)

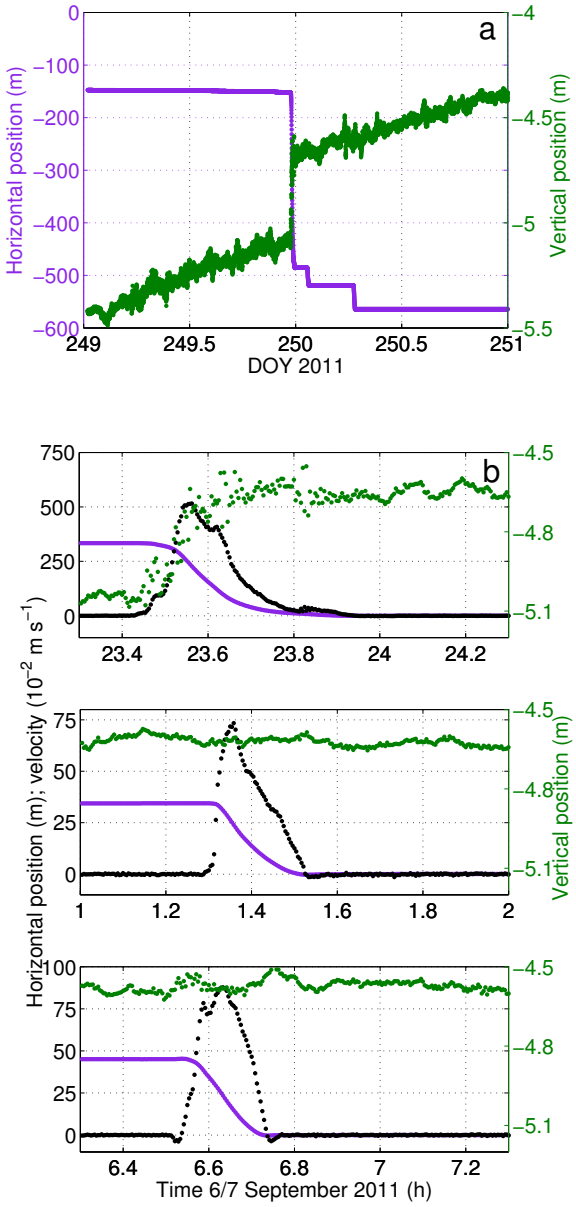

Figure 3.11. A large calving event occurred on 6 September 2011 and was captured by a GPS unit that calved on a large tabular iceberg. a) Horizontal position is depicted in purple, vertical motion is shown in green. Three rapid horizontal displacements were recorded. b) each of the three rapid displacements are shown separately. Horizontal position (purple), vertical position (green) and velocity (black) were recorded on the iceberg during and after the calving event when the iceberg was released. Note scales are different in each panel.

indicate that the west branch tongue thinned by up to 50 m between 2007 and 2010. Equivalent west branch ice thickness changed from ∼190 m on 3 Sept 2007 to 140 m on 26 Aug 2010. This thinning likely weakened the floating ice, which allowed crevasses to transform into rifts, an effect that is commonly observed on other floating ice (e.g. McGrath and others, 2012). Rifts slowly propagated forming a rift system and allowed large tabular icebergs to calve once the rifts intersected. A submerged ridge at a depth of ∼180 m (Fig. 3.3) likely helped buttress the west branch until sufficient thinning floated the tongue off this ridge.

All LiDAR profiles from the east branch showed an inflection point depression around 6.2 km distance (Fig. 3.5d) that became deeper as the ice was thinning. The inflection occurs at about the grounding line, and is likely due to bending forces caused by buoyancy as the tongue transitions from hydrostatic equilibrium to grounding. In 2012, the point of inflection was at about lake level. Similar observations have been made on Mendenhall Glacier (Boyce and others, 2007). There, the depression started to fill with lake water and the floating tongue finally calved off and retreated to its grounding line.

Water filled supraglacial lakes and crevasses have been identified to trigger disintegration of ice shelves in Antarctica (Braun and others, 2009; Scambos and others, 2009) and have been hypothesized to cause increased calving rates on tidewater glaciers (Benn and others, 2007). However, the disintegration of the floating tongue of Yakutat Glacier appears not to have been triggered by supraglacial water-filled features: the floating ice was observed to be very porous without surface streams.

The 2009 profile of the west branch (Fig. 3.5) showed a similar point of inflection as the east branch, but was followed by a surface rise downstream of the depression over the site of the submerged ridge. However, this rise disappeared during the following year, likely because of thinning over the submerged ridge. This ridge could have helped buttress the floating terminus before its break-up and thus the loss of buttressing forces would have allowed the surface rise to spread and thin. Fig. 3.6 shows that the west branch lost a significant amount of its floating tongue after 2009.

3.5.2 Rifting and ice velocity

Strain rates between grounded and floating ice showed a large peak at DOY 182. Ice velocities on the floating ice peaked at the same time. The evidence of this event indicates that a rift must have opened a significant amount between the grounded ice and the floating

part of where the GPS was located. The strain rate between the two sites on the floating ice changed from extension to compression. This varying differential motion suggests the presence of an open rift between the two sites. After the event the GPS units were on ice that resulted in different future icebergs, but they were still connected to the grounded ice. However, the two blocks could move at slightly different speeds, which is reflected in different rift spreading rates. Our time series of rift opening from time lapse imagery showed the same variations as the GPS velocity time series of the floating tongue. Thus, the mechanism causing the large differences in ice speed between grounded and floating ice can be attributed to rift opening.

Here we explore potential mechanisms for rift opening at Yakutat Glacier beginning with subglacial discharge. We examine four different scenarios of how such discharge could influence rifting. (1) Subglacial discharge water at the pressure melting point (-0.18°C) is slightly less dense than deep lake water (0.46°C in May and 0.84°C in September) and therefore hugs the underside of the ice as it flows towards the open lake, dragging the ice out and opening existing rifts. Slightly warmer lake water would then flow towards the grounding line along the lake floor. (2) The sediment load causes the discharge to be denser than lake water and sinks to the bottom of the water column and flows out along the lake floor whereas warmer lake water flows toward the grounding line below the ice. This case would cause the rifts to close and can therefore not explain our observations. Based on silt loads measured on Bench Glacier (Riihimaki, 2005), a sediment load differential between subglacial discharge and lake water of 0.09 g/L (typical sediment loads there were 0.5-4 g/L) would overcome the density difference between water at -0.18°C and 0.84°C. (3) The amount of discharge is large compared to the void between ice and lake bottom, no matter what the density contrast is, the discharge flows in only one direction flushing water towards the open lake and pushing rifts open, especially during periods of increased discharge. (4) Increased supraglacial discharge causes the lake level in the rifts to rise temporarily, which increases rift propagation and opening, similar to the mechanism discussed in Scambos and others (2009). A rough underside such as bottom crevasses would enhance the effect of subglacial flow forcing rifts apart.

Mechanism 1 seems unlikely because the density contrasts are very small. We dismiss mechanism 2 because it operates in the wrong direction. Mechanisms 3 and 4 remain plausible as rifting appears correlated with periods of increased surface melting and/or precipitation; both would increase subglacial discharge.

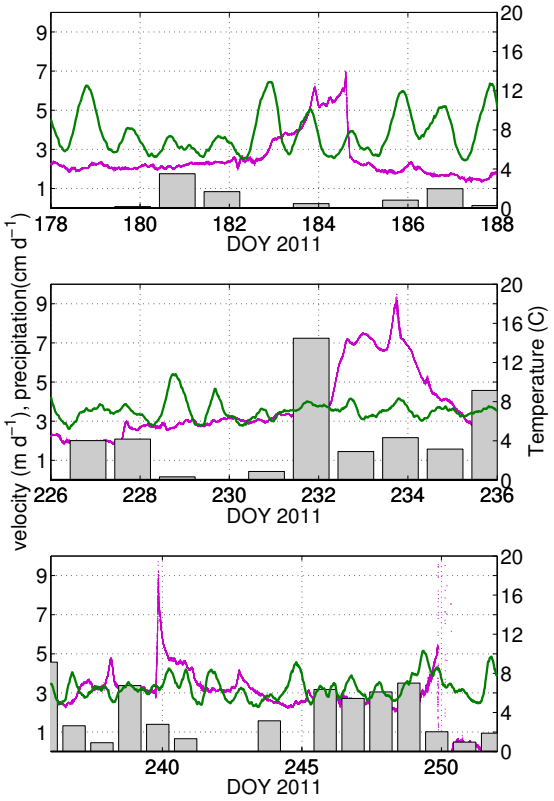

Figure 3.12. Daily precipitation (solid bars), air temperature (green) and velocity (magenta) of the floating tongue for three different time periods in summer 2011. Note temperature is smoothed over 6h intervals.

Additionally, short term lake level fluctuation due to precipitation and melt episodes drive rift opening directly. Such episodes can change the lake level as much as one meter in a week, especially in late summer and thus cause additional flexing, which contributes to the vulnerability of the floating tongue and eventually the break-up. While rift propagation is generally driven by stress and strain rate fields, pre-existing fractures and suture zones do play a critical role (Hulbe and others, 2010). Here we only address the variability in rift opening rates, not its initial formation and propagation.

Another mechanism, unrelated to discharge, are wind regimes that can cause turbulences in the rifts and push the ice towards the lake, as down-glacier is the favored wind direction in a katabatic system, especially in the case when ice surfaces of either side of the rift vary and provide a sail-like surface. Very strong winds have been observed in the terminus area, which destroyed several instruments, including the wind sensor (max gust speeds of 47 m s^{-1} on 27 February 2011, just before the sensor stopped recording). However, the largest wind speeds were recorded in winter when the lake was frozen and rift opening was probably limited. Additional strong and prevalent winds blow from interior Canada (high pressure zone) to the coast (low pressure zone) over the floating tongue and Harlequin Lake, bringing dry air and are thus not expected to be associated with precipitation.

To investigate mechanisms of rifting, we look at data from two GPS units on the floating tongue. The record shows increased velocity and presumably rift opening between 1-3 July 2011 (DOY 182-184, Fig. 3.12a). A non-steady acceleration in ice speed occurred over a period of 38 h, suggesting that the rift opened in a non-steady manner. This episode also resulted in a reversal of strain rates (Fig. 3.9).

A similar high velocity episode occurred on 20-22 August 2011 (Fig. 3.12b). The acceleration was higher and the increase in rift opening occurred therefore faster than during the previous episode (1-3 July 2011). Peak velocities were also higher. However, a velocity peak was also recorded on the grounded ice (Fig. 3.8) and occurred after a high precipitation period. A few days later, on 27 August 2011, another sudden acceleration happened after a period of precipitation episodes. While the largest velocity increases on the floating tongue were mainly due to enhanced rift opening, increased velocities on the grounded ice can partly be attributed to basal sliding. In both cases, increased speeds were observed to follow precipitation episodes and/or high daily temperatures indicating higher surface melt rates.

3.5.3 Motion of an iceberg during a calving event

The large calving event on 6 September 2011 occurred as lake level increased to its seasonal maximum (Fig. 3.10). The event was preceded by accelerated rift opening. Faster rifting resulted in rifts near the grounding line intersecting and ultimately calving of large tabular icebergs. One GPS instrument calved off with such a large iceberg, and it recorded vertical and horizontal displacements (Fig. 3.11). The first event involved both horizontal and vertical displacements, indicating that this was the episode where the iceberg broke loose. We attribute the relatively slow rate of uplift (15 min) of the iceberg at the GPS position to an isostatic imbalance resulting from viscoelastic effects (Boyce and others, 2007) as the iceberg was released close to the grounding line in the area of the depression (Fig. 3.5). The uplift may also have been due to upward rotation as the iceberg transformed into a free floating stage. Horizontal motion that accompanied this first episode consisted of continuous acceleration followed by deceleration over a period of 29 min. The second and third episodes involved only horizontal movement as the iceberg floated away from the glacier. These displacements may have been caused by subsequent calving events that either pushed the iceberg or generated waves that moved the iceberg. The second displacement showed a very asymmetric velocity curve with fast acceleration that followed complete fracture and slow, almost linear deceleration due to viscous drag in water. The three episodes were spaced by 1.8 h and 5.3 h, indicating that the entire calving event consisted of a sequence that took place over a time span of a few hours. It is possible that the later calving events were triggered by a viscoelastic response to the stresses changes caused by the first event.

The majority of calving events of a lacustrine floating tongue result in large tabular icebergs, which detach from the glacier. This is evidenced by the frequent observation of tabular icebergs in other pro-glacial lakes (Molnia, 2007a). However, in July 2009 we observed a different style of calving when a 900 m x 100 m (surface area) iceberg calved off, rotated backwards and broke into many pieces. This calving style has been commonly observed on grounded tidewater glaciers in Greenland (Amundson and others, 2008, 2010). This extreme case indicates that the ice was not isostatically balanced before the calving event. This is also supported by the observation that immediately prior to the event the ice surface level reached down to the lake level at the glacier front. The small aspect ratio (width/depth) contributed to this instability.

3.5.4 Calving of floating ice

Floating glacial ice occurs in three different forms: as ice shelves consisting of cold ice; as ephemeral floating tongues of temperate tidewater glaciers (Walter and others, 2010); and as floating tongues of temperate lacustrine glaciers (Warren and others, 2001; Boyce and others, 2007; Trüssel and others, 2013). All three systems can experience collapse where they lose a significant part of the floating ice. Collapse is generally preceded by a mechanical weakening of the floating ice. In the case of floating tongues in tidewater and lacustrine systems, weakening and destabilization is mostly triggered by thinning. However, the main source for thinning differs substantially for these two types of floating tongues. In a lacustrine system, like Yakutat Glacier, thinning can mostly be attributed to surface ablation, whereas in a tidewater system, such as Jakobshavn, thinning is mainly caused by submarine melt and due to ocean currents and water density contrast (Motyka and others, 2011). Additionally, in a tidewater system, an ephemeral floating tongue is weakened by vertical motion attributed to tidal forcing (Rosenau and others, 2013). Once sufficiently thinned, the floating tongue of either system is then prone to increased rift propagation. These rifts then intersect and allow large icebergs to calve. In a lake environment, tabular icebergs remain floating in the vicinity of the terminus. In a tidewater system on the other hand, large icebergs can disintegrate rapidly as the ice is generally crevassed and rough (Walter and others, 2010). Currents then transport the fragmented icebergs towards the ocean and warmer ocean water enters the terminus area. These currents form an important heat energy exchange mechanism.

Floating ice tongues of lacustrine glaciers show similarities to Antarctic ice shelves. Antarctic ice shelves can function in a steady-state; calving occurs in the form of one or several large icebergs that form every few years and compensate for the ice flux to the shelf during that time. Icebergs detach after a time period of rift opening that is followed by the ice reaching a sufficiently low thickness. However, thinning of these ice shelves results from ice dynamical stretching and basal melting, with surface melting generally negligible on the Antarctic continent. Basal melt rates can be high in places where warm ocean water reaches the continental shelf, such as the Amundson Sea Embayment. An interesting situation arises on the eastern Antarctic Peninsula, where large scale ice shelf collapses have occurred, but ocean water is generally cold. It is at least possible that a more negative surface mass balance led to a thinning of the shelf at Larsen B. Together with the

appearance of surface water, this would have led to a weakening of the shelf.

Generally, there are two different fracture mechanisms causing break-ups of ice shelves, a fast catastrophic failure (brittle) and a slow fracture propagation (ductile), where the latter grow hundreds of meters per year (Braun and others, 2009). Catastrophic failure is accompanied by rapid expansion of fragmented icebergs associated with capsizing of icebergs (MacAyeal and others, 2003). Floating tongues of both, tidewater and lacustrine glaciers appear to experience ductile fracture propagation, as seen on Yakutat Glacier.

3.6 Conclusions

Temperate Yakutat Glacier retreated into an overdeepened basin in the late 1970s. The glacier formed an extensive floating tongue, which was maintained for at least the decade between 2000 and 2010. In 2010 the tongue started a large scale disintegration by calving large tabular icebergs. This led to the separation of the two contributing branches by late 2011. The disintegration of the tongue continued in 2012 and led to the grounding of the western branch. The eastern branch continued to break apart in 2013.

The break-up of the floating tongue was caused by thinning, which can be attributed to the very negative surface mass balance rates. The thinning of up to 50 m between 2007 and 2010 (Trüssel and others, 2013) weakened the floating tongue and led to the formation of large rifts and eventually large tabular ice bergs. Rift opening rates were highly variable and related to precipitation and melt episodes. We hypothesize that this is explained by either the drag of subglacial discharge currents, or the pooling of water in rifts. Increased water discharge also led to higher lake levels, which favored calving events, presumably helped by bending stresses. Flexing over seasonal and inter-annual time scales may have also weakened the tongue.

The tabular calving events at Yakutat Glacier do not appear to be triggered by basal melt. In that regard they might form a useful and easily studied analogue to calving of marine ice shelves that are located in generally cold marine settings, such as those on the Eastern Antarctic Peninsula. Generally, lake calving glaciers are expected to be a common feature in a warming climate, as glaciers retreat into overdeepenings, which are a common erosional feature of glaciated landscapes.

3.7 Acknowledgements

M. Fahnestock provided code for the image correlation analysis. We thank A. Aschwanden, W. Dryer, M. Habermann, S. Herreid, J. Hulth, A. Johnson, J. Kennedy, C. Kienholz, R. McNabb, D. Podrasky, J. Young and L. Zirnheld for assistance with fieldwork. CH2MHill Polar Services provided logistics support, instrument support was provided by the University Navstar Consortium (UNAVCO). Bill Lucey and Tim Ross supported the work in Yakutat, and Temsco Helicopters and Alsek Air provided aircharter services. Funding was provided by NSF-OPP (grant ARC 0806463) and the Center for Global Change.

References

Amundson, J. M., M. Fahnestock, J. Brown, M. Truffer, R. J. Motyka and M. P. Lüthi, 2010. Ice mélange dynamics and implications for terminus stability, Jakobshavn Isbræ, Greenland, *Journal of Geophysical Research*, **115**(F1).

Amundson, J. M., M. Truffer, M. P. Lüthi, M. Fahnestock, M. West and R. J. Motyka, 2008. Glacier, fjord, and seismic response to recent large calving events, Jakobshavn Isbræ, Greenland, *Geophysical Research Letters*, **35**(22), L22501.

Benn, D. I., R. H. Mottram and S. G. Warren, 2007. Calving processes and the dynamics of calving glaciers, *Earth-Science Reviews*, **82**(3-4), 143–179.

Boyce, E. S., R. J. Motyka and M. Truffer, 2007. Flotation and retreat of a lake-calving terminus, Mendenhall Glacier, southeast Alaska, USA, *Journal of Glaciology*, **53**(181), 211–224.

Braun, M., A. Humbert and A. Moll, 2009. Changes of Wilkins Ice Shelf over the past 15 years and inferences on its stability, *The Cryosphere*, **2**(3), 41–56.

Hulbe, C. L., C. LeDoux and K. Cruikshank, 2010. Propagation of long fractures in the Ronne Ice Shelf, Antarctica, investigated using a numerical model of fracture propagation, *Journal of Glaciology*, **56**(197), 459–472.

Jacobs, S. S., H. H. Helmer, C. S. M. Doake, A. Jenkins and R. M. Frolich, 1992. Melting of ice shelves and the mass balance of Antarctica, *Journal of Glaciology*, **38**(130), 375–387.

Johnson, A. J., C. F. Larsen, N. Murphy, A. A. Arendt and S. L. Zirnheld, 2013. Mass balance in the Glacier Bay area of Alaska , USA , and British Columbia , Canada , 1995 âĂŞ 2011 , using airborne laser altimetry, *Journal of Glaciology*, **59**(216), 1995–2011.

Larsen, C. F., R. J. Motyka, A. A. Arendt, K. A. Echelmeyer and P. E. Geissler, 2007. Glacier changes in southeast Alaska and northwest British Columbia and contribution to sea level rise, *Journal of Geophysical Research*, **112**(F1), 1–11.

MacAyeal, D. R., T. A. Scambos, C. L. Hulbe and M. Fahnestock, 2003. Catastrophic ice-shelf break-up by an ice-shelf-fragment-capsize mechanism, *Journal of Glaciology*, **49**(164), 22–36.

McGrath, D., K. Steffen, T. Scambos, H. Rajaram, G. Casassa and J. L. Rodriguez Lagos, 2012. Basal crevasses and associated surface crevassing on the Larsen C ice shelf, Antarctica, and their role in ice-shelf instability, *Annals of Glaciology*, **53**(60), 10–18.

Molnia, B. F., 2007a. Calving Theory and the Thinning, Retreat, and Disarticulation of Bear Glacier, Alaska, *AGU Fall Meeting Abstracts*, A38.

Molnia, B. F., 2007b. Late nineteenth to early twenty-first century behavior of Alaskan glaciers as indicators of changing regional climate, *Global and Planetary Change*, **56**(1-2), 23–56.

Motyka, R. J., L. Hunter, K. A. Echelmeyer and C. L. Connor, 2003. Submarine melting at the terminus of a temperate tidewater glacier, LeConte Glacier, Alaska, U.S.A., *Annals of Glaciology*, **36**(1), 57–65.

Motyka, R. J., M. Truffer, M. Fahnestock, J. Mortensen, S. Rysgaard and I. M. Howat, 2011. Submarine melting of the 1985 Jakobshavn Isbræfloating tongue and the triggering of the current retreat, *Journal of Geophysical Research*, **116**(F1), 1–17.

Pfeffer, W. T., 2007. A simple mechanism for irreversible tidewater glacier retreat, *Journal of Geophysical Research*, **112**(F3), 3.

Raup, B., A. Kääb, J. S. Kargel, M. P. Bishop, G. Hamilton, E. Lee, F. Paul, F. Rau, D. Soltesz, S. Khalsa and M. Beedle, 2007. Remote sensing and GIS technology in the Global Land Ice Measurements from Space (GLIMS) Project, *Computers & Geosciences*, **33**(1), 104–125.

Riihimaki, C. A., 2005. Sediment evacuation and glacial erosion rates at a small alpine glacier, *Journal of Geophysical Research*, **110**(F3), F03003.

Rosenau, R., E. Schwalbe, H.-G. Maas, M. Baessler and R. Dietrich, 2013. Grounding line migration and high-resolution calving dynamics of Jakobshavn Isbrae, West Greenland, *Journal of Geophysical Research: Earth Surface*, **118**(November 2012), n/a—-n/a.

Scambos, T. A., M. J. Dutkiewicz, J. C. Wilson and R. A. Bindschadler, 1992. Application of image cross-correlation to the measurement of glacier velocity using satellite image dataâŸ, *Remote Sensing of Environment*, **42**(3), 177–186.

Scambos, T. A., H. A. Fricker, C.-C. Liu, J. Bohlander, J. Fastook, A. Sargent, R. Massom and A.-M. Wu, 2009. Ice shelf disintegration by plate bending and hydro-fracture: Satellite observations and model results of the 2008 Wilkins ice shelf break-ups, *Earth and Planetary Science Letters*, **280**(1-4), 51–60.

Trüssel, B. L., R. J. Motyka, M. Truffer and C. F. Larsen, 2013. Rapid thinning of lake-calving Yakutat Glacier and the collapse of the Yakutat Icefield, southeast Alaska, USA, *Journal of Glaciology*, **59**(213), 149–161.

Walter, F., S. O'Neel, D. E. McNamara, W. T. Pfeffer, J. N. Bassis and H. A. Fricker, 2010. Iceberg calving during transition from grounded to floating ice: Columbia Glacier, Alaska, *Geophysical Research Letters*, **37**(15), 1–5.

Warren, C., D. I. Benn, V. Winchester and S. Harrison, 2001. Buoyancy-driven lacustrine calving, Glaciar Nef, Chilean Patagonia, *Journal of Glaciology*, **47**(156), 135–146.

Chapter 4

Run-away thinning of the low elevation Yakutat Glacier and its sensitivity to climate[1]

Abstract

Lake calving Yakutat Glacier in Southeast Alaska is undergoing rapid thinning and terminus retreat. We use a simplified glacier model approach to evaluate the future mass loss of Yakutat Glacier. In a first step, we compute glacier wide mass change with a surface mass balance model, and add a mass loss component due to ice flux through the calving front. We then use an empirical elevation change curve to adjust for surface elevation change of the glacier and finally use a flotation criterion to account for terminus retreat due to calving. Surface mass balance is computed on a daily time scale, elevation change and retreat is adjusted on a decadal scale. We use two scenarios to simulate future mass change, 1) keeping the current climate and 2) forcing the model with a projected warming climate. We find that more than 95% of the glacier will have disappeared by 2120 or 2070 under a constant or warming climate, respectively. For the first few decades, the glacier can maintain its current thinning rate by retreating and associated loss of high-ablating low elevation areas. However, once higher elevations have thinned substantially, the glacier can no longer counteract accelerated thinning by retreat and mass loss accelerates.

4.1 Introduction

Low elevation glaciers and icefields are particularly sensitive to a changing climate. Thinning due to a negative surface mass balance can cause the ice surface elevation to drop and expose the ice to warmer climate conditions (Bodvardsson, 1955). Progressively larger areas of the glacier lie below the equilibrium line altitude (ELA). If this effect dominates over the loss of ablation area due to retreat, the volume reaction time scale becomes negative and the glacier will disappear entirely (Harrison and others, 2001), even under constant climate. This effect becomes even more pronounced if the ELA rises to higher elevations due to changing climate.

Many coastal glaciers in Alaska originate at low elevations and extend to sea level. The region has been identified as a significant contributor to global sea level rise (Arendt and others, 2002; Berthier and others, 2010; Arendt and others, 2013). Larsen and others (2007)

[1] Will be submitted to the Journal of Glaciology as: Barbara L. Trüssel, Martin Truffer, Regine Hock, Roman J. Motyka, Matthias Huss and Jing Zhang. Run-away thinning of the low elevation Yakutat Glacier and its sensitivity to climate.

pointed out the large volume loss of lake calving glaciers and identified Yakutat Glacier in Southeast Alaska as one of the most rapidly thinning glaciers since 1948. During the last decade (2000-2010), this glacier experienced a mean thinning of -4.43 m w.e. yr^{-1} and terminus retreat of 14.4 km during the last century (Trüssel and others, 2013).

In addition to the negative surface mass balance Yakutat Glacier also loses ice by calving into Harlequin Lake. Calving may enhance rapid retreat and could dynamically accelerate mass transport to lower elevations causing increased thinning and thereby contributing to the mass balance feedback described above. As glaciers around the world retreat into overdeepened basins, which they have often formed themselves by erosion, they can form pro-glacial lakes (Warren and Aniya, 1999). Once terminating in such a lake, they change their dynamic behaviour from land-terminating to lake calving, which increases ice flow in the terminus area (Kirkbride, 1993). Despite the increasing number of lake calving systems world wide, these systems have previously not been addressed in global glacier change assessments.

In this paper, we use a simplified model that includes surface mass balance, calving and glacier geometry changes, to evaluate the future volume loss of Yakutat Glacier. The model first calculates surface mass balance, adds volume loss from ice flux through the calving front, then adjusts the surface elevation of the glacier by using an empirical elevation change curve and finally computes volume loss due to retreat of the calving front using a flotation criterion. Surface mass balance is calculated on a daily time scale, surface elevation adjustment and calving retreat are performed on a decadal scale.

We consider two climate scenarios. Scenario 1 “constant climate" is based on observations of the period 2000-2010, and scenario 2 “warming climate" is based on monthly temperature trends for the 21^{st} century.

Our model allows us to predict glacier retreat and thinning without a full ice flow model, and is therefore less computationally expensive. This approach can be applied to other glaciers with limited measurements.

4.2 Study area

Yakutat Glacier (337 km^2, Raup and others, 2007) lies on the western (maritime) side of the northern Brabazon Range in southeast Alaska (Fig. 4.1), 50 km east of the town of Yakutat, where the mean annual precipitation is 3576 mm yr^{-1} (1917-2007, http://climate.gi.alaska.edu/climate/location/timeseries/Yakutat.html). Lake-terminating

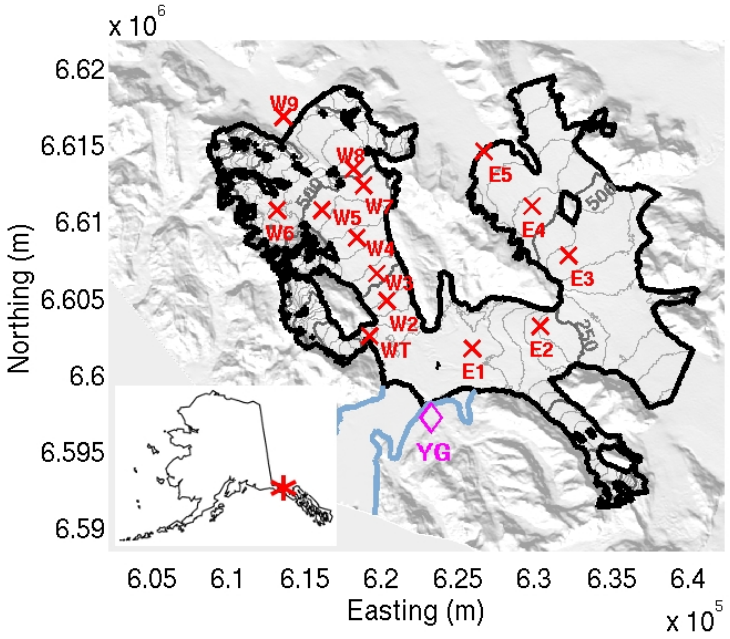

Figure 4.1. Yakutat Glacier - The glacier is outlined in black, contour-line spacing is 50 m (SPOT DEM 2010). Mass balance stake locations are shown by red crosses. The weather station (YG) is located near the terminus and marked by a magenta diamond. Harlequin Lake is outlined in blue.

Yakutat Glacier is part of the low elevation Yakutat Icefield with ice divides at around 650 m a.s.l., which is below the average ELA for this region (Eisen and others, 2001). This glacier has a very small accumulation area ratio (AAR) of 0.03 (2007) and is exposed to much higher thinning rates than the land-terminating glaciers of the icefield (Trüssel and others, 2013).

Yakutat Glacier calves into Harlequin Lake, which is over 330 m deep in places and covered an area of 69 km^2 in 2010, but has increased its surface area due to retreat of the calving front. At the ice divide, the glacier bed lies below the current lake level (radar measurements, see Section 4.3.4), suggesting that Harlequin Lake will continue to grow and may eventually extend up to the ice divide as the glacier retreats.

4.3 Data

To model the evolution of Yakutat Glacier, a digital elevation model (DEM) is required. Further, daily temperature and precipitation data at one location are needed to calculate

the surface mass balance of the glacier. Gridded monthly precipitation data are used to extrapolate precipitation across the glacier. The surface mass balance model is calibrated using measured point balance observations. Finally, to evaluate calving flux and glacier extent for each time interval, information on the ice thickness is required.

4.3.1 Digital elevation model

We use a DEM from Système Pour l'Observation de la Terre (SPOT) imagery (Korona and others, 2009), taken on 20 September 2010 and corrected for the Yakutat Glacier area (Trüssel and others, 2013). Grid spacing of the SPOT DEM is 40 m. The corrected DEM is used as the initial model input and to create an initial slope and aspect grid. The latter two grids are needed to calculate the potential direct solar radiation for each day of the year.

4.3.2 Climate data

Four different climate data sets are used to calculate surface mass balance.
YG data - A weather station was deployed close (<1 km) to the terminus of Yakutat Glacier on bedrock (59°29'35.66" N / 138 °49'22.94" W, 71 m a.s.l.) and collected measurements between 16 July 2009 and 12 September 2011. Temperature data were recorded every 15 min with a HOBO S-THB-M002 temperature sensor 2 m above ground and HOBO U30 NRC data logger (for sensor and logger details see: http://www.onsetcomp.com/).
NOAA data - Daily precipitation and temperature data for the period 1 January 2000 - 31 December 2011 are downloaded from the weather station PAYA maintained by National Oceanic and Atmospheric Administration (NOAA, http://pajk.arh.noaa.gov/cliMap /akCliOut.php). Their weather station PAYA is located at the airport (10 m a.s.l.) in the town of Yakutat, 47.7 km northwest of the weather station close to the terminus of the glacier.
Gridded precipitation data - Monthly gridded (2 km) precipitation data are provided by David Hill (personal communication) from 2002 - 2009. The data is based on re-gridded PRISM monthly precipitation norms between 1971-2000. They calculate and interpolate anomalies between measured monthly precipitation and monthly PRISM norms.They then multiply the anomaly with PRISM norm to create monthly precipitation estimates. For more details see ftp://ftp.ncdc.noaa.gov/pub/data/gridded-nw-pac/.
Projected regional climate data - Simulations from one of Coupled Model Intercomparison

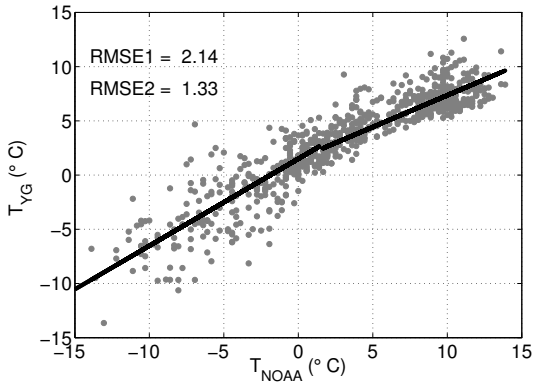

Figure 4.2. Projected daily mean air temperature measured at the NOAA weather station at the airport in Yakutat, AK (10 m a.s.l.), vs. temperature measured close to the terminus of Yakutat Glacier (71 m a.s.l.). A bilinear function with root mean square error RMSE1 for $T_{NOAA} < T_0$ and RMSE2 for $T_{NOAA} > T_0$ was used to fit the data (black solid line).

Project 5th phase (CMIP5) simulation experiments, CCSM4 Community Climate System Model 4 (CCSM4, Gent and others, 2011) historical simulations and future projections, are dynamically downscaled to the Alaska region at a 20 km resolution grid by a regional atmosphere model Weather Research and Forecasting (WRF, Skamarock and others, 2008). The downscaling approach is the same as in previous work using Mesoscale Model version 5 (MM5, the predecessor to WRF) for regional downscaling of CCSM3 (previous version of CCSM4) simulations (Zhang and others, 2007).

NOAA data is used to extend the short YG data series to the period 2001-2010. We compare YG data with NOAA data for the overlapping time period and define a bi-linear transfer function. We apply this transfer function to the full NOAA record, thus providing a longer time series for the YG data location to run the glacier model. The intersection point (T_0 = 1.5 °C/ T_c = 2.5 °C) of the bi-linear fit was picked based on minimal root mean square errors (2.14 for $T_{NOAA} < T_0$ and 1.33 for $T_{NOAA} > T_0$). The best-fit transfer function

$$T = \begin{cases} 0.59\,(T_{NOAA} - T_0) + T_c, & T_{NOAA} < T_0 \\ 0.80\,(T_{NOAA} - T_0) + T_c, & T_{NOAA} >= T_0. \end{cases} \tag{4.1}$$

with T_0 = 1.5 °C and T_c = 2.5°C.

For scenario 1 (constant climate), we create a time series using the corrected NOAA temperature and uncorrected measured NOAA precipitation data (2001-2010). We then

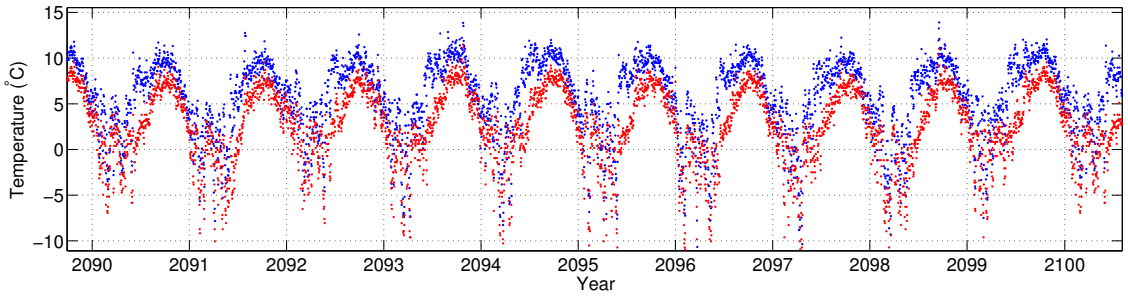

Figure 4.3. Daily mean temperatures at the terminus of Yakutat Glacier between 2090 and 2100. Red: scenario 1 (constant climate); blue: scenario 2 (warming climate).

repeat this ten year interval until 2120. Repeating a time interval allows us to conserve extreme temperature and precipitation events and preserves the observed variability over the past decade without a longer term trend. We use this scenario to explore the magnitude of the mass balance feedback due to surface lowering.

To account for spatial variations of snow accumulation we use gridded monthly precipitation data (Hill, personal communication), as described at ftp://ftp.ncdc.noaa.gov/pub/data/gridded-nw-pac/, to create a mean precipitation index grid. For spatial distribution, we only consider winter data (October - April, 2002-2009), because only solid precipitation is relevant for the surface mass balance model. For each glacier grid cell the mean deviation from the glacier wide precipitation average over the winter months 2002-2009 is computed. This produces a spatial grid of precipitation correction factors with values ranging between 0.76 and 1.24 with a mean of 1.

For scenario 2, we calculate linear trends from projected regional climate data for each month over the 21^{st} century, which are extracted from a dynamically downscaled CMIP5 (Coupled Model Intercomparison Project 5th phase) simulation and based on monthly means. We superimpose these trends on observed temperatures from 2000-2010 to preserve variability on shorter time scales. Trends for each month are shown in Tab. 4.1. Largest slopes and therefore highest temperature increases are found for June, followed by July, May and February. Increased June temperatures cause earlier melt onset. Overall, the predicted melt seasons will be more extended and warmer, as shown for the period 2090-2100 in Fig. 4.3.

Projected precipitation data do not show seasonally/monthly varying trends. However, the data shows a linear annual trend with a slope of 2.07 10^{-5} mm day^{-1} that is

Table 4.1. Monthly temperature trends (δ T) extracted from dynamically downscaled CMIP5 and root mean square errors (RMSE).

Month	δ T (K yr^{-1})	RMSE
January	0.0247	2.771
February	0.0385	3.116
March	0.0214	2.459
April	0.0244	1.454
May	0.0377	1.449
June	0.0757	2.726
July	0.0516	2.164
August	0.0322	1.431
September	0.0296	1.283
October	0.0253	1.728
November	0.0211	2.568
December	0.0161	2.621

applied to precipitation data from scenario 1 to produce a data set for scenario 2.

4.3.3 Surface mass balance

Point balance observations are used to calibrate the surface mass balance model. In total data are available at 14 locations in 2009, 12 locations in 2010 and 13 locations in 2011. Each year the measurements were done in late May and early September. Winter point balances are derived from snow depth measurements in May. Snow density is assumed to be 500 kg m^{-3}. Due to high summer melt rates (more than 6 m at lower elevations) ablation was measured with wires drilled into the ice rather than the widely used technique of ablation stakes.

Surface mass balance measurements for 2009-2011 are shown in Table 4.2. Note, that E1MB shows a less negative summer mass balance compared to other points at higher elevation. This is due to the fact that the lower east branch was covered with moss and other small dirt piles in the vicinity of E1MB, which appears to have an insulating influence on the ice.

Table 4.2. Surface mass balance measurements between 2009 and 2011. The values in parentheses represent snow water equivalent (m w.e.) at the start day of each period (May). Station names starting with E were located on the east branch of Yakutat Glacier, W stands for west branch. Elevation is given as the 2010 surface elevation in WGS84.

Station	Elevation	20 May - 3 Sept 2009	20 May - 29 Aug 2010	25 May - 11 Sept 2011
E1MB	51	-3.63 (0)	-3.65 (0)	-3.99 (0)
E2MB	222	-5.04 (0)	-5.11 (0.55)	-5.37 (0)
E3MB	444	-3.70 (1.85)	-3.30 (1.58)	-4.91 (0.75)
E4MB	551	-2.10 (3.50)	-2.91 (1.78)	-3.66 (1.52)
E5MB	639	-2.48 (2.45)	-2.18 (2.45)	-2.26 (1.85)
W1MB	118	-5.75 (0.54)	n/a (0.65)	-5.51 (0)
W2MB	217	n/a (0.75)	n/a (1.05)	-6.86 (0)
W3MB	295	-4.11 (2.37)	-4.70 (1.80)	n/a (1.15)
W4MB	398	-3.24 (2.05)	-3.07 (2.35)	-3.63 (1.88)
W5MB	489	-3.25 (2.50)	-3.24 (2.70)	-3.39 (2.09)
W6MB	589	-3.00 (4.00)	-2.88 (3.70)	-2.52 (4.00)
W7MB	496	-4.02 (2.13)	-3.46 (2.35)	-3.41 (1.69)
W8MB	538	-3.06 (n/a)	n/a (n/a)	n/a (2.10)
W9MB	691	-2.97 (3.65)	-2.53 (3.23)	-2.60 (3.40)
WTMB	155	-4.95 (1.00)	-4.71 (1.10)	-6.13 (0)

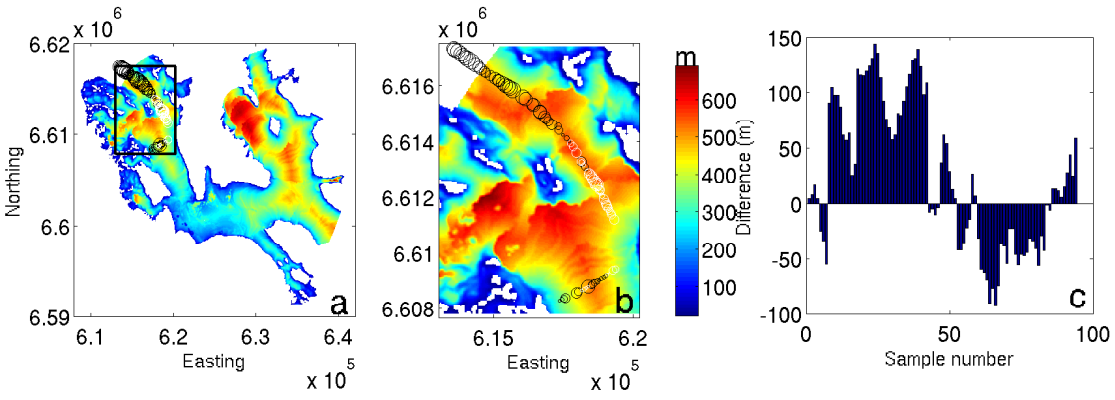

Figure 4.4. Modeled ice thickness (m) of a) the entire Yakutat Glacier and b) a subregion in the upper reaches of the western branch based on the methods by Huss and Farinotti (2012). Circles mark location of radar measurements. Black circles indicate ice that is thicker than modeled and white circles indicate shallower than modeled ice. c) Differences between radar measurements and modeled thickness along sampling track (sample numbers do not correspond to a constant distance).

4.3.4 Ice thickness

Ice thickness data are calculated using the method of Huss and Farinotti (2012) who use surface mass balance to derive a volumetric balance flux and then derive ice thickness through Glen's flow law (Fig. 4.4 a). These simulations are calibrated with ground-based radio echo sounding data that were collected 19-20 May 2010 along several profiles on the upper west branch of Yakutat Glacier with a ski-towed low frequency radio echo sounding system. Errors in bed returns are influenced by uncertainties in wave propagation velocity, but dominated by the accuracy of the return pick, which we estimate at 0.1 μs. The mean difference between measured and modeled ice thicknesses along the center line is 25.1 m. Larger discrepancies occur mostly towards the glacier margins, where the glacier is shallower (Fig. 4.4b). Therefore, we expect that these differences have little effect on our results.

4.4 Methods

The glacier model includes four steps: First it calculates the surface mass balance with daily resolution. Then each year volume loss due to calving assuming a constant position of the calving front is modeled and subtracted from the volume change due to the annual surface mass balance. Third, the combined glacier-wide volume change is converted into

an elevation change for each grid cell accounting for both changes due to surface mass balance and ice flow. Finally, each decade, volume loss due to the retreat of the calving front is added.

4.4.1 Surface mass balance model

We use the open access Distributed Enhanced Temperature Index Model (DETIM) to compute the glacier's surface mass balance (Hock, 1999). DETIM is freely available at http://regine.github.com/meltmodel/. The model runs fully distributed, meaning that calculations are performed for each grid cell of a digital elevation model. Melt $\mathcal{M}$ (mm d^{-1}) is calculated by

$$\mathcal{M} = \begin{cases} (M_f + a_{snow/ice} I)\, T, & T > 0 \\ 0, & T <= 0. \end{cases} \tag{4.2}$$

where M_f is the melt factor (mm $d^{-1}\,^{\circ}C^{-1}$), $a_{snow/ice}$ describes a radiation factor for snow and ice ($m^3W^{-1}d^{-1}\,^{\circ}C^{-1}$), respectively, T is the daily mean air temperature ($^{\circ}$C) and I is the potential clear-sky direct solar radiation (W m^{-2}). Eqn. (4.2) is an empirical relationship that was found to work well in Hock (1999).

I is computed from topographic shading and solar geometry. Since this is computationally expensive, we keep the daily grids of I constant in time rather than recalculating I as the glacier surface evolves. Sensitivity tests show negligible impact on our results.

DETIM is forced with daily climate data, and calculates surface mass balance for each glacier grid point of a DEM. Temperature data at YG station are extrapolated to the grid using surface elevation and a lapse rate. Daily precipitation is adjusted by a precipitation correction factor and then distributed using a precipitation index grid (see Section 4.3.2). Snow accumulation is computed from a threshold temperature that distinguishes between solid versus liquid precipitation. Solid precipitation is added to the surface mass balance, whereas rain is not considered.

Five parameters are used to adjust the model to Yakutat Glacier: precipitation factor (p_{cor}), temperature lapse rate (γ), melt factor (M_f), radiation factor for ice (a_{ice}) and radiation factor for snow (a_{snow}). p_{cor} accounts for precipitation under-catch of the gauges, especially for snow measurements and for topographic differences between the NOAA and YG station, specifically their proximity to mountainous terrain. γ describes temperature

change with elevation, and often varies between -0.45 and -1.00 x 10^{-2} °C m^{-1} (Rolland, 2003). M_f, a_{ice} and a_{snow} are empirical parameters, the only limitation is that a_{ice} must be equal or higher than a_{snow} to account for generally higher albedo over snow than ice.

4.4.2 Calving

Calving flux Q_c (m^3 yr^{-1}) is defined as the difference between the ice flux arriving at the calving front Q and the volume change due to terminus advance or retreat $\frac{dV}{dt}$:

$$Q_c = Q - \frac{dV}{dt} \tag{4.3}$$

We first determine Q based on recent surface velocity observations (Trüssel and others, 2013), thus assuming $dV/dt = 0$. The resulting volume loss is added to the volume change calculated by DETIM. The total volume change is then comparable to volume change as measured with DEM differencing. In a later step, after the surface elevation has been adjusted, $\frac{dV}{dt}$ will be determined. For simplicity we ignore potential dynamical feedbacks after large calving events, such as speed-ups. This is justifiable because ice speed and thus changes in ice flux to the calving front are small compared to surface mass balance (Trüssel and others, 2013).

Ice flux

For each decadal time step, we calculate ice flux at the terminus by assuming a spatially constant mean speed along the terminus of 74.3 m yr^{-1} for the west branch and 30.0 m yr^{-1} for the east branch, using results from Trüssel and others (2013). These velocity observations result from feature tracking on satellite imagery between 2000-2010, for more details see Trüssel and others (2013), and are assumed to be temporally constant. The ice speed is expected to be constant throughout the entire ice column, because the ice will be floating at the terminus and will therefore not experience resistance from the glacier bed. The flow direction is assumed to be along the centerline, which is anticipated to remain constant for the future as long as there is calving. We then identify the terminus by finding the ice-covered pixels that neighbor water, and find the flux Q by integrating along the length L of the terminus:

$$Q = \int_L h\, \mathbf{v} \cdot \mathbf{n}\, dl, \tag{4.4}$$

where h is the ice thickness in, and $\mathbf{n}$ is the unit normal vector to the line L.

Calving retreat

In the past, Yakutat Glacier was able to build and maintain a floating tongue for at least a decade until the ice was sufficiently weakened by thinning, which allowed rifts to open and propagate, and caused large tabular ice bergs to calve. To address such a calving style in a simplified way, we apply a flotation criterion to determine calving retreat. This flotation criterion is based on measured lake level, bed topography and ice thickness and allows floating tongues to disintegrate after the chosen time interval (ten years). Cells fulfilling the flotation criterion will transform from glacier cells to lake cells.

4.4.3 Surface elevation adjustment

In order to account for the surface mass balance feedbacks due to retreat/advance and thinning/thickening, the DEM of the glacier surface must be adjusted, as changes in surface elevation and glacier extent expose the ice to different climate conditions. We determine the total volume change (without calving retreat) by subtracting the ice flux through the calving front from the volume change from surface mass balance calculated with DETIM. We then use an empirical glacier specific elevation change relationship, which includes dynamic components to redistribute the total volume loss (again without calving retreat), using a similar concept as proposed in Huss and others (2010). The resulting new surface elevation of the glacier is then used to compute retreat due to calving (see Section 4.4.2) and retreat of grounded ice due to thinning. The latter is determined by glacier cells with a negative thickness, which are transformed into bedrock cells. The DEM is adjusted every ten years.

Model description

Each grid point of the glacier experiences a rate of surface elevation change $\frac{\partial h}{\partial t}$ given by

$$\frac{\partial h}{\partial t} = \dot{b} + w \tag{4.5}$$

where $\dot{b}$ is the specific surface mass balance (calculated by DETIM and converted to ice equivalent change) and w is the vertical velocity. If calving retreat is ignored, glacier wide rate of volume change $\dot{V}$ can be described as

$$\dot{V} = \int_A \dot{b}\, da + Q = \int_A \frac{\partial h}{\partial t}\, da \tag{4.6}$$

where A is the glacier map area. Observations show that elevation change Δh is a function of elevation f(z) and has a typical shape for each glacier with higher $\frac{\partial h}{\partial t}$ at lower elevations (Johnson and others, 2013). This glacier specific f(z) will shift up towards larger mean $\frac{\partial h}{\partial t}$ during a period of colder climate and down during warmer periods:

$$\dot{V} = \int_A (f(z) + C)\, da = \int_A f(z)\, da + C \cdot A \tag{4.7}$$

$$C = \frac{1}{A}(\int_A \dot{b}\, da + Q - \int_A f(z)\, da) \tag{4.8}$$

We then find the surface elevation change Δh for each grid cell as a function of elevation.

$$\Delta h = f(z) + C \tag{4.9}$$

The amount of shifting C changes for each time interval (here ten years).

Elevation change curve f(z)

We use surface elevation change data from DEM differencing for the period 2000-2010 (Trüssel and others, 2013) to find the typical *z-dz* curve shape for each branch of Yakutat Glacier separately. We fit both quadratic and exponential functions to the data. The RMSE fit of both functions are nearly identical: $\sim$0.87 m yr^{-1} for the West Branch and $\sim$0.77 m yr^{-1} for the East Branch. The exponential function is chosen as slightly better and is used for both branches.

This elevation change curve works well for thinning glaciers. However, for glaciers with a large positive mass balance, f(z) would allow glacier thickening, but more so at higher elevations, resulting in steep slopes. Advances would happen very slowly or not at all. Further, f(z) cannot be used for dynamically complicated glaciers, such as surge-type glaciers. However f(z) is generated from glacier specific data of a rapidly thinning glacier, if the climate and thus mass balance and glacier characteristics would change dramatically, f(z) might have to be adjusted with current measurements.

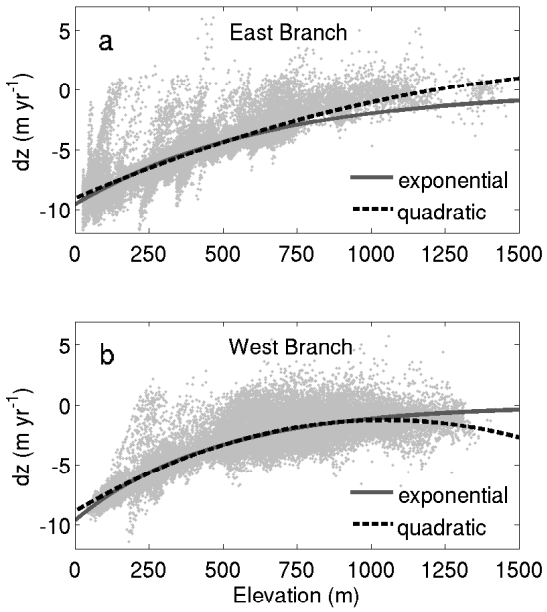

Figure 4.5. Elevation vs. elevation change (*z-dz*) from DEM differencing (2000-2010) with exponential and quadratic fits. Typical *z-dz* curve for a) east branch and b) west branch of Yakutat glacier.

4.4.4 Calibration

Model calibration proceeds by finding best values and ranges for sensitivity analysis for the following parameters: precipitation factor (p_{cor}), lapse rate (γ), melt factor (M_f), radiation factor for ice (a_{ice}) and snow (a_{snow}). We perform a grid search for these parameters and compare the results to two types of observations: seasonal point mass balances measured over different time periods between 2009 and 2011 and total glacier mass change due to surface mass balance derived from DEM differencing between 2000 and 2010. The DEM differencing results are corrected for a calving flux derived in Trüssel and others (2013) to make them directly comparable to the integrated surface mass balance ($\dot{B}$). As a final step we apply the full model with dynamic corrections over the time period 2000 - 2010 and compare it to measured DEM differences.

We determine an initial set of all parameter values by trial and error, seeking to minimize discrepancies with measured point balance data. We find p_{cor}=1.6 to provide good fits to measured snow water equivalent. Compared to measured precipitation in Yakutat (3576 mm yr^{-1}, http://climate.gi.alaska.edu/climate/location/timeseries/Yakutat.html), p_{cor}=1.6 corresponds to an increase in precipitation of 22% at the glacier terminus, 58% at the ice divide and 98% at the highest point of the glacier. Increasing p_{cor} can further improve the fit to winter balance data, but balances measured in summer will be represented less accurately with a precipitation increase of over 100% in certain parts of the glacier. We therefore keep p_{cor} fixed for the additional parameter runs. We then perform a grid search of γ, M_f, a_{ice} and a_{snow} over the intervals specified in Table 4.3. For each parameter combination we calculate the root mean square error (RMSE) to measured point balances and we also compare the three-year average total $\dot{B}$ to the ten-year average DEM difference, corrected for calving flux. From the parameter sets that produce acceptable fits to the mean three year balance, we select the ten sets that produced the lowest RMSE to point balances (Tab. 4.3, Fig. 4.6). The calculated ten-year average $\dot{B}$ of these ten sets lies within $\pm$0.05 m of the three-year average total $\dot{B}$. These sets are then run over the full 2000-2010 period with the full model (including dynamic adjustments and calving) and compared to DEM differencing data. We restrict the comparison to the grounded portion of the ice, because the model calves back to the grounding line after each decade, as discussed above. This comparison is used to find a calibrated parameter set, which produces an area-averaged mean difference of 0.26 m over the ten years (Fig. 4.7c). This best parameter set slightly

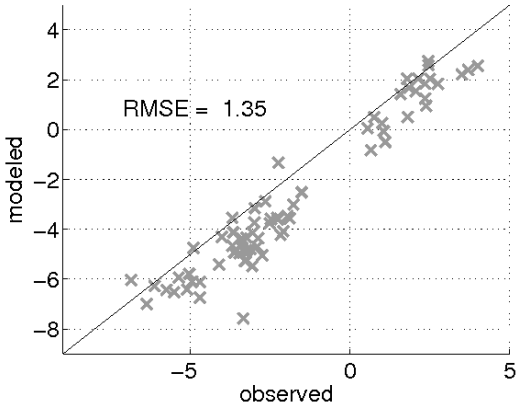

Figure 4.6. Calibration of DETIM. Modeled mass balance vs. measured stake data from 2009 to 2011 using γ of -0.45°C 100 m^{-1}, M_f of 4.1$\cdot$ 10^{-3} m^3 d^{-1}K^{-1}, a_{ice} of 0.9$\cdot$ 10^{-6} m^3 W^{-1}d^{-1}K^{-1} and a_{snow} of 0.7$\cdot$ 10^{-6} m^3 W^{-1}d^{-1}K^{-1}.

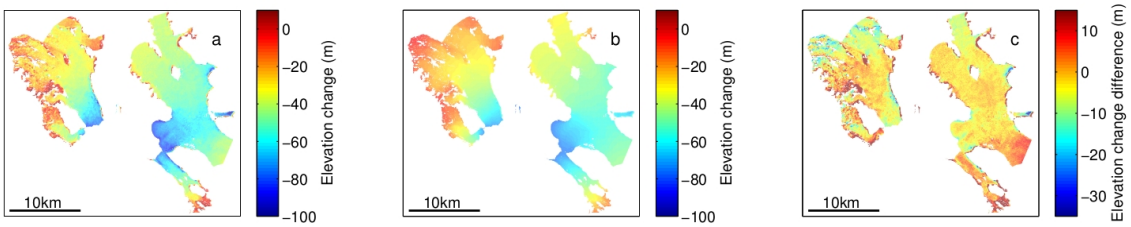

Figure 4.7. Surface elevation change. a) Measured surface elevation change from DEM differencing 2000 - 2010, b) modeled surface elevation change between 2000 and 2010, c) difference between measured and modeled surface elevation change.

underestimates the mass loss.

The calibrated parameter set is used for all projection runs; the remaining nine parameter sets are used in the sensitivity study.

4.5 Results

We first calculate the evolution of Yakutat Glacier under a constant climate (scenario 1). Fig. 4.8a shows the ice thickness between 2020 and 2120. Assuming scenario 1, Yakutat Glacier will have lost over 95% of its volume and surface area by 2120 and will have vanished by 2130. Under a warming trend, the entire glacier will have disappeared by 2080 (Fig. 4.8b). In 2070, Yakutat Glacier will have lost 77% of its 2010 volume under scenario

Table 4.3. Parameters of best ten DETIM input variable sets, including parameter ranges and intervals. Lapse rate (γ) in 10^{-2} °C m^{-1}; melt factor (M_f) in 10^{-3} m $d^{-1}K^{-1}$; radiation factor for ice (a_{ice}) and snow (a_{snow}) in 10^{-6} m^3 $W^{-1}d^{-1}K^{-1}$; and precipitation factor (p_{cor}). Root mean square errors (RMSE) between measured and modeled point balances and mean annual balance ($\dot{B}$) from 20 September 2009 - 11 September 2011 for each parameter set.

Parameter	1	2	3	4	5	6	7	8	9	10	Range	Interval
γ	−0.45	−0.45	−0.45	−0.45	−0.45	−0.45	−0.45	−0.45	−0.45	−0.45	−0.9 to −0.45	0.05
M_f	4.2	3.9	4.0	3.7	4.0	4.1	3.7	3.8	3.5	3.6	3.5 to 4.2	0.1
a_{ice}	0.9	1.0	1.0	1.1	0.9	0.9	1.0	0.9	1.0	0.9	0.7 to 1.1	0.1
a_{snow}	0.6	0.6	0.6	0.6	0.7	0.7	0.7	0.8	0.8	0.9	0.6 to 1.0	0.1
p_{cor}	1.6	1.6	1.6	1.6	1.6	1.6	1.6	1.6	1.6	1.6	1.5 to 2.0	0.1
RMSE	1.28	1.29	1.34	1 .34	1.30	1.35	1.31	1.31	1.32	1.32		
$\dot{B}$	−3.95	−3.93	−4.01	−3.98	−3.96	−4.04	−3.95	−3.95	−3.96	−3.94		

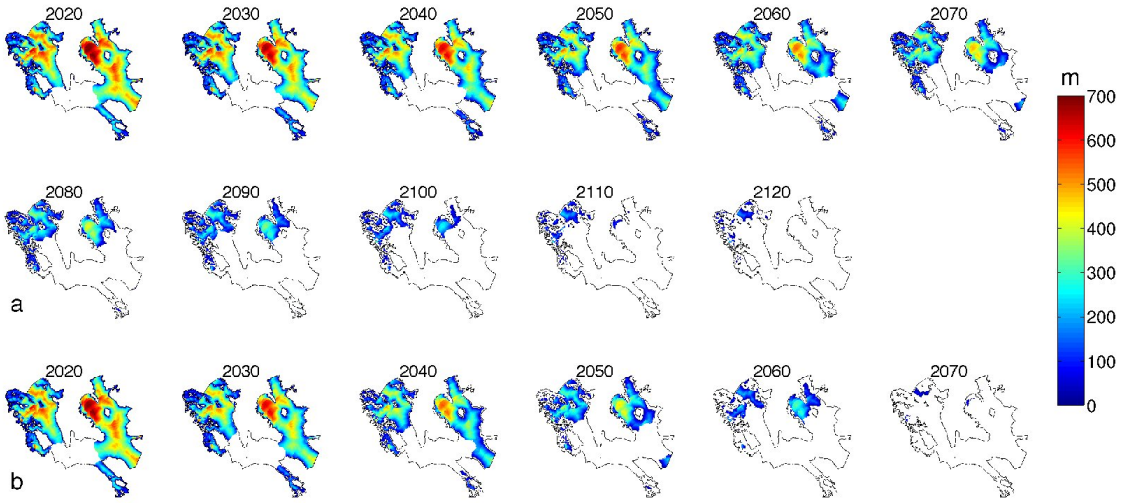

Figure 4.8. Evolution of Yakutat Glacier under a) scenario 1 (2020-2120) and b) scenario 2 (2020-2070). Rapid thinning can be observed in ice thickness maps (m), the east branch will have totally disappeared by 2120 under scenario 1. Under scenario 2, the east branch will have mostly disappeared by 2070, only small ice patches will be left.

1 vs. more than 95% under scenario 2. The mean surface elevation under a scenario 1 in 2070 will be 393 m a.s.l. vs. 100 m a.s.l. under scenario 2.

We use all ten parameter sets (parameters: γ, M_f, a_{ice} and a_{snow}; mean annual balance ($\dot{B}$) 2009-2011: -4.5 to -3.9 m w.e. yr^{-1} and RMSE to point balance data < 1.35 m w.e. yr^{-1}) to run the model to explore the range of volume loss of Yakutat Glacier. The differences between the ten cases are relatively small and represent the uncertainty due to parameter choice. For the two scenarios, the largest difference between the highest and lowest model under constant projections is found in 2070 with a value of 1.8 km^3 and occurs under changing projections in 2050 with a volume change difference of 4.7 km^3.

Fig. 4.9 shows the cumulative volume loss for both climate scenarios, starting with an initial volume of 115 km^3 in 2010. For the best performing parameter set, the volume loss under scenario 1 is -114.1 km^3 in 2120, and under scenario 2, it is -114.8 km^3 in 2070. Due to decadal surface elevation adjustments, small patches of ice will remain at the end of each model run.

The contribution from calving to the total volume loss is shown in Fig. 4.9a (red).

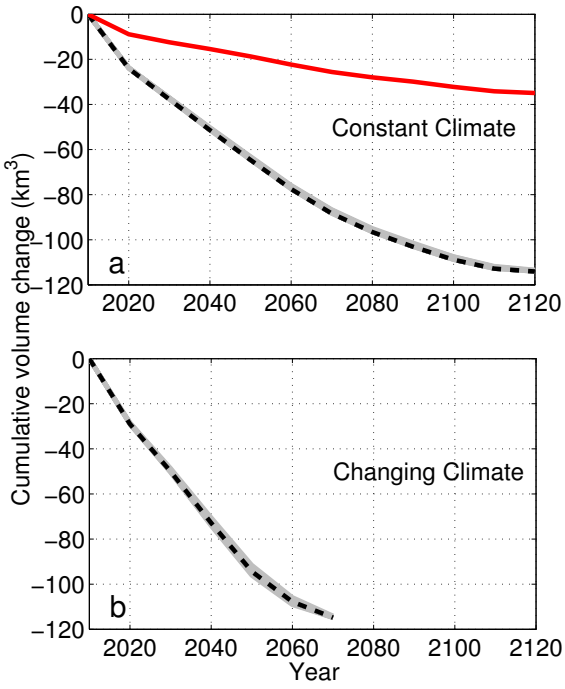

Figure 4.9. Mean cumulative volume change for ten parameter sets, including calving, a) under scenario 1 and b) under scenario 2. The best performing parameter combination when comparing modeled volume change to DEM differencing, is shown in black, its cumulative contribution from calving flux is illustrated in red.

4.6 Discussion

4.6.1 Parameter range

We compare the parameter range of these ten best combinations to parameters found by Schneeberger and others (2003) for the two Alaskan glaciers Gulkana (interior mountain range) and Wolverine (coastal mountain range). Our best results are found with a lapse rate of $-0.45\ 10^{-2}\,^{\circ}\mathrm{C\ m^{-1}}$, whereas Schneeberger and others (2003) found lapse rates between -0.5 and $-0.7\ 10^{-2}\,^{\circ}\mathrm{C\ m^{-1}}$. Our melt factors M_f ranged between 3.6 - 4.2, while they report values between 5.6 - 32.5; where the upper bound is from coastal Wolverine Glacier, which is exposed to a climate similar to Yakutat Glacier. Also radiation factors a_{ice} and a_{snow} varied greatly in their study, between 0.28 - 1.52$\cdot\ 10^{-6}$ $\mathrm{m^3\ W^{-1}d^{-1}K^{-1}}$ and 0.26 - 1.60$\cdot\ 10^{-6}$ $\mathrm{m^3\ W^{-1}d^{-1}K^{-1}}$, respectively. In comparison, our a_{ice} varied between 0.9 - 1.1$\cdot\ 10^{-6}$ $\mathrm{m^3\ W^{-1}d^{-1}K^{-1}}$ and a_{snow} between 0.6 - 0.9$\cdot\ 10^{-6}$ $\mathrm{m^3\ W^{-1}d^{-1}K^{-1}}$. These large differences could partly be due to temporally different input data. However, Schneeberger and others (2003) allowed their snow radiation factor to be larger than the ice radiation factor, which is unphysical. Also, these models are highly empirical and incorporate a large variety of physical processes, so a close agreement between different glaciers, even in the same area cannot be expected.

4.6.2 Influence of calving

To assess the importance of calving to the overall volume loss we run the model without the calving module, hence assuming the glacier is land-terminating and compared results to simulations including calving. Results show that in 2050, 46.7% of the initial volume would be left if the glacier is not exposed to calving, vs. 43.8% including calving (53.7 $\mathrm{km^3}$ vs. 50.4 $\mathrm{km^3}$ from initially 115.0 $\mathrm{km^3}$). The glacier would cover 20.5 $\mathrm{km^2}$ (9.6%) more surface area if there was no calving.

Calving will remain a volume loss mechanism for this glacier, because the glacier bed is well below lake level in large parts of the glaciated area. However, calving will be more important during the first few decades after 2010 than later in the glacier's future, as illustrated in Fig. 4.9a (red). The decrease in calving flux is due to both, bedrock geometry and reduced ice mass causing slower ice flux. For our model, this means that the ice thickness at the calving front is decreasing with time resulting in a smaller calving front (Fig. 4.8a).

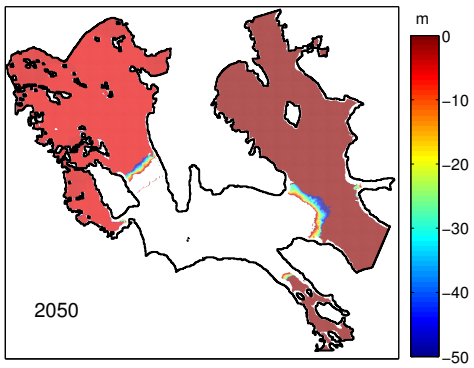

Figure 4.10. Difference in surface elevation in 2050 between a model run including volume loss by calving (Eqn. 4.3) and a run excluding calving, i.e assuming the glacier was land-terminating. The model was forced by scenario 1 (constant climate).

Two main differences between a lake calving and land-terminating system are illustrated in Fig. 4.10. First, there is an area with steep elevation change gradient, which depicts the area of calving retreat. Second, glacier area with a constant negative elevation change (west branch:-5.7 m, east branch: -1.3 m) illustrates that calving dynamics increase thinning. These differences are small in our model, but still account for 0.14 m yr^{-1} of surface lowering on the west branch between 2010-2050.

However, even under the most conservative future predictions, constant climate and no calving, in 2120 Yakutat Glacier will have lost more than 95% of its initial volume from 2010, indicating that this glacier is well into its collapse already.

4.6.3 Feedbacks

Yakutat Glacier is experiencing two separate feedback mechanisms during its collapse. First, as the ice surface is continuously thinning, the ice will be exposed to higher temperatures, which in turn increases thinning rates, a positive feedback mechanism known as the Bodvardsson effect (Bodvardsson, 1955). Second, as thinning rates increase, especially at lower elevations, the glacier cannot support the rapid thinning in the terminus area and starts retreating. By losing the area with highest thinning rates and thus decreasing the ablation area, the glacier can maintain a constant glacier-wide thinning rate resulting in a negative feedback mechanism (Harrison and others, 2001).

To investigate the positive (surface lowering) and the negative feedback mechanism's (terminus retreat) influence on the glacier's mass balance, we compare conventional mass balance calculations with results where the surface elevation and geometry of the glacier are kept constant, known as reference-surface mass balance (Elsberg and others, 2001). The latter excludes terminus retreat and thinning and therefore neither of the feedback mechanisms influence the mass balance. During the first few decades after 2010 the conventional surface mass balance is less negative compared to the reference-surface mass balance, due to the negative feedback mechanism (Fig. 4.11). Similar observations are made by Huss and others (2012) on 36 glaciers in the Alps. The glacier maintains a relatively small mean thinning rate by retreating to higher elevations and thus losing area at low elevations. However, after a few decades, rapid thinning on the glacier can no longer be counteracted by retreat to higher elevations. The mean thinning rates will now continue to increase. This transformation is projected to occur around 2055 under scenario 1. In a changing climate, the glacier will react much faster and switch to this unstable situation already in 2034. Once the positive feedback of the Bodvardsson effect starts to dominate over the negative feedback, the glacier will accelerate its volume loss.

4.6.4 Can the retreat of Yakutat Glacier be stopped?

If climate change would reverse drastically, the glacier could theoretically return into a steady-state situation in its present size with a zero mass balance. We systematically decrease temperature and change precipitation to estimate what climate conditions would allow a zero mass balance for Yakutat Glacier (Fig. 4.12). In order to maintain its current volume, the temperature would have to drop by an unrealistic 1.5°C if the precipitation stayed constant. Raising precipitation by 50% under current temperatures would still be inadequate to achieve zero mass balance. Such an increase in precipitation would make Yakutat Glacier the wettest place on earth.

If it requires a temperature decrease of -1.5°C to reach equilibrium presently, it will require a larger temperature drop in the future as the mean surface elevation of the glacier will be lower. The terminus will likely be at lake level for most of the glacier's existence, because of a glacier bed at around sea level at the ice divide, therefore retreating to higher elevation to reach equilibrium is only possible when the glacier disintegrates into small fragments.

Once the glacier retreats into a few small cirque glaciers, they can exist for decades,

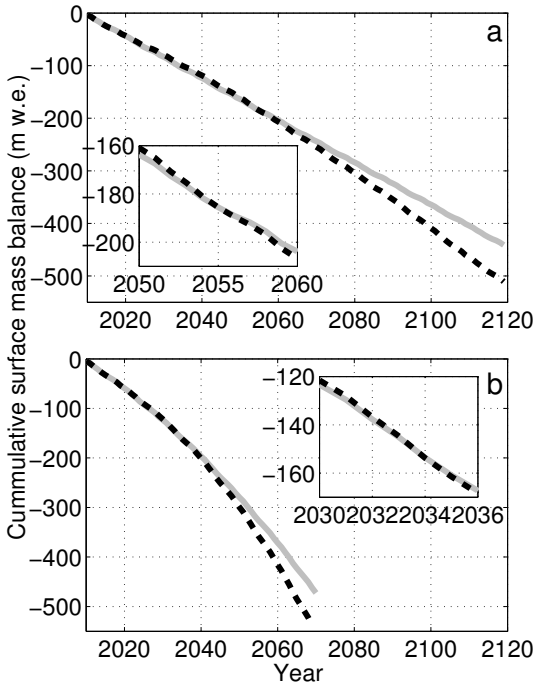

Figure 4.11. Comparison of reference-surface mass balance (grey) and conventional surface mass balance (black) for a) scenario 1 and b) scenario 2.

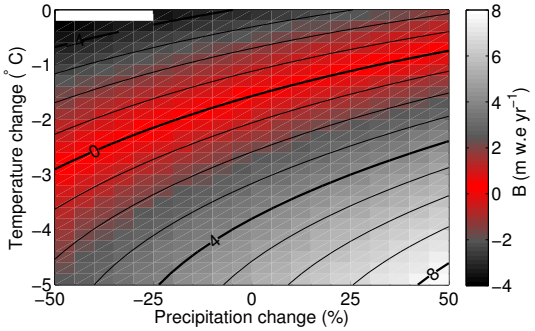

Figure 4.12. Glacierwide $\dot{B}$ (m w.e. yr^{-1}) for mass-balance years 2000-2010 calculated with DETIM as a function of temperature and precipitation changes applied to the original input data. Zero $\dot{B}$ are highlighted in red.

but they will be influenced by the two following mechanisms. First, thinning and retreat may be slowed down by the influence of topography and location. Aspect and therefore shading as well as increased accumulation due to wind drift and avalanches may become important in the glacier's mass balance (DeBeer and Sharp, 2009). Second, these small patches of ice will not be exposed to calving dynamics and losses.

We show here that climate conditions would have to change significantly in order to transform Yakutat Glacier into an equilibrium. This raises the question of how this low elevation glacier exposed to lacustrine calving originated. If it would already require large changes in climate to maintain its current geometry, climate changes alone appear to be an unrealistic source for the initial formation of Yakutat Glacier. In Trüssel and others (2013) we hypothesized that, in addition to colder climate conditions, ice spilled over from adjacent Art Lewis and Vern Ritchie glaciers, both of which have high elevation accumulation basins. In addition, Nunatak and Hidden Glaciers (both glaciers of Yakutat Icefield) thickened as a result of nearby Hubbard Glacier damming Russell Fjord and ice from these glaciers helped grow Yakutat Glacier.

4.6.5 Influence of lacustrine dynamics

Collapses as we project for Yakutat Glacier and possibly the entire icefield have been observed previously in Glacier Bay (Larsen and others, 2005), only a few hundred kilometers south of Yakutat Glacier. However, Glacier Bay was primarily occupied by tidewater glaciers, the rapid retreat and thinning was mostly attributed to maritime regimes and their dynamic effects. The collapse of Yakutat Glacier on the other hand will mostly be caused by its low elevation and lake calving dynamics.

Many coastal glaciers in Alaska are presently lake terminating. With current retreat rates, the number of such lacustrine systems will increase in the near future and some of these glaciers may experience similar rapid retreat and thinning as we project here. As shown by Trüssel and others (2013), Yakutat Glacier is exposed to the highest thinning rates of the Yakutat Icefield, which is attributed to calving dynamics. Therefore the formation of a pro-glacial lake is important for two reasons: 1) a previously land-terminating glacier will change its dynamic behaviour into a lake calving system with highest ice speeds at the terminus and 2) the terminus area will remain at lake levels, where the ice surface will be exposed to higher air temperatures, similar to the description by Mercer (1961).

Compared to tidewater glaciers, a lake calving system is influenced by different mech-

anisms. First, the glacier is not exposed to tidal forcing. Second, the density difference between subglacial discharge and lake water is not strong enough to drive circulations as seen in a tidewater system where the subglacial discharge fresh water is buoyant compared to ocean water (Motyka and others, 2011). Third, a lake forms a closed system without energy exchange, whereas ocean circulations continuously transport warmer water to the calving front and remove the cold melt water. If a glacier retreats into an overdeepened basin, these differences may allow a persistent floating tongue to form in a lake calving system, as hypothesized in Trüssel and others (2013). Such floating tongues can then collapse rapidly, once the ice has thinned enough.

4.7 Conclusions

To predict future retreat and thinning of Yakutat Glacier, we combine a surface mass balance model with a dynamic correction, include a simple calving law and adjust the glacier surface after each decade. Surface elevation change can influence mass balance of the sequential time period by two competing feedback mechanisms. First, the lowest elevation area will decrease as the glacier retreats, a negative feedback loop. Second, as the glacier thins, the surface elevation will lower and expose the ice to warmer air temperatures, which forms a positive feedback. The negative feedback will lose its importance as the glacier thins and highest elevations are low enough that the positive feedback will become dominant.

Yakutat Glacier demonstrates that a low elevation glacier is particularly sensitive to change. Even under present climate conditions, the glacier will retreat and thin substantially, by 2120 less than 5% of its initial volume of 115.0 km^3 in 2010 will remain and by 2130 it will have disappeared. When forcing the same model with scenario 2 projections, the entire glacier will have disappeared by 2080. Only two little ice patches will be left by 2070.

To prevent such a collapse, air temperatures would have to become much lower (1.5 K) and precipitation would have to increase by more than 50%, both unrealistic prerequisites (Fig. 4.12). Our results show that Yakutat Glacier is far from equilibrium and will not transition back to steady-state in the near future. Many low elevation glaciers around the globe will experience similar scenarios.

4.8 Acknowledgements

We thank David Hill for providing gridded precipitation data. The downscaled climate data were generated under support of NSF award EAR-0943742. We thank Chris Larsen and David Podrasky for discussions, which helped to improve this manuscript. The SPOT-5 images used for DEM differencing was provided by the SPIRIT program (CNES). Funding was provided by NSF-OPP (grant ARC 0806463).

References

Arendt, A., S. Luthcke, A. Gardner, S. O'Neel, D. Hill, G. Moholdt and W. Abdalati, 2013. Analysis of a GRACE global mascon solution for Gulf of Alaska glaciers, *Journal of Glaciology*, **59**(217), 913–924.

Arendt, A. A., K. A. Echelmeyer, W. D. Harrison, C. S. Lingle and V. B. Valentine, 2002. Rapid wastage of Alaska glaciers and their contribution to rising sea level, *Science*, **297**(5580), 382–386.

Berthier, E., E. Schiefer, G. K. C. Clarke, B. Menounos and F. Rémy, 2010. Contribution of Alaskan glaciers to sea-level rise derived from satellite imagery, *Nature Geoscience*, **3**(2), 92–95.

Bodvardsson, G., 1955. On the flow of ice-sheets and glaciers, *Jokull*, **5**.

DeBeer, C. M. and M. J. Sharp, 2009. Topographic influences on recent changes of very small glaciers in the Monashee Mountains, British Columbia, Canada, *Journal of Glaciology*, **55**(192), 691–700.

Eisen, O., W. D. Harrison and C. F. Raymond, 2001. The surges of Variegated Glacier, Alaska, U.S.A., and their connection to climate and mass balance, *Journal of Glaciology*, **47**(158), 351–358.

Elsberg, D. H., W. D. Harrison, K. A. Echelmeyer and R. M. Krimmel, 2001. Quantifying the effects of climate and surface change on glacier mass balance, *Journal of Glaciology*, **47**(159), 649–658.

Gent, P. R., G. Danabasoglu, L. J. Donner, M. M. Holland, E. C. Hunke, S. R. Jayne, D. M. Lawrence, R. B. Neale, P. J. Rasch, M. Vertenstein, P. H. Worley, Z.-L. Yang and M. Zhang, 2011. The Community Climate System Model Version 4, *Journal of Climate*, **24**(19), 4973–4991.

Harrison, W. D., D. H. Elsberg, K. A. Echelmeyer and R. M. Krimmel, 2001. On the characterization of glacier response by a single time-scale, *Journal of Glaciology*, **47**(159), 659–664.

Hock, R., 1999. A distributed temperature-index ice- and snowmelt model including potential direct solar radiation, *Journal of Glaciology*, **45**(149), 101–111.

Huss, M. and D. Farinotti, 2012. Distributed ice thickness and volume of all glaciers around the globe, *Journal of Geophysical Research*, **117**(F4), F04010.

Huss, M., R. Hock, A. Bauder and M. Funk, 2012. Conventional versus reference-surface mass balance, *Journal of Glaciology*, **58**(208), 278–286.

Huss, M., G. Jouvet, D. Farinotti and A. Bauder, 2010. Future high-mountain hydrology: a new parameterization of glacier retreat, *Hydrology and Earth System Sciences*, **14**(5), 815–829.

Johnson, A. J., C. F. Larsen, N. Murphy, A. A. Arendt and S. L. Zirnheld, 2013. Mass balance in the Glacier Bay area of Alaska, USA, and British Columbia, Canada, 1995 âĂŞ 2011, using airborne laser altimetry, *Journal of Glaciology*, **59**(216), 1995–2011.

Kirkbride, M. P., 1993. The temporal significance of transitions from melting to calving termini at glaciers in the central Southern Alps of New Zealand, *The Holocene*, **3**(3), 232–240.

Korona, J., E. Berthier, M. Bernard, F. Rémy and E. Thouvenot, 2009. SPIRIT. SPOT 5 stereoscopic survey of Polar Ice: Reference Images and Topographies during the fourth International Polar Year (2007âĂŞ2009), *ISPRS Journal of Photogrammetry and Remote Sensing*, **64**(2), 204–212.

Larsen, C. F., R. J. Motyka, A. A. Arendt, K. A. Echelmeyer and P. E. Geissler, 2007. Glacier changes in southeast Alaska and northwest British Columbia and contribution to sea level rise, *Journal of Geophysical Research*, **112**(F1), 1–11.

Larsen, C. F., R. J. Motyka, Jeffrey T. Freymueller, K. A. Echelmeyer and Erik R. Ivins, 2005. Rapid viscoelastic uplift in southeast Alaska caused by post-Little Ice Age glacial retreat, *Earth and Planetary Science Letters*, **237**(3-4), 548–560.

Mercer, J. H., 1961. The Response of Fjord Glaciers to Changes in the Firn Limit, *Journal of Glaciology*, **3**(29), 850–858.

Motyka, R. J., M. Truffer, M. Fahnestock, J. Mortensen, S. Rysgaard and I. M. Howat, 2011. Submarine melting of the 1985 Jakobshavn Isbræ floating tongue and the triggering of the current retreat, *Journal of Geophysical Research*, **116**(F1), 1–17.

Raup, B., A. Kääb, J. S. Kargel, M. P. Bishop, G. Hamilton, E. Lee, F. Paul, F. Rau, D. Soltesz, S. Khalsa and M. Beedle, 2007. Remote sensing and GIS technology in the Global Land Ice Measurements from Space (GLIMS) Project, *Computers & Geosciences*, **33**(1), 104–125.

Rolland, C., 2003. Spatial and Seasonal Variations of Air Temperature Lapse Rates in Alpine Regions, *Journal of Climate*, **16**(7), 1032–1046.

Schneeberger, C., H. Blatter, A. Abe-Ouchi and M. Wild, 2003. Modelling changes in the mass balance of glaciers of the northern hemisphere for a transient 2ÃŮCO2 scenario, *Journal of Hydrology*, **282**(1-4), 145–163.

Skamarock, W. C., J. B. Klemp, D. O. Gill, D. M. Barker, M. G. Duda, W. Wang and J. G. Powers, 2008. A Description of the Advanced Research WRF Version 3, (June).

Trüssel, B. L., R. J. Motyka, M. Truffer and C. F. Larsen, 2013. Rapid thinning of lake-calving Yakutat Glacier and the collapse of the Yakutat Icefield, southeast Alaska, USA, *Journal of Glaciology*, **59**(213), 149–161.

Warren, C. and M. Aniya, 1999. The calving glaciers of southern South America, *Global and Planetary Change*, **22**(1-4), 59–77.

Zhang, J., U. S. Bhatt, W. V. Tangborn and C. S. Lingle, 2007. Response of glaciers in northwestern North America to future climate change: an atmosphere/glacier hierarchical modeling approach, *Annals of Glaciology*, **46**(1), 283–290.

Chapter 5
Conclusions

Yakutat Icefield in Southeast Alaska has been experiencing rapid thinning. The entire icefield is low in elevation with an accumulation to total area ratio (AAR) of 0.04 and its ice divides lie below the region's equilibrium line altitude (Eisen and others, 2001). Thinning lowers the surface elevation of the ice, exposing it to warmer climate and additionally increasing thinning, a positive feedback known as the Bodvardsson effect (Bodvardsson, 1955). Such a small AAR raises questions about the origin and the transformation into a remnant icefield. Our favored explanation includes a combination of factors, including a spillover of glacier ice from the Art Lewis and Vern Ritchie glaciers, which possess much higher elevation accumulation areas, a colder climate during the little ice age (LIA) and thickening of the Nunatak and Hidden Glaciers (both glaciers of Yakutat Icefield) as a result of nearby Hubbard Glacier occupying Russell Fjord. The post-LIA collapse was driven by the tidewater calving retreats of Nunatak and Hidden glaciers, the lake calving retreat of Yakutat Glacier, a warming climate, and recently by the Bodvardsson feedback mechanism.

Despite rapid thinning of the entire icefield, lacustrine Yakutat Glacier has stood out with significantly higher thinning rates than the land-terminating glaciers of the icefield. Increased thinning and rapid retreat can therefore be attributed to the influence of calving dynamics. However, different thinning rates between lake calving Yakutat Glacier and the remaining land-terminating glaciers in the icefield cannot be explained by calving flux itself, despite similar AARs.

As Yakutat Glacier retreated into an overdeepened basin, it was able to form a floating tongue that persisted for at least a decade. Temperate tidewater glacier ungrounding in an overdeepened basin would be exposed to density driven circulations and heat exchange with the open ocean, which would increase submarine melt and rapidly thin the ungrounded ice tongue. The weakened floating ice would then experience calving retreat. In contrast, a lacustrine ungrounded tongue is not exposed to similar density driven circulations, subaqueous melt would be comparably small and the glacier could form a persistent floating tongue. Once this tongue is weakened sufficiently by thinning, it will start to disintegrate by calving large tabular icebergs. This potentially explains the very different morphology of tidewater and lacustrine glaciers.

Thinning and breaking up of the floating tongue was observed starting in early 2010

when thinning led to rift opening. Thinning was mostly attributed to surface mass balance, which weakened the floating ice and allowed crevasses to penetrate through the ice and form rifts. Rift opening rates were highly variable and were related to precipitation and melt episodes. We hypothesize that this correlation can be explained by either the drag of sub-aqueous discharge currents, or the pooling of water in rifts. Increased water discharge additionally led to higher lake levels, which favored calving events, possibly due to increased bending stresses.

During the break-up event, large tabular icebergs calved into the lake and remained there until they melted. In late 2011, the west branch retreated back to its grounding line. Once the floating part was fully disintegrated, the calving style changed from tabular to smaller, fragmented icebergs.

As part of a remnant icefield, Yakutat Glacier will be exposed to thinning and retreat. Ice thickness measurements even suggest that the glacier will continue calving as the glacier bed lies below lake level at the ice divide. Assuming future climate to be constant at current levels, the entire east branch and more than 95% of the west branch of Yakutat Glacier will have disappeared by 2120. Under warming projections, the glacier will experience even faster retreat and thinning, only small patches of ice will be left by 2070.

At the beginning of the 21^{st} century, Yakutat Glacier can maintain relatively stable thinning rates by retreating up to higher elevations. This is a negative feedback, which will dominate in the next few decades. However, at one point in time, thinning on the upper glacier cannot be compensated by retreat and loss of low elevation areas. Thinning lowers the surface elevation, which exposes the ice surface to higher temperatures, causing increased thinning. Once this positive feedback mechanism dominates, the glacier will transfer into an unstable situation where thinning rates will increase rapidly and cause the collapse of the glacier, even under current climate conditions.

In order to stop mass loss and maintain the glaciers present volume, current climate conditions would have to change drastically. To transition into an equilibrium situation with a zero mass balance, air temperatures would have to drop by 1.5°C if the precipitation stays constant. Similarly, increasing precipitation by 50% under current temperatures would still not be sufficient to achieve zero mass balance. Both, such a decrease in temperature and an increase in precipitation appear unrealistic for Yakutat Glacier. With time passing, the required temperature drop and precipitation increase will continue to grow

and the glacier will move farther away from its equilibrium. Yakutat Glacier is irreversibly wasting mass.

5.0.1 Outlook

When a glacier retreats into an overdeepended basin, it can form a proglacial lake. Such overdeepened basins are common erosional features in glaciated areas. Once a proglacial lake exists, the glacier will transform into a lacustrine system and calving is initiated. Similarly to observations from Yakutat Glacier, thinning and retreat rates may increase due to calving dynamics, which will accelerate the mass wastage. Such lacustrine systems can be found in almost every icefield in costal Alaska, but also in most other glaciated areas around the globe. Under the present climate, the number of lake calving systems will increase.

In addition to exposure to calving dynamics, Yakutat Glacier is part of a low elevation icefield where the equilibrium line altitude (ELA) is above the ice divides. Such icefields are unstable and can rapidly lose mass or even collapse. Retreating and thinning icefields are also found outside coastal Alaska in other parts of the world, such as Arctic Canada and Patagonia. Current changes in climate increase the vulnerability of icefields, even icefields with a much higher AAR than Yakutat Icefield can transfer into a system that undergoes irreversible changes.

In summary, Yakutat Glacier is an example showing that lacustrine calving dynamics increase mass loss and that a low elevation glacier and icefield can experience a collapse even under a constant climate. With climate change, currently land-terminating margins of icefields can transform into calving systems, causing mass loss to increase and potentially lower the elevation of the entire glacier and icefield. Not only small icefileds will be exposed to such changes, also large icesheets like the Greenland Icesheet will be influenced. Along its west coast, the number of proglacial lakes is increasing. It remains to be seen how our results scale to much larger systems such as Greenland

References

Bodvardsson, G., 1955. On the flow of ice-sheets and glaciers, *Jokull*, **5**.

Eisen, O., W. D. Harrison and C. F. Raymond, 2001. The surges of Variegated Glacier, Alaska, U.S.A., and their connection to climate and mass balance, *Journal of Glaciology*, **47**(158), 351–358.